



THE HONG KONG  
POLYTECHNIC UNIVERSITY

香港理工大學

Pao Yue-kong Library

包玉剛圖書館

---

## Copyright Undertaking

This thesis is protected by copyright, with all rights reserved.

**By reading and using the thesis, the reader understands and agrees to the following terms:**

1. The reader will abide by the rules and legal ordinances governing copyright regarding the use of the thesis.
2. The reader will use the thesis for the purpose of research or private study only and not for distribution or further reproduction or any other purpose.
3. The reader agrees to indemnify and hold the University harmless from and against any loss, damage, cost, liability or expenses arising from copyright infringement or unauthorized usage.

### IMPORTANT

If you have reasons to believe that any materials in this thesis are deemed not suitable to be distributed in this form, or a copyright owner having difficulty with the material being included in our database, please contact [lbsys@polyu.edu.hk](mailto:lbsys@polyu.edu.hk) providing details. The Library will look into your claim and consider taking remedial action upon receipt of the written requests.

**LINEAR REGRESSION POSITION  
ESTIMATION METHODS FOR  
SWITCHED RELUCTANCE MOTORS**

**CHANG, YAN TAI**

**Ph.D**

**The Hong Kong Polytechnic University**

**2014**



**The Hong Kong Polytechnic University**

**Department of Electrical Engineering**

**Linear Regression Position Estimation  
Methods for Switched Reluctance Motors**

**Chang, Yan Tai**

**A Thesis Submitted in Partial Fulfillment of the Requirements for  
the Degree of Doctor of Philosophy**

**October 2012**

# Certificate of Originality

I hereby declare that this thesis is my own work and that, to the best of my knowledge and belief, it reproduces no material previously published or written nor material that has been accepted for the award of any other degree or diploma, except where due acknowledgement has been made in the text.

\_\_\_\_\_ (Signed)

Chang, Yan Tai (Name of student)

# Abstract

In this research different sensorless methods that could reliably help to remove the need to use position sensors in switched reluctance motors(SRM) are developed. These methods are different to the conventional ones by providing unique rotor positions without relying on premeasured motor magnetic characteristics. The approach is systematic and mathematical.

The relationship among motor phase inductance profiles is investigated and three types of functions to model their relationship are presented. Through regression analysis the function coefficients are found. Methods to linearize these functions for regression are explained. These coefficients are then used to calculate the rotor positions at standstill or flying restart. The estimation accuracies and efficiencies of the methods using the three functions are compared. These methods are collectively called the Linear Regression Position Estimation Methods(LRP EM).

Two methods for position estimation on a running motor are also developed. A special event called Adjacent Phase Inductance Profiles Crossing(APC) when an SRM is running is used to turn the motor into a low resolution encoder. The speed and position values obtained from this encoder are fed to a Kalman filter where detailed rotor position values are produced. The low resolution encoder is used to commutate the phases with limited speed and torque capability, while the high resolution outputs from the Kalman filter are used for fine commutations. The two commutation methods are compared and the effects from mutual couplings, voltage drops and magnetic saturation are shown.

# List of Publications

## Technical Papers in Refereed Journals

- [1] Yan Tai Chang, K.W.E. Cheng, "Sensorless Position Estimation of Switched Reluctance Motor at Startup using Quadratic Polynomial Regression", IET Electric Power Applications, vol.7, issue 7, pp.618-626, Aug. 2013.
- [2] Yan Tai Chang, K.W.E. Cheng, S.L. Ho, "Type-V Exponential Regression for Online Sensorless Position Estimation of Switched Reluctance Motor", IEEE/ASME Transactions on Mechatronics, in press, accepted on May 2014.
- [3] Yan Tai Chang, K.W.E. Cheng, "Sensorless Position Estimation of Switched Reluctance Motor at Startup Based on Relative Inductance Profile", Electric Power Components & Systems Journal. (Under revision)

## Conference Papers in Refereed Proceedings

- [4] Yan Tai Chang, K.W.E. Cheng, "Waveform analysis and control scheme for variable voltage controller and its applications for energy saving", New Energy Generation Control and Power Electronics Technology conference, Guangzhou, pp 67-73, Nov 25-29, 2007.

- [5] Yan Tai Chang, K.W.E. Cheng, Jiongkang Lin “A 200kW Wind Turbine Power Chain”, 3<sup>rd</sup> International Conference on Power Electronics Systems and Applications, 2009.
- [6] Yan Tai Chang, K.W.E. Cheng, “A simulation model for a 4 phase switched reluctance motor for PSIM”, 4<sup>th</sup> International Conference on Power Electronics Systems and Applications, pp 290-294, 2011.

# Acknowledgements

First and foremost, I would like to express my deepest gratitude to my supervisor, Prof. K. W. Eric Cheng, of the Department of Electrical Engineering, the Hong Kong Polytechnic University, who has given me numerous inspiration, guidance, advice, and support.

My sincere thanks go to Prof. S. L. Ho, Dr. Norbert Cheung, Dr. Xiangdang Xue, Dr. Paul Chan, Dr. Benny Yeung, Mr. Jiongkang Lin, Mr. Ivan Chan, Mr. K.Y. Tse, and Mr. Jones Chan, for their great supports in various aspects of my research work. Special thanks to the members of Power Electronics Research Center in the Hong Kong Polytechnic University for their kind help and encouragement in my study, as well as their friendship: Mr. K. F. Kwok, Ms. Cuidong Xu, Dr. Zhanghai Shi, Mr. Daohong Wang, Mr. Yanjie Bao, Dr. Kai Ding, Dr. Shuxiao Wang, Mr. T. W. Ng, Mr. M. K. Wong, Dr. C. K. Lee, Mr. Junfeng Liu, Dr. Zhu Zhang, Dr. Weimin Wang, Mr. Dickson Chau, Mr. Yuanmao Ye, Mr. Ray Tai, Mr. W. F. Choi.



# Table of Contents

Certificate of Originality.....	I
Abstract.....	II
List of Publications .....	III
Acknowledgements.....	V
Table of Contents.....	VI
List of Figures .....	IX
List of Tables .....	XIII
List of Abbreviations .....	XIV
List of Symbols .....	XV
Chapter 1 Introduction .....	1
1.1 Foreword.....	1
1.2 Background .....	3
1.2.1 Inductance Profile of SRM .....	3
1.2.2 Regression Analysis.....	4
1.2.3 Kalman Filter .....	5
1.3 Thesis Outline.....	8
Chapter 2 Position Estimation Using Polynomial Regression .....	10
2.1 Polynomial Regression.....	10
2.2 Principle of the Proposed Method.....	13
2.3 Illustration of LQRPEM.....	19
2.4 Simulation Results.....	24
2.5 Hardware Descriptions .....	27
2.5.1 System Setup.....	27
2.5.2 Converter .....	29
2.5.3 Motor .....	29
2.5.4 Load.....	30

2.5.5	Control .....	30
2.6	Experimental Results .....	31
2.7	Summary .....	36
Chapter 3 Position Estimation Using Type V Exponential Function.....		37
3.1	Introduction .....	37
3.2	Type V Exponential Function .....	37
3.3	Method Derivation.....	40
3.4	An Example of LERPEM .....	42
3.5	Simulation Results.....	45
3.6	Experimental Results .....	49
3.7	Summary .....	50
Chapter 4 Position Estimation Using Co-sinusoidal function.....		51
4.1	Introduction .....	51
4.2	Co-sinusoidal Regression Model.....	51
4.2.1	IEEE Standard 1057 .....	51
4.2.2	Cosine Regression Function .....	52
4.2.3	Method Derivation.....	54
4.3	Simulation Results.....	56
4.4	Experimental Results .....	58
4.5	Models Comparison .....	59
4.6	Summary .....	63
Chapter 5 Position Estimation under Dynamic Conditions.....		64
5.1	Introduction .....	64
5.2	General Phase Inductance Profile property.....	65
5.3	Using Kalman Filter For SRM Control.....	67
5.4	The State Space model.....	69
5.4.1	Conventional State Space model .....	69

5.4.2	Proposed State Space model .....	70
5.5	Position Estimation Procedure and Phase Switching Strategy .....	71
5.5.1	Type I Switching Mode.....	71
5.5.2	Type II Switching Mode.....	75
5.6	Some Implementation Issues.....	78
5.6.1	Update frequency of the Kalman filter .....	78
5.7	Simulation Results.....	81
5.7.1	Type I only switching with applied load.....	82
5.7.2	Type II switching.....	84
5.7.3	Type I to Type II transition .....	86
5.8	Experimental Results .....	88
5.9	Comparison to other methods.....	104
5.10	Summary .....	104
Chapter 6 Conclusion .....		106
6.1	Developed Techniques for Position Estimations .....	107
6.2	Main Contributions .....	108
6.3	Future Research .....	110
References .....		111

# List of Figures

Fig. 1–1 General Inductance Profile of a switched reluctance motor .....	4
Fig. 2–1 Inductance of all phases at an arbitrary rotor position .....	13
Fig. 2–2 Phase inductance profile repeated for 2 periods and superimposed with 2 parabolas .....	14
Fig. 2–3 Results from polynomial regression. ....	21
Fig. 2–4 Startup angle estimation simulation results of a 3kW four-phase 8/6 switched reluctance motor using LQRPEM and the function with negative concavity and larger <i>rms</i> residuals. a) Actual angle. b) Estimated angle c) Error in estimations .....	25
Fig. 2–5. Startup angle estimation simulation results of a 5kW four-phase 8/6 switched reluctance motor using LQRPEM and the function with negative concavity and larger <i>rms</i> residuals. a) Actual angle. b) Estimated angle c) Error in estimations .....	25
Fig. 2–6 Startup angle estimation simulation results of a 3kW four-phase 8/6 switched reluctance motor using LQRPEM and the function with positive concavity with smaller <i>rms</i> residuals. a) Actual positions. b) Estimated positions c) Error in estimations.....	26
Fig. 2–7 Startup angle estimation simulation results of a 5kW four-phase 8/6 switched reluctance motor using LQRPEM and the function with positive concavity and smaller <i>rms</i> residuals. a) Actual positions. b) Estimated positions c) Error in estimations.....	26
Fig. 2–8 System schematic of the experiment setup. ....	28
Fig. 2–9 Experiment setup .....	28
Fig. 2–10 Converter used for the experiments. ....	29
Fig. 2–11 Inductance profile for all phases for the two periods used in the experiments for static position estimation. ....	30
Fig. 2–12 Current waveforms for all phases at Phase 1 mechanical positions of a)0° b)10° c)30° d)50°. Trace 1,2,3,4 corresponds to Phase 1,2,3,4 respectively. ....	32
Fig. 2–13 Startup angle estimation experiment results of a 1.5kW four phase 8/6 switched reluctance motor using LQRPEM. a)Actual positions. b)Estimated positions using functions with smallest <i>rms</i> residuals c)Estimated positions using functions with the smallest <i>rms</i> residuals with opposite concavities as the functions in b). d)Error in estimations: blue curve – errors for b). red curve –errors for c). e)Concavity of the curve with the smallest <i>rms</i> residuals. ....	35
Fig. 3–1 Inductance of the phases repeated for 2 periods and superimposed with 2 Type V exponential functions .....	41

Fig. 3–2 Results from exponential regression.....	44
Fig. 3–3 Startup angle estimation simulation results of a 3kW four phase 8/6 switched reluctance motor using the curve with positive concavity. a) Actual angle. b) Estimated angle c) Error in estimation .....	46
Fig. 3–4 Startup angle estimation simulation results of a 5kW four phase 8/6 switched reluctance motor using the curve with positive concavity. a) Actual angle. b) Estimated angle c) Error in estimations.....	46
Fig. 3–5 Startup angle estimation simulation results of a 3kW four phase 8/6 switched reluctance motor using the preferred curve. a) Actual angle. b) Estimated angle c) Error in estimation .....	47
Fig. 3–6 Startup angle estimation simulation results of a 5kW four phase 8/6 switched reluctance motor using the preferred curve. a) Actual angle. b) Estimated angle c) Error in estimations.....	47
Fig. 3–7 Startup angle estimation simulation results of a 1.5kW four phase 8/6 switched reluctance motor using the preferred curve. a) Actual positions. b) Estimated positions c) Error in estimations. ....	48
Fig. 3–8 Startup angle estimation experiment results of a 1.5kW four-phase 8/6 switched reluctance motor using LERP EM. a)Actual positions. b)Estimated positions c)Error in estimations d)rms residuals from the curve fit. ....	49
Fig. 4–1 Inductance of the phases repeated for 2 periods and superimposed with one cosinusoidal function.....	52
Fig. 4–2 Startup angle estimation simulation results using LSRPEM of a 3kW four-phase 8/6 switched reluctance motor. a) Actual angle. b) Estimated angle c) Error in estimation .....	57
Fig. 4–3 Startup angle estimation simulation results using LSRPEM of a 5kW four-phase 8/6 switched reluctance motor. a) Actual angle. b) Estimated angle c) Error in estimation .....	57
Fig. 4–4 Startup angle estimation experimental results using LSRPEM of a 1.5kW four-phase 8/6 switched reluctance motor. a) Actual angle. b) Estimated angle c) Error in estimation ..	59
Fig. 4–5 Position estimation errors and <i>rms</i> residuals for the different methods using simulation result from the 3kW motor. a)Estimation Error. b) <i>rms</i> residuals.....	60
Fig. 4–6 Position estimation errors and <i>rms</i> residuals for the different methods using simulation result from the 5kW motor. a)Estimation Error. b) <i>rms</i> residuals.....	61
Fig. 4–7 Position estimation errors and <i>rms</i> residuals for the different methods using experimental result from the 1.5kW motor. a)Estimation Error. b) <i>rms</i> residuals .....	62
Fig. 5–1 General phase inductance profiles for all phases of an 8/6 SRM. Inductance profile crossing points for adjacent phases shown. ....	66

Fig. 5–2 Current switching waveforms for all phases of an 8/6 SRM under Type I Switching Mode. a)Current waveforms. b) Actual Electrical Positions .....	72
Fig. 5–3 Current switching waveforms for all phases of an 8/6 SRM under Type II Switching Mode. a)Current waveforms. b)Actual Electrical Positions c) Estimated Phase 1 Electrical Position from filter .....	76
Fig. 5–4 Expanded current switching waveforms for all phases of an 8/6 SRM under Type II Switching Mode. a)Current waveforms. b)Actual Electrical Positions .....	77
Fig. 5–5 Simulation results using Type I switching method with and without load a)Set Current and Load. b)Actual Speed c)Estimated Speed Error d)Estimated Position Error .....	83
Fig. 5–6 Simulation results using Type II switching method with and without load a)Set Current and Load. b)Actual Speed c)Estimated Speed Error d)Estimated Position Error .....	85
Fig. 5–7 Simulation results using Type I and Type II switching methods with load a)Set Current. b)Actual speed c)Speed Estimation delta d)Position Estimation delta. ....	87
Fig. 5–8 Current waveforms under Type I switching without load a)Phase Currents. b)Phase 1 Mechanical Position .....	88
Fig. 5–9 Current waveforms under Type I switching with load a)Phase currents. b)Phase 1 Mechanical Position .....	90
Fig. 5–10 Current waveforms under Type I switching mode with load in expanded view. a)Phase currents. b)Phase 1 Mechanical Position .....	91
Fig. 5–11 Kalman Filter performance under Type I switching. a)Actual Speed b)Filter Speed Estimation error c)Filter Position Estimation Error .....	92
Fig. 5–12 Current waveforms under Type II switching without load a)Phase currents. b)Phase 1 Mechanical Position .....	93
Fig. 5–13 Current waveforms under Type II switching with load a)Phase currents. b)Phase 1 Mechanical Position .....	93
Fig. 5–14 Kalman Filter performance under Type II switching. a)Actual Speed b)Filter Speed Estimation error c)Filter Position Estimation error .....	94
Fig. 5–15 Kalman Filter performance with no switching. a)Actual Speed b)Filter Speed Estimation error c)Filter Position Estimation error .....	95
Fig. 5–16 Kalman Filter performance when switching goes from Type I to Type II. a)Actual Speed b)Filter Speed Estimation error c)Filter Position Estimation error .....	96
Fig. 5–17 Position variations from expected at APC4/1 under different switching conditions with no load. Red lines indicate mean values. a)No switching. b)Type I switching c)Type II switching .....	100

Fig. 5–18 Position variations from expected at APC1/2 under different switching conditions with no load. Red lines indicate mean values. a)No switching. b)Type I switching c)Type II switching ..... 100

Fig. 5–19 Position variations from expected at APC2/3 under different switching conditions with no load. Red lines indicate mean values. a)No switching. b)Type I switching c)Type II switching ..... 101

Fig. 5–20 Position variations from expected at APC3/4 under different switching conditions with no load. Red lines indicate mean values. a)No switching. b)Type I switching c)Type II switching ..... 101

Fig. 5–21 Position variations from expected at APC4/1 under different switching conditions under load. Red lines indicate mean values. a)Type I switching b)Type II switching ..... 102

Fig. 5–22 Position variations from expected at APC1/2 under different switching conditions under load. Red lines indicate mean values. a)Type I switching b)Type II switching ..... 102

Fig. 5–23 Position variations from expected at APC2/3 under different switching conditions under load. Red lines indicate mean values. a)Type I switching b)Type II switching ..... 103

Fig. 5–24 Position variations from expected at APC3/4 under different switching conditions under load. Red lines indicate mean values. a)Type I switching b)Type II switching ..... 103

# List of Tables

TABLE 2-1 SIMULATION MOTOR PARAMETERS.....	20
TABLE 2-2 MEASURED PHASE CURRENTS AND ACTUAL PHASE 1 MECHANICAL POSITION .....	34
TABLE 4-1 COMPARISON OF THE DIFFERENT ESTIMATION METHODS.....	63
TABLE 5-1 SIMULATION SETTINGS FOR TYPE I SWITCHING .....	82
TABLE 5-2 SIMULATION SETTINGS FOR TYPE II SWITCHING .....	84
TABLE 5-3 SIMULATION SETTINGS FOR TYPE I TO II TRANSITION.....	86
TABLE 5-4 COMPARISON OF DIFFERENT DYNAMIC METHODS .....	104



## List of Abbreviations

APC	Adjacent Phase Inductance Profiles Crossing
APC $n/m$	Adjacent Phase Inductance Profiles Crossing Event of phase $n$ and phase $m$
CSMO	Current Sliding Mode Observer
FEA	Finite Element Analysis
FSMO	Flux linkage Sliding Mode Observer
LERPEM	Linear Exponential Regression Position Estimation Method
LQRPEM	Linear Quadratic Regression Position Estimation Method
LRPEM	Linear Regression Position Estimation Method
LSRPEM	Linear Sinusoidal Regression Position Estimation Method
SRM	Switched Reluctance Motor

# List of Symbols

$\mathbf{A}_k$	State Transition Matrix
$\mathbf{B}_k$	Discrete Input Matrix
$\mathbf{D}$	Regression Matrix
$\mathbf{F}$	System Dynamics Matrix
$\mathbf{G}$	Input Matrix
$\mathbf{H}$	Measurement Matrix
$\mathbf{H}_k$	Discrete Measurement Matrix
$I$	Current
$\mathbf{K}$	Kalman Gain Matrix
$L_{relative}(\theta_e)$	Relative Inductance at $\theta_e$
$N_R$	Rotor Pole Number
$\mathbf{P}_k$	State Estimation Error Covariance Matrix
$\mathbf{Q}_k$	Discrete Noise Process Covariance Matrix
$\mathbf{R}_k$	Discrete Measurement Noise Covariance Matrix
$\Delta T$	Period

$\theta_e$	Phase Electrical Position
$\theta_m$	Phase Mechanical Position
$\mathbf{u}$	Input Column Vector
$\mathbf{u}_k$	Discrete Input Column Vector
$V$	Voltage
$\mathbf{v}$	Zero Mean White Measurement Noise vector
$\mathbf{v}_k$	Zero Mean Discrete White Measurement Noise Vector
$\mathbf{w}$	Zero Mean White-Noise Process Column Vector
$\mathbf{w}_k$	Zero Mean Discrete White-Noise Process Column Vector
$\mathbf{x}$	State Vector
$\mathbf{x}_k$	Discrete State Vector
$\mathbf{y}$	Sampled Data Column Vector
$\mathbf{z}$	Measurement Vector, Coefficients Vector
$\mathbf{z}_k$	Discrete Measurement Vector

# Chapter 1

## Introduction

### 1.1 Foreword

Switched-reluctance motors are reliable and simple to manufacture. They do not need permanent magnet for flux generation and therefore do not have the risks of demagnetization or bear the high costs of rare earth metals. On the other hand they must be driven by power converters and they cannot run directly off main power. Adding to this it is also difficult to control the smoothness of torque and speed. Much work has been done on reducing the torque ripples[1-9] and the resulting noisy operations[10-16]. Dynamic performance is also greatly improved by various torque control strategies[17-24]. In recent years, thanks to advances in power electronics and control elements, these types of machines are gaining in popularity and the cost of implementation is dropping. But to truly compete with other technologies like the induction motor, which is also robust and economical, there are still many hurdles to overcome, one of them being the need for position feedback devices. This issue has been addressed by many researchers, and many sensorless methods for starting and running of switched reluctance motors had been developed[6, 25-46]. For starting the motor, the simplest way is to align the rotor to an energized phase. If for some reasons rotating the motor arbitrarily is not allowed or becomes difficult, some rough estimation of the phase positions are needed. Different starting methods have been studied. In [26], flux linkage is obtained by calculating the volt-seconds applied to the phases. Then the inductances for the three phases are found by dividing the flux

linkage by the measured current. Assuming identical inductance profiles for all the phases the positions are then estimated using vector transformations. But this method is limited to three-phase SRM. In [32] currents are again measured after an equal amount of volt-seconds are applied to a four-phase SRM. By ordering the currents by magnitude and using a lookup table, the best phase for starting is determined. In [36] the phase next to the phase with the largest current after an equal amount of volt-seconds is applied is chosen for starting. In [42] cubic spline interpolation is used to find the starting position after finding the best phases for the operation. In [39] mutual inductance is utilized to estimate the positions of a four-phase SRM. By exciting Phase A and B of a four-phase SRM by an alternating current, the induced voltages of the adjacent phases are compared and the rotor positions can be determined to within  $15^\circ$  mechanical accuracy. In [47] the authors describe a method to find the linear regions between the aligned and unaligned position by measuring the time for each phase to reach a certain threshold current. These methods usually involve applying voltage to the motor, and by measuring the resultant phase currents and sometimes together with calculated flux linkage, estimate the positions or just determine the best phases to turn on [25, 32, 42, 47]. There are also many studies on sensorless control the running of SRM. In [26, 48] the phase inductances from a three-phase motor are combined into a rotating vector and by orthogonal decomposition the rotor angle is found. In [49] a similar vector based method is used to determine the inductance vector and direct torque control technique is applied. [38] describes a method that relies on premeasured flux-current characteristic of the motor to determine the switching position of the phases using flux linkage value. Observers and artificial intelligence are sometimes used for position detection during running [6, 28, 30, 35, 45, 49-54]. In [6] two fuzzy neural network modules are used to identify the turn-on and

turn-off positions separately. In [45] a neural network is trained with predefined data and a 2D lookup table is created for finding the rotor position. In [51] FEA data is used to train the neural network for estimating the positions during running. In [30] two sliding mode observers namely the Flux linkage Sliding Mode Observer (FSMO) and the Current Sliding Mode Observer (CSMO) are combined to estimate the positions of a running SRM.

In this study methods for both static and dynamic rotor position estimation will be presented. These methods do not require knowledge of specific magnetic characteristics of the motor used. The static methods provide direct mathematical estimations of the positions and the dynamic methods turn the motor into a low resolution encoder. These methods can be used in areas where speed control is required such as in pumps, fans and electric vehicles.

## **1.2 Background**

### **1.2.1 Inductance Profile of SRM**

Fig. 1–1 shows a general inductance profile for one phase for one electrical period of an SRM. The profile takes on a rounded triangular shape with a small slope towards the aligned and unaligned positions. The inductance is a function of the rotor angular position and current and has its maximum value at the fully aligned position and minimum value at the fully unaligned position. The inductance profiles of all phases take on a similar shape with an angle offset to the adjacent phases' determined by the number of phases. For a four-phase SRM, each phase is separated by  $90^\circ$  electrical. The actual mechanical position of each phase is determined by the number of rotor poles on the motor, and is given by:

$$\theta_m = \frac{\theta_e}{N_R} \quad (1-1)$$

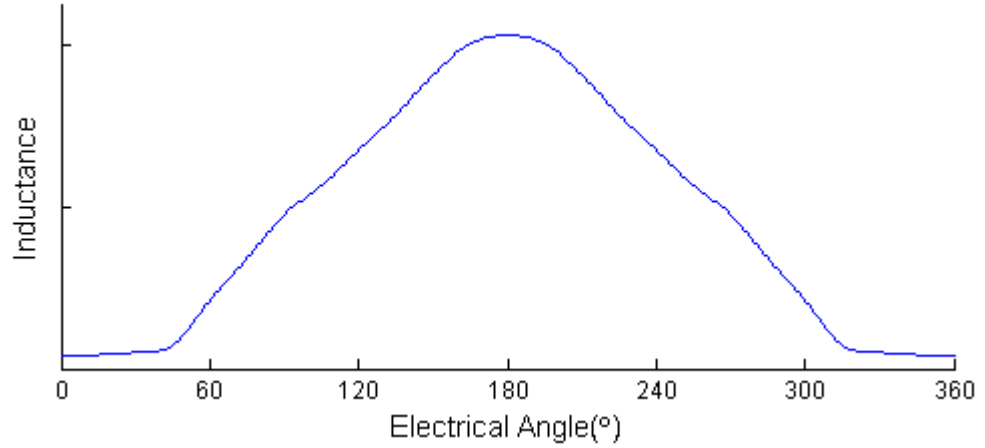


Fig. 1-1 General Inductance Profile of a switched reluctance motor

where  $\theta_m$  represents the mechanical angle,  $\theta_e$  represents the electrical angle, and  $N_R$  the number of rotor poles. Therefore for an 8/6 SRM, each phase's inductance profile has an offset to the adjacent phase's by  $15^\circ$  mechanical. In this thesis,  $0^\circ$  and  $180^\circ$  electrical are defined as the fully unaligned and aligned positions respectively. All angle values are assumed electrical unless explicitly stated.

### 1.2.2 Regression Analysis

Regression analysis is a statistical process originally developed for data analysis[55]. In the case of single independent variable it models the relationship between the value of independent variable  $x$  such and the corresponding conditional mean of dependent variable  $y(x)$ . When a set of observed data is collected, it uses a parametrically defined function known as a regression function to model these data in order to understand the trend and characteristics of the data set. To find the coefficients of the regression functions many techniques have been developed, both linear and nonlinear.

Linear techniques include ordinary least squares and maximum likelihood estimation and nonlinear techniques there are the Gauss-Newton algorithm, gradient descent and the Levenberg-Marquardt algorithms.

In this research for static rotor position estimations, regression analysis will be used extensively and the method of ordinary least squares will be used to find the model parameters.

### **1.2.3 Kalman Filter**

The Kalman Filter was developed in the 1960s by Rudolf E. Kalman. It was first described in his paper “*A New Approach to Linear Filtering and prediction problems*”[56]. Since then it has been widely used in navigation, missile guidance, and unmanned automobiles. It is a kind of state estimators, by using the system model and sensors measuring the states, it employs a correction algorithm with a variable estimator gain based on process and measurement noise covariance, to estimate the states of the target online even in noisy measurements environment. It is a two-step process, in the first step known as the time update step the process model is used to predict the current state. In the second called the measurement update step, information from sensors is then used to correct the model predicted states. Its power lies in the ability to filter out measurements and modeling errors through continuous updates of the state predictions with new measurements. It is also an optimal filter, as it guarantees that the state estimation minimizes the least squares error. Measurements from different sensors with different accuracies and measuring frequencies can also be combined to improve states estimations.

To apply the Kalman filter a model of the target system must be known. It is described by a set of differential equations, cast in matrix or state-space format:



$$\dot{\mathbf{x}} = \mathbf{F}\mathbf{x} + \mathbf{G}\mathbf{u} + \mathbf{w} \quad (1-2)$$

where  $\mathbf{x}$  being a column vector containing the states,  $\mathbf{F}$  the system dynamics matrix,  $\mathbf{u}$  the input or control column vector,  $\mathbf{G}$  the input matrix, and finally  $\mathbf{w}$  as a zero mean white-noise process column vector. The filter also requires that the measurements are linear related to the states as follow:

$$\mathbf{z} = \mathbf{H}\mathbf{x} + \mathbf{v} \quad (1-3)$$

where  $\mathbf{z}$  is the measurement vector,  $\mathbf{H}$  the measurement matrix, and  $\mathbf{v}$  the white measurement noise vector. These requirements are actually in line with the definition of a linear system model and the measurements from the sensors are considered as the system output. In this thesis the discrete Kalman filter is used. Therefore the above equations must be converted to their discrete equivalence. The discrete state-space equation is given by:

$$\mathbf{x}_{k+1} = \mathbf{A}_k \mathbf{x}_k + \mathbf{B}_k \mathbf{u}_k + \mathbf{w}_k \quad (1-4)$$

where  $\mathbf{x}_k$ ,  $\mathbf{u}_k$ ,  $\mathbf{w}_k$  are the discrete versions of their continuous counterparts  $\mathbf{x}$ ,  $\mathbf{u}$ ,  $\mathbf{w}$ , in (1-2) at the sampling instant  $k$ .  $\mathbf{A}_k$  is known as the state transition matrix. It is related to the system dynamics matrix  $\mathbf{F}$  by

$$\mathbf{A}_k = e^{\mathbf{F}T} \quad (1-5)$$

where  $\mathbf{F}$  is assumed constant and  $T$  the sampling period for the discrete system.  $\mathbf{B}_k$  is related to the input matrix  $\mathbf{G}$  by

$$\mathbf{B}_k = \int_0^T e^{\mathbf{F}(T-t)} \mathbf{G}(t) dt \quad (1-6)$$

The discrete measurement equation is given by

$$\mathbf{z}_k = \mathbf{H}_k \mathbf{x}_k + \mathbf{v}_k \quad (1-7)$$

which is the discrete counterpart of (1-3). There are also two very important parameters, one is the discrete process noise covariance matrix  $\mathbf{Q}$  given by

$$\mathbf{Q}_k = E[\mathbf{w}_k \mathbf{w}_k^T] \quad (1-8)$$

and the discrete measurement noise covariance matrix  $\mathbf{R}$  given by

$$\mathbf{R}_k = E[\mathbf{v}_k \mathbf{v}_k^T] \quad (1-9)$$

where  $E[\_]$  is the expected value operator and  $\mathbf{w}_k$  and  $\mathbf{v}_k$  has zero mean. These parameters are needed to calculate the Kalman gain factor.

The Kalman-filtering equation is then given by:

$$\hat{\mathbf{x}}_{k+1} = \mathbf{A}_k \hat{\mathbf{x}}_k + \mathbf{B}_k \mathbf{u}_k + \mathbf{K}_{k+1} (\mathbf{z}_{k+1} - \mathbf{H}_k \mathbf{A}_k \hat{\mathbf{x}}_k - \mathbf{H}_k \mathbf{B}_k \mathbf{u}_k) \quad (1-10)$$

Basically the filter uses the discrete state-space system model to calculate the next state from the current state and then added a correction term based on the new measurements. The matrix  $\mathbf{K}$  is what is known as the Kalman gain matrix. The Kalman gain and the covariance matrix of the state estimation error at the sampling instant  $k$ , represented by  $\mathbf{P}_k$ , is obtained through (1-11) to (1-13) of the following Riccati equations:

$$\mathbf{P}_k^- = \mathbf{A}_{k-1} \mathbf{P}_{k-1}^+ \mathbf{A}_{k-1}^T + \mathbf{Q}_{k-1} \quad (1-11)$$

$$\mathbf{K}_k = \mathbf{P}_k^- \mathbf{H}_k^T (\mathbf{H}_k \mathbf{P}_k^- \mathbf{H}_k^T + \mathbf{R}_k)^{-1} \quad (1-12)$$

$$\mathbf{P}_k^+ = (\mathbf{I} - \mathbf{K}_k \mathbf{H}_k) \mathbf{P}_k^- \quad (1-13)$$

The sign superscript indicates whether the covariance is for the state estimation obtained from the previous state through the system model only (minus sign), known as *a priori* error covariance matrix, or for the state estimation after the measurement correction step (plus sign), known as *posterior* error covariance matrix. (1-10) shows that a new state vector can be obtained at every execution of the filter equation. It is interesting to note that the Kalman gain and the error covariance can be calculated offline before running the filter.

The Kalman filter is used in Chapter 5 for a dynamic position sensorless control method.

### 1.3 Thesis Outline

This Thesis is organized as follows: Chapter 2 through Chapter 4 introduce 3 different regression functions to model the phase inductance for a four-phase 8/6 SRM. Through the coefficients obtained from the functions, the rotor position is estimated. A quadratic function is used in Chapter 2 to model the inductance. In this chapter the procedure for finding the least squares solution is introduced, and the position estimation method is demonstrated. The system overview and hardware used for the experiments are also presented. Chapter 3 and Chapter 4 investigate the use of type V exponential functions and co-sinusoidal functions to model the inductance, and the approach to extract the position information is shown. The merits and drawbacks of the different models are then compared. Chapter 5 presents two methods to estimate the rotor positions while the motor is running. The first method makes use of a special

magnetic property of a four-phase SRM and the second method utilizes the Kalman filter to determine the commutation positions.

# Chapter 2

## Position Estimation Using Polynomial Regression

### 2.1 Polynomial Regression

Polynomial regression is a form of regression analysis[57]. It uses a polynomial regression function to model the characteristics of the data set. Polynomial regression models usually employ the method of least squares to minimize the difference between the regression function and the actual data. Although the dependent and independent variables do not have a linear relationship above the first order, it is linear in the parameters[57] and linear techniques could be used to find the coefficients for the function.

A polynomial function  $y(x)$  with one independent variable  $x$  can be represented by:

$$y(x) = \sum_{n=0}^m a_n x^n \quad (2-1)$$

where  $m$  represents the order of the polynomial and  $a_n$  the constant coefficients for each power of  $x$ . A second order polynomial regression function(i.e. a quadratic regression function) is pertinent to the method to be developed and its corresponding equation is:

$$y(x) = a_2 x^2 + a_1 x^1 + a_0 \quad (2-2)$$

Given a sequence of data  $y_1, y_2, \dots, y_L$ , taken at points  $x_1, x_2, \dots, x_L$ , it is desired to find

the unknown coefficients  $a_n$  of the regression function  $y(x)$  to minimize the following sum of squared differences  $S_s$  :

$$S_s = \sum_{n=1}^L (y_n - y(x))^2 = \sum_{n=1}^L (y_n - a_2 x_n^2 - a_1 x_n^1 - a_0)^2 \quad (2-3)$$

To find the values of  $a_2$ ,  $a_1$ , and  $a_0$  the following matrices are first created:

$$\mathbf{D} = \begin{bmatrix} x_1^2 & x_1 & 1 \\ x_2^2 & x_2 & 1 \\ \bullet & \bullet & \bullet \\ \bullet & \bullet & \bullet \\ \bullet & \bullet & \bullet \\ x_L^2 & x_L & 1 \end{bmatrix} \quad (2-4)$$

$$\mathbf{y} = \begin{bmatrix} y_1 \\ y_2 \\ \bullet \\ \bullet \\ \bullet \\ y_L \end{bmatrix} \quad (2-5)$$

$$\mathbf{z} = \begin{bmatrix} a_2 \\ a_1 \\ a_0 \end{bmatrix} \quad (2-6)$$

where  $\mathbf{D}$  is a variation of the Vandermonde Matrix[58],  $\mathbf{y}$  the vector containing the sampled data and  $\mathbf{z}$  the vector of coefficient values.

In matrix notation, the sum of squared differences in equation (2-3) is then given by

$$S_s = (\mathbf{y} - \mathbf{Dz})^T (\mathbf{y} - \mathbf{Dz}) \quad (2-7)$$

The purpose is to find a set of coefficients  $\mathbf{z}$  that would minimize  $S_s$ . This least squares solution is given by:

$$\hat{\mathbf{z}} = (\mathbf{D}^T \mathbf{D})^{-1} (\mathbf{D}^T \mathbf{y}) = \mathbf{T} \mathbf{y} \quad (2-8)$$

where  $\hat{\mathbf{z}}$  is the set of coefficients which provides the least squares solution. The polynomial regression function is then expressed as:

$$\hat{y}_n(x_n) = \hat{a}_2 x_n^2 + \hat{a}_1 x_n + \hat{a}_0 \quad (2-9)$$

and the residuals  $r_n$  of the solution is given by

$$r_n = y_n - \hat{y}_n \quad (2-10)$$

The coefficients thus can be found directly from the least squares operation (2-8).

To locate the vertex of function (2-9), its derivative is taken:

$$\hat{y}'_n(x_n) = 2\hat{a}_2 x_n + \hat{a}_1 \quad (2-11)$$

The root of (2-11) is then given by

$$x_r = -\frac{\hat{a}_1}{2\hat{a}_2} \quad (2-12)$$

$x_r$  therefore represents the  $x$  coordinate of the vertex of (2-9). To determine whether the vertex is the maximum or minimum of the function, the 2<sup>nd</sup> derivative of equation (2-9) is taken and is given by:

$$\hat{y}''_n(x_n) = 2\hat{a}_2 \quad (2-13)$$

Therefore by inspecting the polarity of coefficient  $\hat{a}_2$ , the concavity of the curve can be known. It follows that  $x_r$  is at the maximum if  $\hat{a}_2 < 0$  and minimum if  $\hat{a}_2 > 0$ .

## 2.2 Principle of the Proposed Method

The last section has provided the background of the method to be developed in this section. The method to be developed is for a four-phase 8/6 SRM, but could easily be extended to motors with at least three phases.

As mentioned in Section II, the inductance profile of a phase takes on a rounded triangular shape, and each profile is shifted from that of the next phase by  $90^\circ$ . If a snapshot of all the phase inductance is taken at any one rotor position, their values can be mapped on a single profile. This is shown in Fig. 2-1 which shows the inductance of all phases when phase 1 is at  $300^\circ$ .

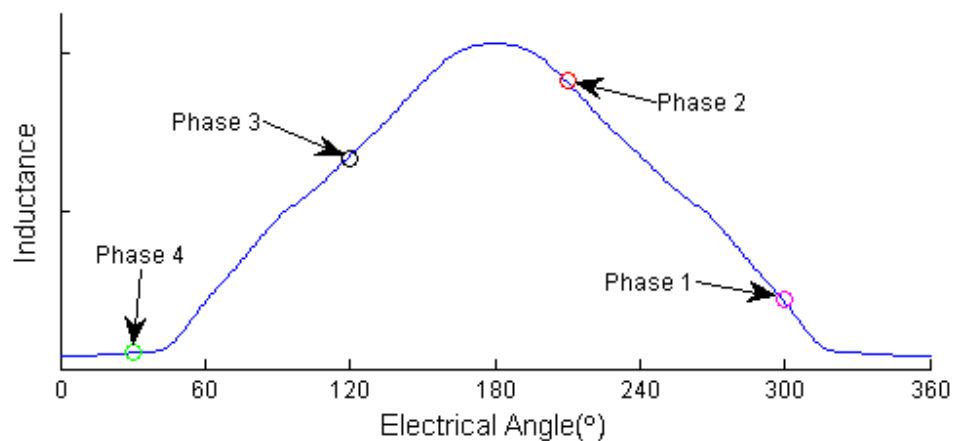


Fig. 2-1 Inductance of all phases at an arbitrary rotor position

It is assumed that all motor phases have the same inductance profile. Although the profiles among phases might not be exactly the same, they usually will not differ by a



large extent. By superimposing two 2<sup>nd</sup> order polynomials on the plot and repeating the profile for two periods, Fig. 2–2 follows:

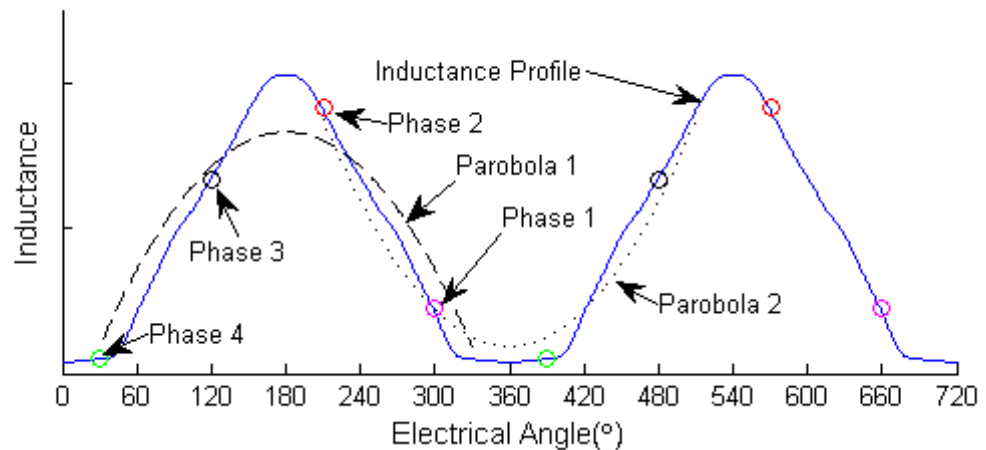


Fig. 2–2 Phase inductance profile repeated for 2 periods and superimposed with 2 parabolas

Parabola 1 is a polynomial with its maximum vertex vertically aligned with the fully aligned position of the inductance profile, and parabola 2 has its minimum vertex vertically aligned with the fully unaligned position of the profile. It can be observed that although the polynomials do not follow the actual inductance profile, they have great resemblance in the sense that all are symmetric to the midpoint and possess one vertex. It is proposed that by best fitting several quadratic functions of phase position to a scaled version of the phase inductances, which will be called the relative inductances, two curves with the same characteristics as parabola 1 and 2 can be obtained. Through solving for the position of one of their vertices, the positions of all the phases can be estimated.

Referring back to Fig. 2–1, at any moment in time the inductances from the 4 phases are represented by 4 points on the inductance profile. In order to carry out the best-fit operation it is necessary to find these 4 points. To do so a voltage is applied to all phases for an equal amount of time and the currents are then measured. In the method

to be developed only the ratio of the inductances is needed and therefore it is not necessary to calculate the flux linkage as long as all phases are given the same volt-seconds. The relationship between volt-seconds and inductance for each phase is:

$$L(\theta_e) = \frac{V \cdot \Delta T}{I} \quad (2-14)$$

where mutual coupling, inductance saturation and resistance are ignored because the current to be used will be small. The inductance is a function of the electrical phase position  $\theta_e$ . The product of  $V$  and  $\Delta T$  represents the volt-seconds applied to a fully demagnetized phase, and  $I$  is the resultant phase current. Since only the relative inductance is of interest and volt-seconds are equal for all phases, (2-14) can be normalized by  $V \cdot \Delta T$ . The expression becomes:

$$L_{relative}(\theta_e) = \frac{1}{I} \quad (2-15)$$

Therefore by measuring the currents after an equal amount of volt-seconds is applied to each phase, the relative inductances can be calculated.

The proposed quadratic equation to represent the relationship between the relative inductance  $L_{relative}(\theta_e)$  and the electrical phase angle is:

$$L_{relative}(\theta_e) = a_2 \theta_e^2 + a_1 \theta_e^1 + a_0 \quad (2-16)$$

The next step is to apply the regression technique in Section II to find the coefficients  $a_2$ ,  $a_1$  and  $a_0$ . This is done by replacing the variables  $x_n$  in the  $\mathbf{D}$  matrix (2-4) with  $\theta_{ne}$ , where  $\theta_{ne}$  represents the electrical angle for phase  $n$ , and variables  $y_n$  in the  $\mathbf{y}$  vector (2-5) with  $L_{relative\_n}$ , where  $L_{relative\_n}$  represents the relative inductance for phase

*n.*

The **D** matrix becomes:

$$\mathbf{D} = \begin{bmatrix} \theta_{1e}^2 & \theta_{1e} & 1 \\ \theta_{2e}^2 & \theta_{2e} & 1 \\ \theta_{3e}^2 & \theta_{3e} & 1 \\ \theta_{4e}^2 & \theta_{4e} & 1 \end{bmatrix} \quad (2-17)$$

Four arbitrary angles 90° apart within one electrical period will be assigned to the phases. The actual values are not important, as they will not affect the results as will be explained later. Here arbitrary angles of 270°, 180°, 90° and 0° for phase 1 through 4, respectively, are used. The **D** matrix then becomes:

$$\mathbf{D} = \begin{bmatrix} 270^2 & 270 & 1 \\ 180^2 & 180 & 1 \\ 90^2 & 90 & 1 \\ 0 & 0 & 1 \end{bmatrix} \quad (2-18)$$

that evaluates to:

$$\mathbf{D} = \begin{bmatrix} 72900 & 270 & 1 \\ 32400 & 180 & 1 \\ 8100 & 90 & 1 \\ 0 & 0 & 1 \end{bmatrix} \quad (2-19)$$

And vector **y** (2-5) becomes:

$$\mathbf{y} = \begin{bmatrix} L_{relative\_1} \\ L_{relative\_2} \\ L_{relative\_3} \\ L_{relative\_4} \end{bmatrix} \quad (2-20)$$

Substituting **D** and **y** into the least squares solution equation (2-8) and simplifying,

the following equation is obtained:

$$\hat{\mathbf{z}} = \begin{bmatrix} 3.0864e-5 & -3.0864e-5 & -3.0864e-5 & 3.0864e-5 \\ -0.0050 & 0.0094 & 0.0072 & -0.0117 \\ 0.0500 & -0.1500 & 0.1500 & 0.9500 \end{bmatrix} \begin{bmatrix} L_{relative\_1} \\ L_{relative\_2} \\ L_{relative\_3} \\ L_{relative\_4} \end{bmatrix} \quad (2-21)$$

where the 3 by 4 matrix is  $\mathbf{T}$  of equation (2-8). The coefficients of the regression function are thus easily found by one matrix operation.

But there is a problem with this procedure: the polynomial function is found by assuming phase 1 at the largest angle and phase 4 the smallest, which is not always the situation. In order to find the right curve like parabola 1 or 2 in Fig. 2-2, it is necessary to try all the phase order combinations. Therefore the matrix operation of equation (2-21) has to be done four times with each phase assigned with the largest angle once. This assignment is achieved by circular shifting the relative inductance vector  $\mathbf{y}$  in equation (2-21). So for example if now phase 2 is assumed to be at the largest angle,  $\mathbf{y}$  becomes:

$$\mathbf{y} = \begin{bmatrix} L_{relative\_2} \\ L_{relative\_3} \\ L_{relative\_4} \\ L_{relative\_1} \end{bmatrix} \quad (2-22)$$

and  $\mathbf{D}$  becomes:

$$\mathbf{D} = \begin{bmatrix} \theta_{2e}^2 & \theta_{2e} & 1 \\ \theta_{3e}^2 & \theta_{3e} & 1 \\ \theta_{4e}^2 & \theta_{4e} & 1 \\ \theta_{1e}^2 & \theta_{1e} & 1 \end{bmatrix} \quad (2-23)$$

Notice that although the variables in the  $\mathbf{D}$  matrix have changed, their values remain

the same and therefore matrix  $\mathbf{T}$  does not need to be recalculated.

Now the coefficients of the new regression function are found by recalculating equation (2-21) with the new  $\mathbf{y}$  vector. This operation is repeated until every phase has been assigned with the largest assumed angle, and thus four regression polynomials with one for each phase-ordering are found. The *rms* residuals, vertex positions and concavities of the four functions are then calculated. A candidate function for estimation that resembles parabola 1 or 2 must have its vertex located between the two phases in the middle, which means between  $90^\circ$  and  $180^\circ$  with our angle assumption. This is because there must be at least one phase on any side of the fully aligned position or the fully unaligned position in one period of the inductance profile. Even if a different angle assumption was made for the  $\mathbf{D}$  matrix, the vertex will still lie between the positions of the two phases in the middle. Therefore the choice of the assumed angle values only affects the boundary angle values for choosing the right curve. The polynomial with the smallest *rms* residuals is also preferred, although not strictly required, for the estimation, as its form would resemble best to the relative inductance profile it is trying to fit.

The root of the derivative of the found polynomial would then locate the maximum of parabola 1 (thus the fully aligned position) or the minimum of parabola 2 (the fully unaligned position) in Fig. 2–2, depending on the concavity of the curve found. For an inductance profile with  $0^\circ$  defined as the fully unaligned position (thus  $180^\circ$  as the fully aligned position), the root represents the phase shift from  $0^\circ$  or  $180^\circ$ . Therefore the assumed phase positions can be shifted accordingly to find the real positions. The estimated electrical positions for the phases are then simply:

$$\hat{\theta}_{ne} = \theta_{ne} + 180^\circ - \theta_r \quad (2-24)$$

if the regression function which concaves downward is used for fitting

or

$$\hat{\theta}_{ne} = \theta_{ne} - \theta_r \quad (2-25)$$

if the regression function which concaves upward is used for fitting

where  $\theta_r$  represents the root of the function derivative(i.e. the electrical position of the vertex). Other co-ordinate systems with the unaligned position defined as other than  $0^\circ$  can be accommodated by proper shifting. The mechanical angle is then given by dividing the electrical angle by the number of rotor poles:

$$\hat{\theta}_{nm} = \frac{\hat{\theta}_{ne}}{N_R} \quad (2-26)$$

Therefore the mechanical positions for all four phases are found. This method will be called the Linear Quadratic Regression Position Estimation Method(LQRPEM). An example in the next section will illustrate the method.

### 2.3 Illustration of LQRPEM

In the last section the LQRPEM to estimate startup phase positions was described. In this section an example based on simulation of a motor with known magnetic characteristic will illustrate the method. The characteristic of the motor chosen is as follows:

TABLE 2-1  
SIMULATION MOTOR PARAMETERS

Parameter	Value
Maximum output power	3kW
Maximum speed	1500 rpm
Number of phases	4
Number of stator poles	8
Number of rotor poles	6
Aligned Inductance	0.0838H
Unaligned Inductance	0.0063H
Phase resistance	0.192 ohm

The positions chosen to be estimated are 150°, 60°, 330°, 240° for phase 1 through phase 4, respectively. Using Matlab for the simulation and applying volt-seconds of 0.01Vs, we obtain a corresponding current of 0.1332A, 0.5408A, 1.4706A, and 0.1709A. By taking the inverse of the current, the relative inductances are found. Substituting the values into  $\mathbf{y}$  of equation (2-21), it becomes:

$$\hat{\mathbf{z}} = \begin{bmatrix} 3.0864e-5 & -3.0864e-5 & -3.0864e-5 & 3.0864e-5 \\ -0.0050 & 0.0094 & 0.0072 & -0.0117 \\ 0.0500 & -0.1500 & 0.1500 & 0.9500 \end{bmatrix} \begin{bmatrix} 7.5075 \\ 1.8491 \\ 0.6800 \\ 5.8514 \end{bmatrix} \quad (2-27)$$

The coefficients for the regression function assuming phase 1 at 270° are thus found. As mentioned in Section 2.2, the other functions' parameters with different angle orderings are found by circular shifting the  $\mathbf{y}$  vector and redoing the multiplication in (2-21). Their *rms* residuals, derivatives' roots and concavities are subsequently calculated. The final results are shown in Fig. 2-3.

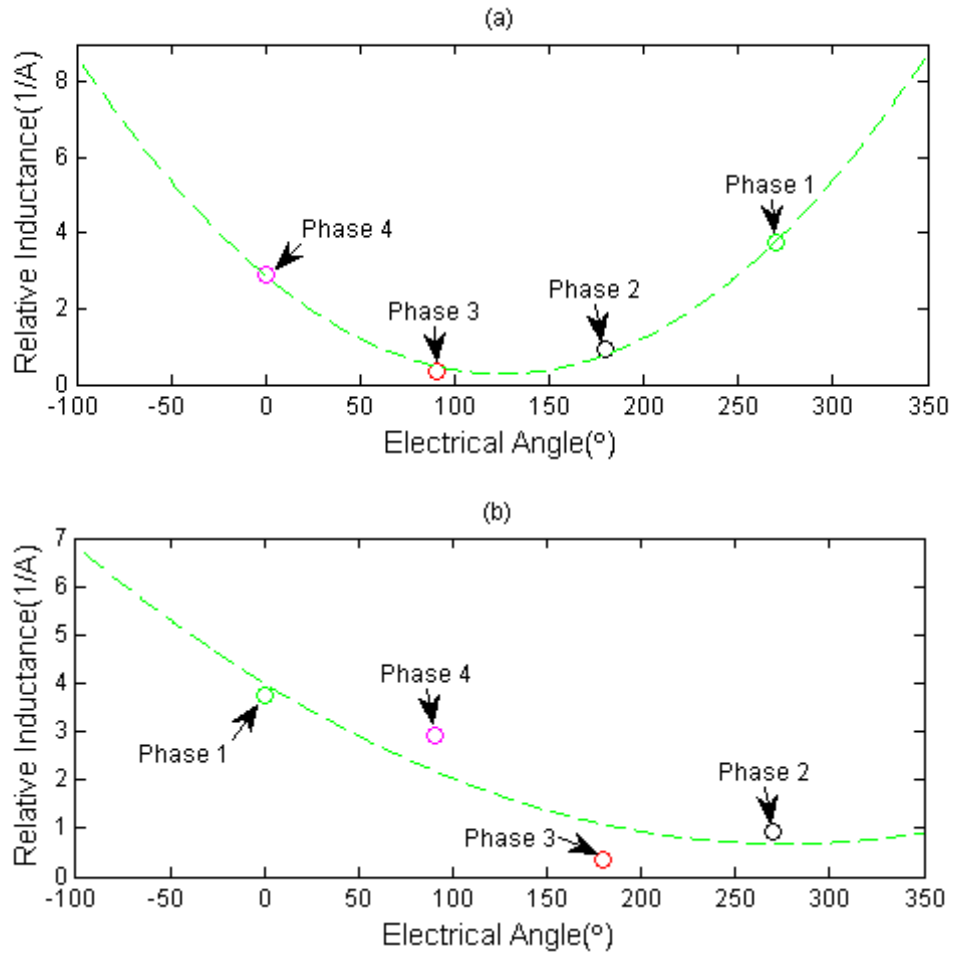
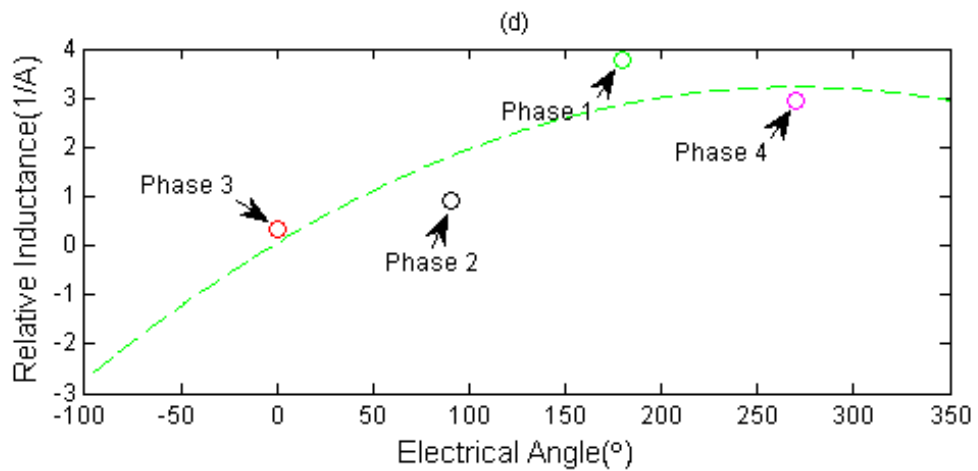
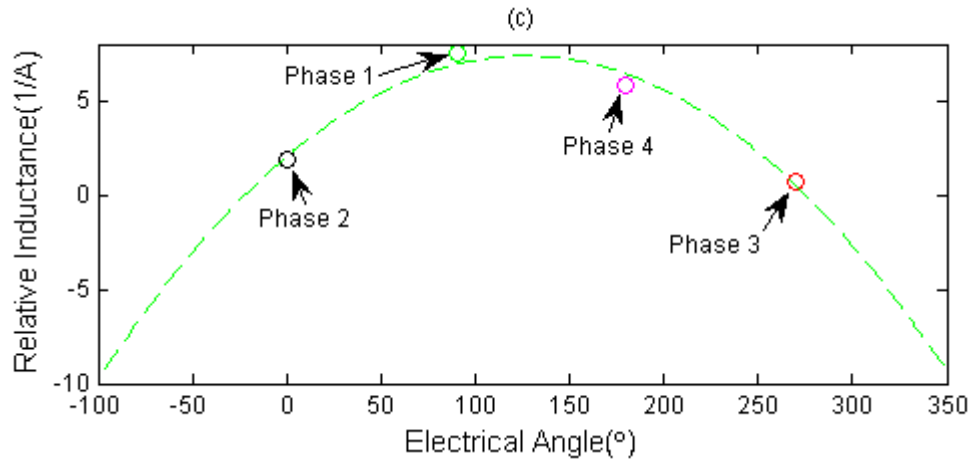


Fig. 2-3 Results from polynomial regression.

a)Phase 1 assumed at  $270^\circ$ .  $\hat{a}_2=0.000334$ ,  $\hat{a}_1=-0.083415$ ,  $\hat{a}_0=5.757846$ , *rms* residuals= $0.413836^\circ$ , function minimum at angle= $124.80^\circ$

b)Phase 2 assumed at  $270^\circ$ .  $\hat{a}_2=0.000087$ ,  $\hat{a}_1=-0.048152$ ,  $\hat{a}_0=7.999665$ , *rms* residuals= $2.203262^\circ$ , function minimum at angle= $276.06^\circ$





(Cont.)Fig. 2-3 Results from polynomial regression.

c)Phase 3 assumed at  $270^\circ$ .  $\hat{a}_2=-0.000334$ ,  $\hat{a}_1=0.084498$ ,  $\hat{a}_0=2.039142$ ,  $rms$  residuals= $0.849871^\circ$ , function maximum at angle= $126.42^\circ$

d)Phase 4 assumed at  $270^\circ$ .  $\hat{a}_2=-0.000087$ ,  $\hat{a}_1=0.047069$ ,  $\hat{a}_0=0.089824$ ,  $rms$  residuals= $2.639296^\circ$ , function maximum at angle= $269.85^\circ$

It is suggested in the last section that the regression function with the smallest *rms* residuals is preferred for the estimation, but it is not the only choice. As long as the function has a minimum or maximum between the angle of  $90^\circ$  and  $180^\circ$ , it could be used for the estimation. In fact for each set of relative inductances two curves like parabola 1 and parabola 2 of Fig. 2-2 will exist in all situations with one curve aligned with the fully aligned position and the other with the fully unaligned position. From Fig. 2-3 it could be seen that the curves of (a) and (c) are the right candidates

for the estimation, since curve (a) has a minimum at  $124.80^\circ$  and curve (c) has a maximum at  $126.42^\circ$ . If curve (a) is chosen, the root of its derivative is then the phase shift of the unaligned position. Otherwise if curve (c) is chosen, the root would then be the phase shift of the fully aligned position. The concavities of the candidate functions are used to determine if the vertex is a maximum or minimum and thus deciding whether the root is the phase shift of the aligned or unaligned position.

Therefore if curve (a) is chosen, the estimated angles could be calculated using equation (2-25):

$$\begin{bmatrix} \hat{\theta}_{1e} \\ \hat{\theta}_{2e} \\ \hat{\theta}_{3e} \\ \hat{\theta}_{4e} \end{bmatrix} = \begin{bmatrix} 270^\circ \\ 180^\circ \\ 90^\circ \\ 0^\circ \end{bmatrix} - 124.8^\circ = \begin{bmatrix} 145.2^\circ \\ 55.2^\circ \\ -34.8^\circ \\ -124.8^\circ \end{bmatrix} \quad (2-28)$$

And by adjusting the angles to positive values, we have:

$$\begin{bmatrix} \hat{\theta}_{1e} \\ \hat{\theta}_{2e} \\ \hat{\theta}_{3e} \\ \hat{\theta}_{4e} \end{bmatrix} = \begin{bmatrix} 145.2^\circ \\ 55.2^\circ \\ 325.2^\circ \\ 235.2^\circ \end{bmatrix} \quad (2-29)$$

If curve (c) is chosen, the estimated angles are calculated using (2-24):

$$\begin{bmatrix} \hat{\theta}_{3e} \\ \hat{\theta}_{4e} \\ \hat{\theta}_{1e} \\ \hat{\theta}_{2e} \end{bmatrix} = \begin{bmatrix} 270^\circ \\ 180^\circ \\ 90^\circ \\ 0^\circ \end{bmatrix} + 180^\circ - 126.42^\circ = \begin{bmatrix} 323.58^\circ \\ 233.58^\circ \\ 143.58^\circ \\ 53.58^\circ \end{bmatrix} \quad (2-30)$$

Rearranging the order, (2-30) becomes:

$$\begin{bmatrix} \hat{\theta}_{1e} \\ \hat{\theta}_{2e} \\ \hat{\theta}_{3e} \\ \hat{\theta}_{4e} \end{bmatrix} = \begin{bmatrix} 143.58^\circ \\ 53.58^\circ \\ 323.58^\circ \\ 233.58^\circ \end{bmatrix} \quad (2-31)$$

Comparing with the actual angles chosen, both choices will give acceptable estimations. But the regression function with the smallest *rms* residuals should be used, the reason for that would be shown in the next section.

## 2.4 Simulation Results

The LQRPEM is simulated using data from 2 different motors with known magnetic characteristics. A lookup table that takes phase angle and flux linkage as input is created for each motor to supply the current information for the simulations. An arbitrary volt-seconds value of 0.01 is chosen. The method is tested on different angles for 2 periods starting from one aligned position of 30° mechanical in 0.1° increment. Angle estimations are done using both functions of opposite concavities. The results for phase 1 are shown in Fig. 2-4 through Fig. 2-7.

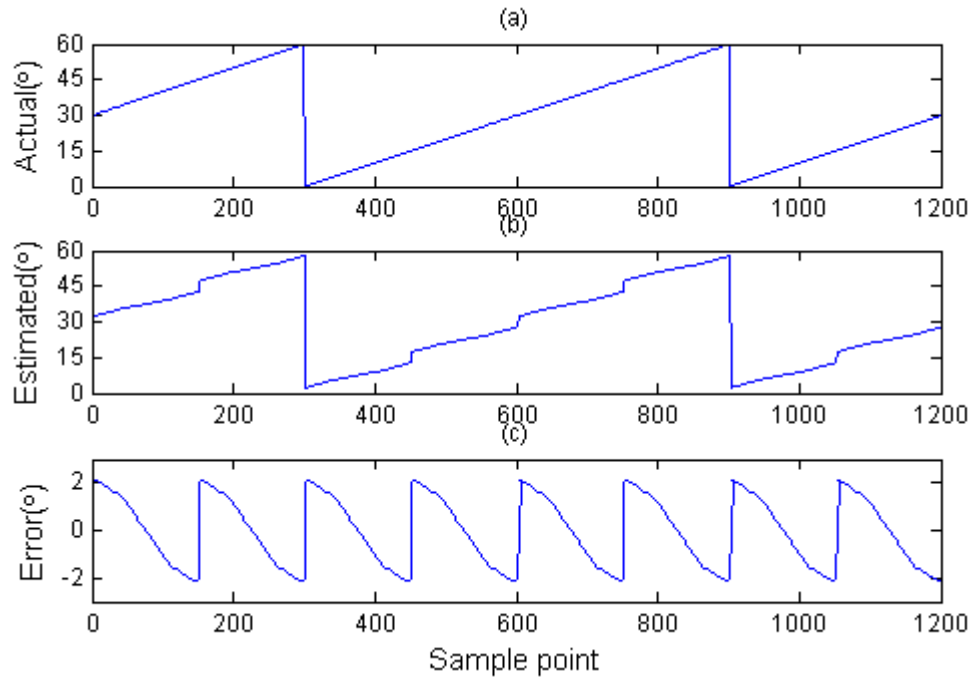


Fig. 2-4 Startup angle estimation simulation results of a 3kW four-phase 8/6 switched reluctance motor using LQRPEM and the function with negative concavity and larger *rms* residuals. a) Actual angle. b) Estimated angle c) Error in estimations

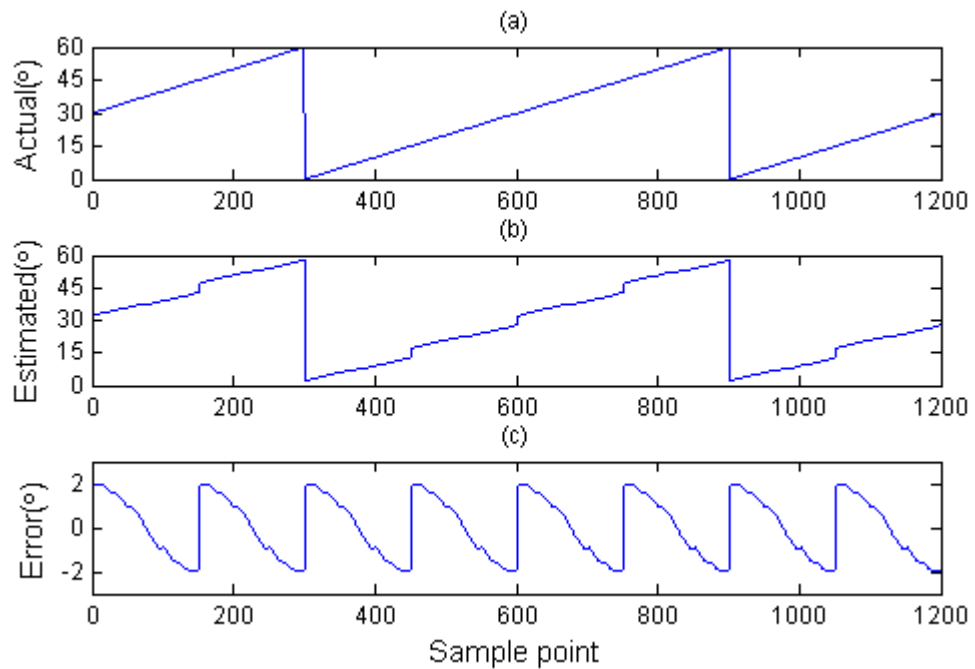


Fig. 2-5. Startup angle estimation simulation results of a 5kW four-phase 8/6 switched reluctance motor using LQRPEM and the function with negative concavity and larger *rms* residuals. a) Actual angle. b) Estimated angle c) Error in estimations

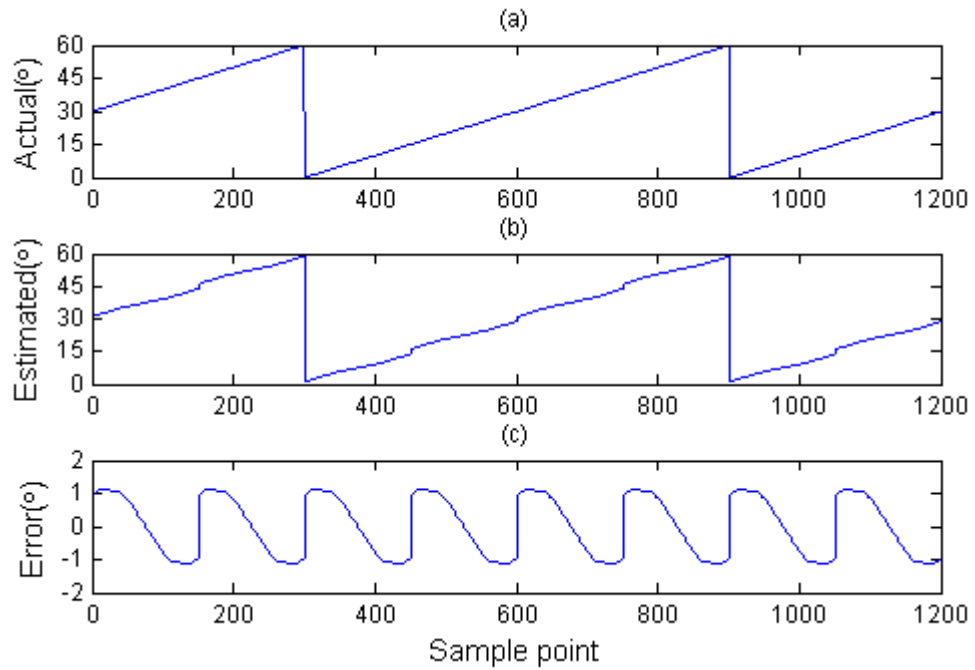


Fig. 2-6 Startup angle estimation simulation results of a 3kW four-phase 8/6 switched reluctance motor using LQRPEM and the function with positive concavity with smaller *rms* residuals. a) Actual positions. b) Estimated positions c) Error in estimations

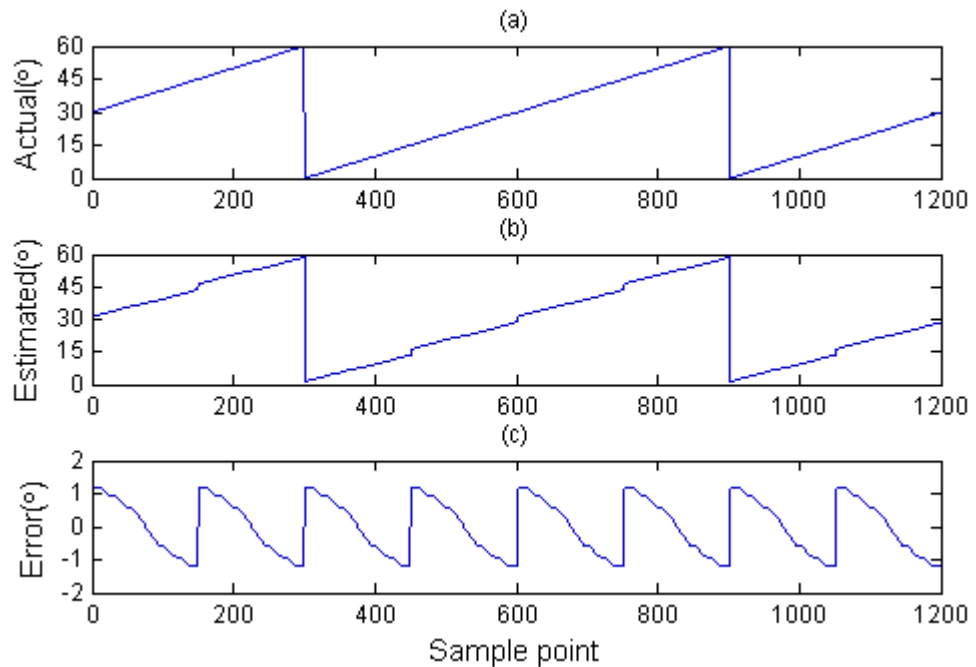


Fig. 2-7 Startup angle estimation simulation results of a 5kW four-phase 8/6 switched reluctance motor using LQRPEM and the function with positive concavity and smaller *rms* residuals. a) Actual positions. b) Estimated positions c) Error in estimations

It can be seen that the error profiles are periodic in  $15^\circ$  mechanical for all the

estimations. This is because the motor phases are  $15^\circ$  mechanical apart, and by using identical inductance profile for all the phases in the simulation the current data from the lookup table repeat every  $15^\circ$  mechanical. In real situation this would not be the case because the inductance profiles of different phases are not exactly equal. An abrupt change can also be observed at the same angle because for every  $15^\circ$  two phases change from one side of the profile to the other, and therefore the regression function used for the position estimations are changed at this same point. This condition creates such discontinuities.

For the two motor inductance profiles used it is observed that the functions with positive concavities always give smaller *rms* residuals than those with negative concavities, meaning they fit better to the data. It is believed that is due to the relatively flat valley close to the fully unaligned position in most SRM designs, and this valley has more resemblance to a parabola. Comparing Fig. 2–4 with Fig. 2–6 and Fig. 2–5 with Fig. 2–7 it can also be seen that curve-fits with smaller *rms* residuals give better estimations of the angles and reduce the magnitude of the step change at every  $15^\circ$ . Again this is contributed by the fact that a tighter fit follows the inductance profile better and at the same time introduces less abrupt changes at the end of a  $15^\circ$  period when the function used for the position estimations changes.

## **2.5 Hardware Descriptions**

### **2.5.1 System Setup**

The system schematic is shown in Fig. 2–8 and the setup shown in Fig. 2–9

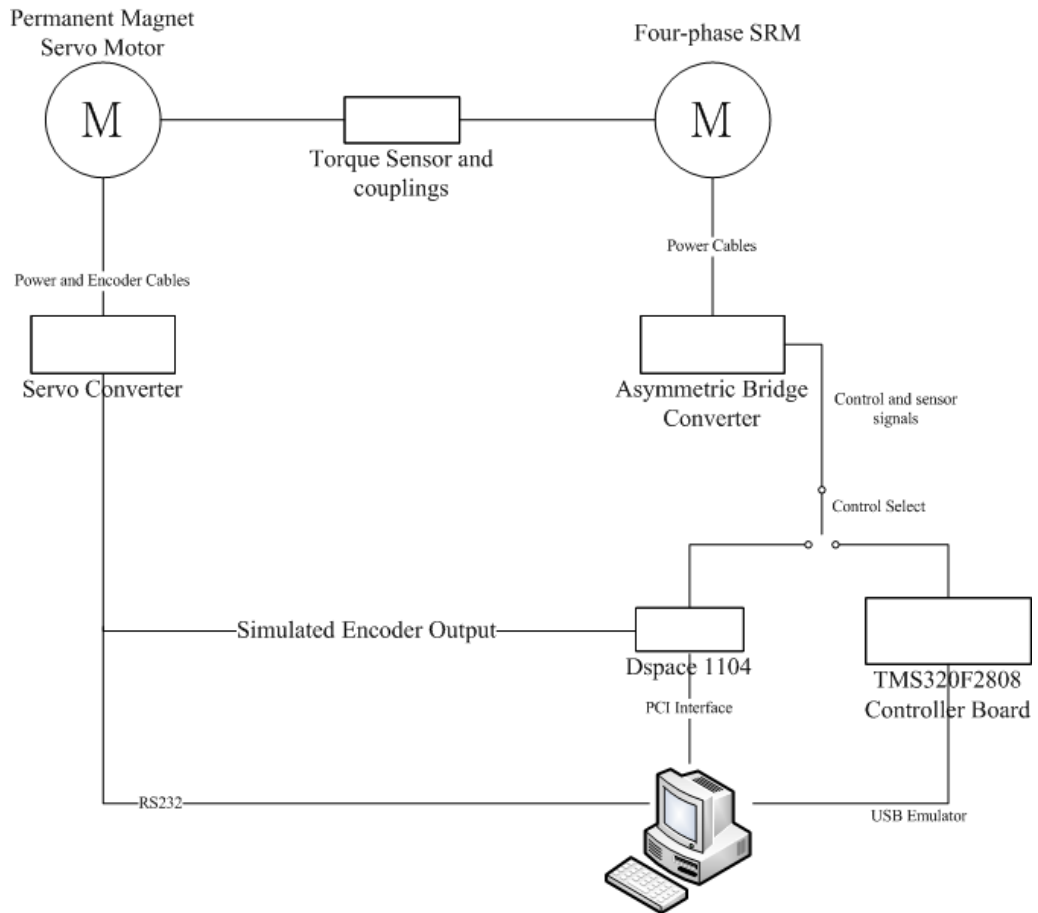


Fig. 2-8 System schematic of the experiment setup.

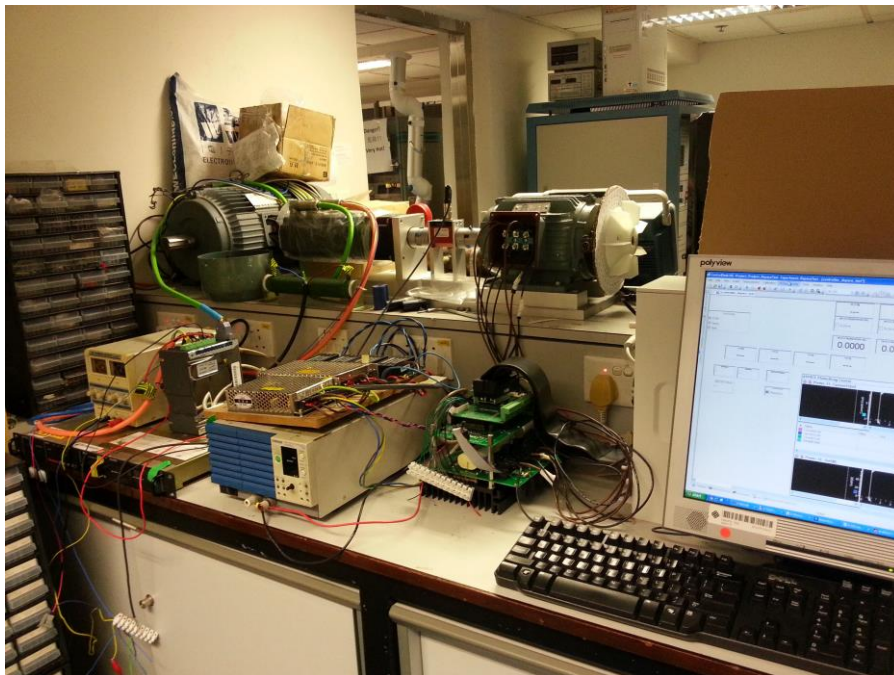


Fig. 2-9 Experiment setup

## 2.5.2 Converter

A conventional asymmetric bridge converter is used to drive the SRM. Each phase is equipped with a current sensor for control and position estimations. The schematic is shown in Fig. 2–10. Hysterisis current control and hard chopping conduction mode is used in the dynamic sensorless methods. For the static estimations, a DC bus voltage of 36V is used. For the dynamic algorithms the DC bus voltage is set to 65V. A higher voltage is used for the dynamic experiments such that a wider speed range can be achieved.

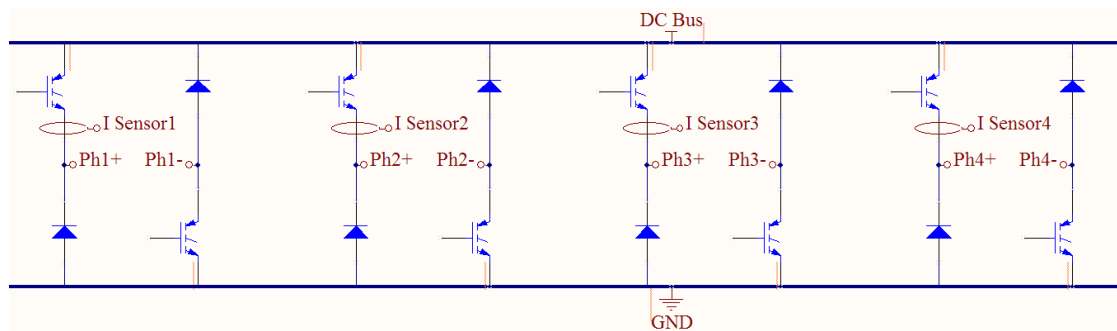


Fig. 2–10 Converter used for the experiments.

## 2.5.3 Motor

A four-phase 8/6 switched reluctance motor is used in the experiments. The nameplate power is 1.5kW. It is discovered that there is a defect in the inductance profile of Phase 2, which has a substantially lower aligned inductance than the others, as shown in Fig. 2–11 below:



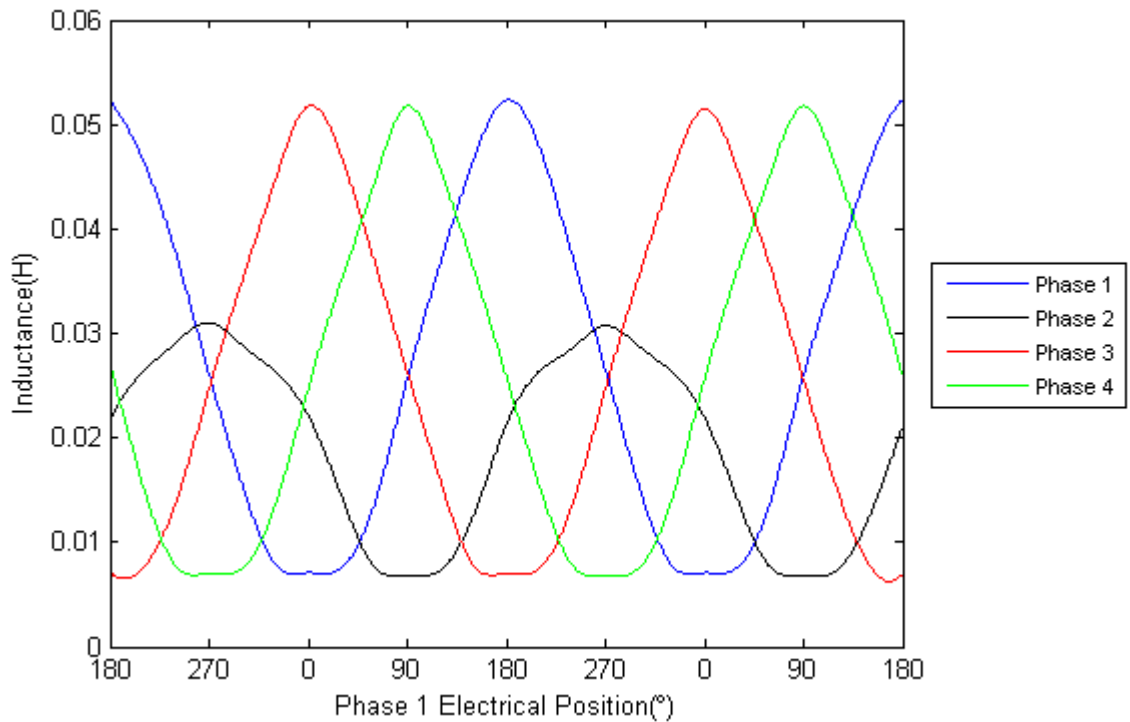


Fig. 2–11 Inductance profile for all phases for the two periods used in the experiments for static position estimation.

But this defect can serve to verify that even though the inductance profiles are not ideal, the algorithms to be introduced will still work satisfactorily.

### 2.5.4 Load

The load is provided by a permanent magnet servomotor connected to the SRM via couplings with a torque sensor in between. The position read from the servomotor's encoder is used as the position reference.

### 2.5.5 Control

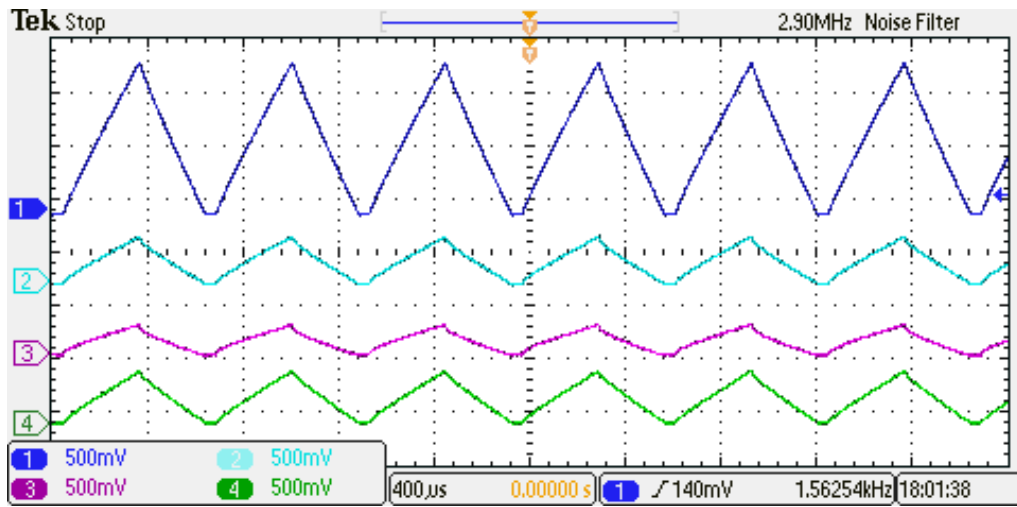
The voltage probing and current measuring control for the static position estimation algorithms is implemented on a TMS320F2808 DSP board running at 25kHz, and the position estimation is done offline in Matlab. The dynamic position estimation and

control algorithms introduced in Chapter 5 are implemented on the dSPACE DS1104 board running at a cycle time of  $60\mu\text{s}$ .

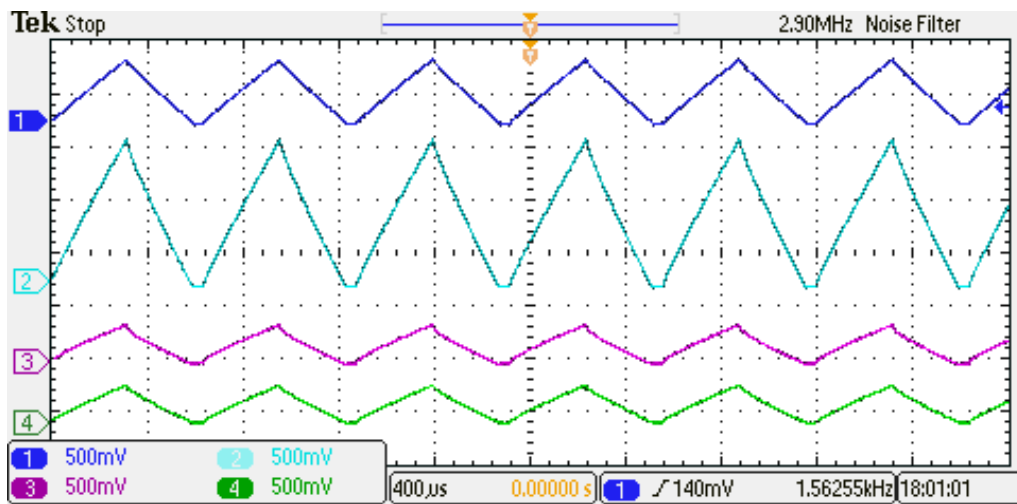
## 2.6 Experimental Results

To measure the currents a train of voltage pulses is applied to all phases simultaneously at each tested position. The motor phases are energized for about  $400\mu\text{s}$ , and then de-energized for an equal amount of time plus some delay. The delay is to make sure that the phases are fully demagnetized before the next pulse is applied. The volt-seconds add up to about  $0.0144\text{Vs}$  but this information is not needed. Note that the energizing time might not be exactly  $400\mu\text{s}$  as the voltage is applied such that the phases are turned off if any phase current reaches above  $1\text{A}$ . It is also ensured that a resultant current of about  $1.5\text{A}$  does not cause much saturation or induce a movement of the motor. The peak current is measured at turn off and the current probes produce  $1\text{V/A}$ . The measurement process is repeated at mechanical angles of  $2.5^\circ$  apart for  $120^\circ$  starting from a phase 1 aligned position, producing 48 current samples for each phase. The measurement results are tabularized in Table 2-2. The current waveforms are shown for all phases at phase 1's mechanical angles of  $0^\circ$ ,  $10^\circ$ ,  $30^\circ$  and  $50^\circ$  in Fig. 2-12. The results from the estimations are shown in Fig. 2-13. (11b) shows the results for estimation done using the regression function with the smallest *rms* residuals and (11c) with the function with opposite concavities and smallest *rms* residuals. Both give acceptable results but estimations using the smallest *rms* residuals functions have smaller errors in general. Estimations in (11b) have a mean absolute error of  $1.555^\circ$  and in (11c)  $2.112^\circ$  mechanical. The obtained results have thus verified that the developed LQRPEM can indeed provide a good estimation

of the rotor position.

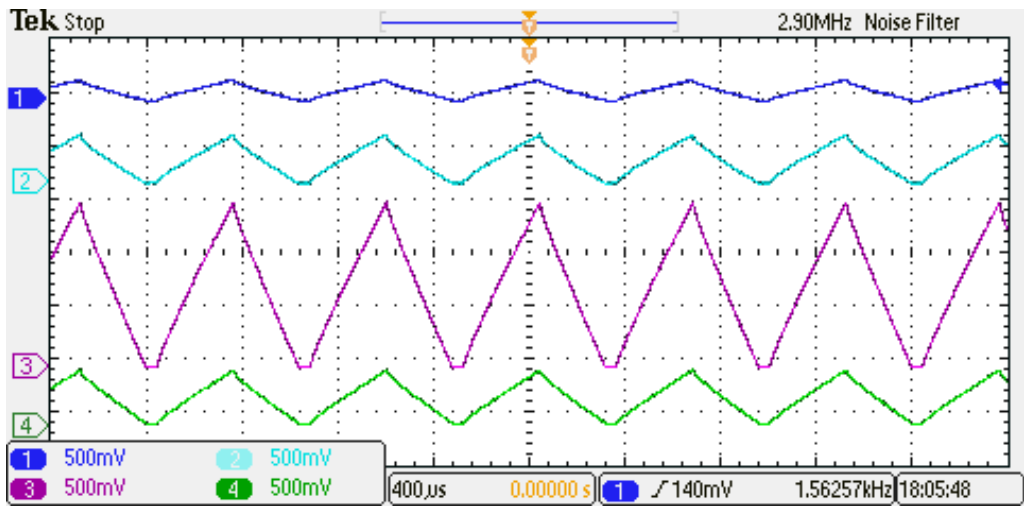


(a)

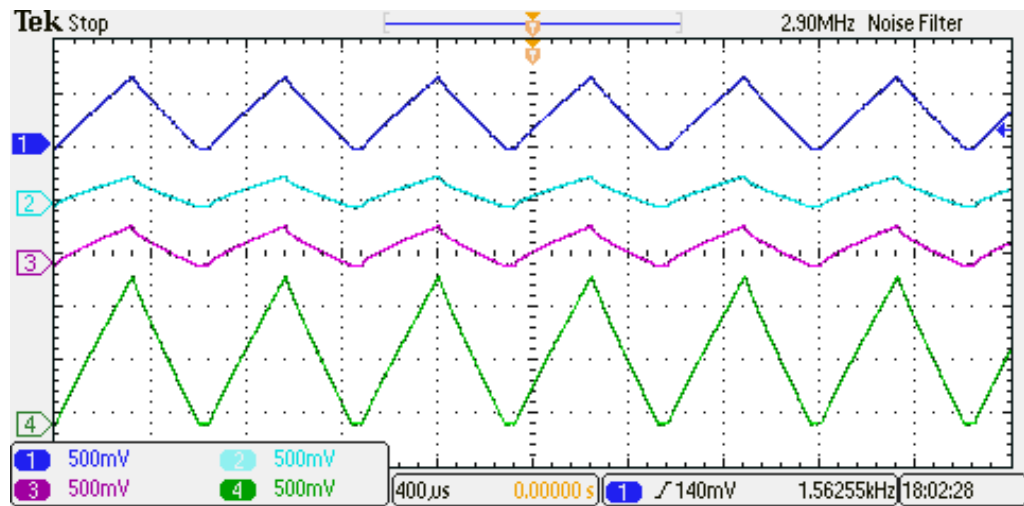


(b)

Fig. 2-12 Current waveforms for all phases at Phase 1 mechanical positions of a)0° b)10° c)30° d)50°. Trace 1,2,3,4 corresponds to Phase 1,2,3,4 respectively.



(c)



(d)

(Cont.)Fig. 2–12 Current waveforms for all phases at Phase 1 mechanical positions of a)0° b)10° c)30° d)50°. Trace 1,2,3,4 corresponds to Phase 1,2,3,4 respectively.

TABLE 2-2  
MEASURED PHASE CURRENTS AND ACTUAL PHASE 1 MECHANICAL POSITION

Phase 1 current(A)	Phase 2 current(A)	Phase 3 current(A)	Phase 4 current(A)	Actual phase 1 angle(deg)
0.184	0.42	1.44	0.5	30
0.22	0.42	1.56	0.62	32.5
0.24	0.38	1.44	0.82	35
0.26	0.34	1.18	1.24	37.5
0.3	0.3	0.82	1.44	40
0.34	0.28	0.62	1.54	42.5
0.42	0.28	0.52	1.54	45
0.52	0.3	0.46	1.52	47.5
0.74	0.32	0.4	1.42	50
1.16	0.34	0.38	1.14	52.5
1.36	0.36	0.34	0.76	55
1.44	0.4	0.32	0.62	57.5
1.46	0.48	0.32	0.5	0
1.42	0.58	0.32	0.46	2.5
1.3	0.78	0.34	0.44	5
1.06	1.16	0.36	0.4	7.5
0.68	1.42	0.38	0.38	10
0.5	1.52	0.44	0.36	12.5
0.38	1.56	0.52	0.34	15
0.32	1.54	0.62	0.36	17.5
0.26	1.42	0.84	0.38	20
0.24	1.22	1.2	0.4	22.5
0.22	0.78	1.46	0.42	25
0.22	0.62	1.56	0.44	27.5
0.2	0.48	1.6	0.5	30
0.22	0.42	1.56	0.6	32.5
0.24	0.38	1.46	0.78	35
0.26	0.34	1.2	1.2	37.5
0.3	0.32	0.82	1.44	40
0.34	0.3	0.64	1.52	42.5
0.4	0.28	0.52	1.54	45
0.5	0.28	0.46	1.52	47.5
0.7	0.3	0.4	1.42	50
1.1	0.32	0.38	1.2	52.5
1.34	0.36	0.34	0.78	55
1.42	0.4	0.32	0.62	57.5
1.44	0.48	0.3	0.5	0
1.4	0.58	0.32	0.46	2.5
1.28	0.8	0.34	0.42	5
0.98	1.24	0.36	0.4	7.5
0.64	1.46	0.4	0.38	10
0.48	1.56	0.44	0.36	12.5
0.36	1.58	0.52	0.34	15
0.32	1.54	0.64	0.36	17.5
0.26	1.4	0.9	0.38	20
0.24	1.06	1.32	0.42	22.5
0.22	0.72	1.52	0.44	25
0.22	0.58	1.58	0.46	27.5
0.2	0.46	1.58	0.52	30

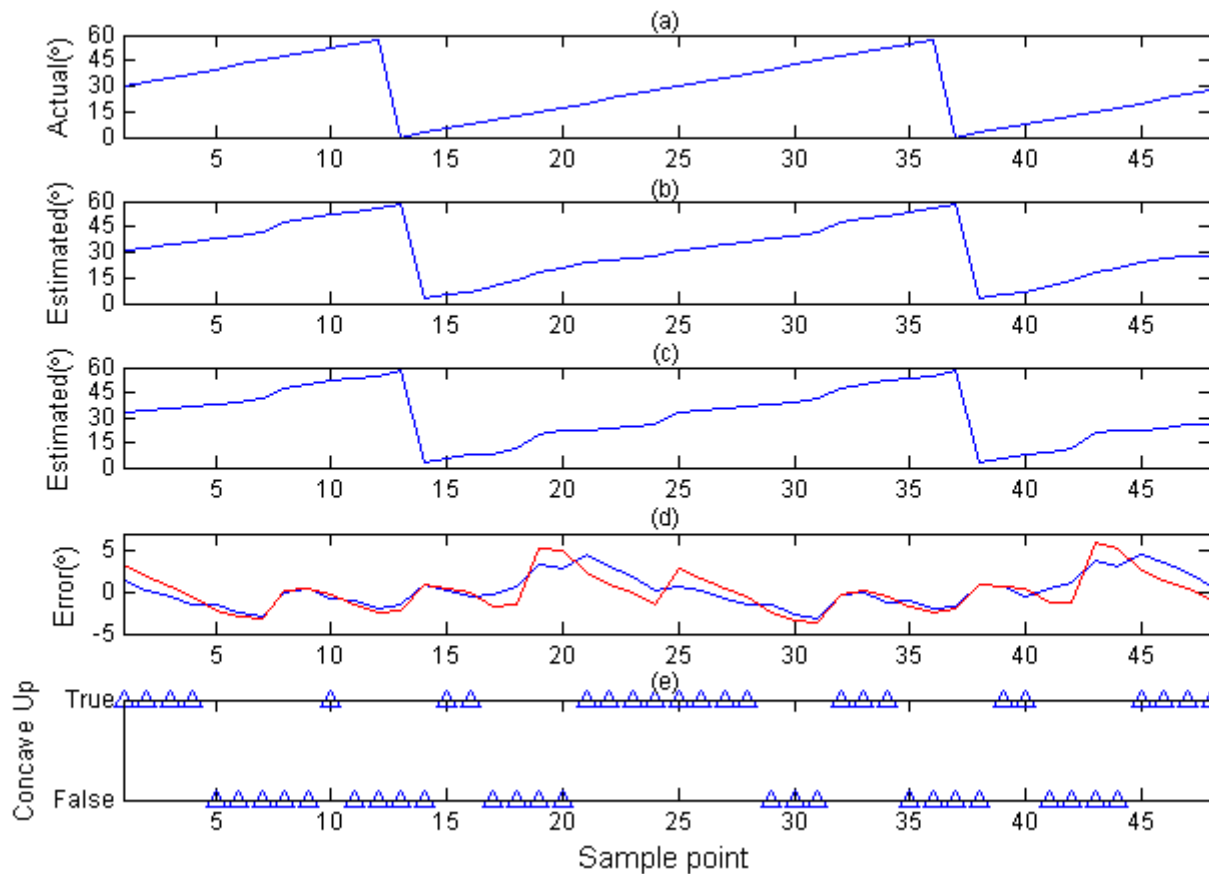


Fig. 2–13 Startup angle estimation experiment results of a 1.5kW four phase 8/6 switched reluctance motor using LQRPEM. a)Actual positions. b)Estimated positions using functions with smallest *rms* residuals c)Estimated positions using functions with the smallest *rms* residuals with opposite concavities as the functions in b). d)Error in estimations: blue curve – errors for b). red curve –errors for c). e)Concavity of the curve with the smallest *rms* residuals.

## 2.7 Summary

In this chapter the LQRPEM for sensorless starting of switched-reluctance motor has been developed. It is based on a polynomial model of the phase inductance profiles of the motor. The main feature is that no specific magnetic information is needed and no calculation of flux linkage or current gradients is necessary. Only current measurement is needed and hence the method is robust and can be easily adapted to any switched-reluctance motor. The calculations are straight forward that they only involve simple matrix and algebraic operations. The utilization of all four phases for the estimations also reduces errors introduced by individual phase. The validity of LQRPEM has been confirmed by both simulation and experiments. The error in the estimation of the position is very small with a mean absolute error of  $1.555^\circ$  in the experiment. It is therefore believed to be a promising method for sensorless driving of SRM.

## Chapter 3

# Position Estimation Using Type V Exponential Function

### 3.1 Introduction

In the last chapter a quadratic function is utilized to estimate the positions of the motor phases at startup. It provides acceptable results although a polynomial function does not follow the inductance profile closely. In this chapter we will investigate a new type of function that has more resemblance to the inductance profile and therefore provide even more accurate results.

### 3.2 Type V Exponential Function

A type V exponential function is described by V. Sit and M. Poulin-Costello for modeling data[59]. It will be used in this chapter to model the inductance profile. Again the function parameters will be found using regression analysis where linear least squares technique will be used to estimate the coefficients of the function.

A type V exponential function  $f(x)$  with one independent variable  $x$  takes the following form:

$$f(x) = ab^{(x-c)^2} \quad (3-1)$$

where parameter  $a$  controls the maximum or minimum value of the function,  $b$  the



concavity, and  $c$  the  $x$  co-ordinate of the vertex of  $f(x)$ . This function cannot be used directly in linear regression analysis and has to be linearly transformed into the following form:

$$\ln(f(x)) = a_2x^2 + a_1x^1 + a_0 \quad (3-2)$$

where

$$a = e^{(a_0 - \frac{a_1^2}{4a_2})} \quad (3-3)$$

$$b = e^{a_2} \quad (3-4)$$

$$c = \frac{-a_1}{2a_2} \quad (3-5)$$

Given a sequence of data  $y_1, y_2, \dots, y_L$ , taken at points  $x_1, x_2, \dots, x_L$ , it is desired to find the unknown coefficients  $a_n$  of the regression function to minimize the following sum of squared differences  $S_s$  :

$$S_s = \sum_{n=1}^L (\ln(y_n) - \ln(f(x)))^2 = \sum_{n=1}^L (\ln(y_n) - a_2x_n^2 - a_1x_n^1 - a_0)^2 \quad (3-6)$$

Note from equation (3-6) that instead of trying to find the least squares solution from the original data, it is proposed here to find the least squares solution from their

natural logarithm instead. This greatly simplifies the calculation and gives sufficient accuracy. To find the values of  $a_2$ ,  $a_1$ , and  $a_0$  the same  $\mathbf{D}$  and  $\mathbf{z}$  matrix (2-4) and (2-6) from the last chapter are used. But the  $\mathbf{y}$  vector now becomes:

$$\mathbf{y} = \begin{bmatrix} \ln(y_1) \\ \ln(y_2) \\ \bullet \\ \bullet \\ \bullet \\ \ln(y_L) \end{bmatrix} \quad (3-7)$$

Using the least squares solution equation (2-8), the following exponential function is found:

$$\hat{f}(x_n) = \hat{y}_n = e^{\hat{a}_2 x_n^2 + \hat{a}_1 x_n + \hat{a}_0} \quad (3-8)$$

Like the quadratic function from last chapter, type V exponential function also has a vertex, which can be found from its first derivative:

$$\hat{y}_n' = (2\hat{a}_2 x_n + \hat{a}_1) e^{\hat{a}_2 x_n^2 + \hat{a}_1 x_n + \hat{a}_0} \quad (3-9)$$

And its root is:

$$x_r = -\frac{\hat{a}_1}{2\hat{a}_2} \quad (3-10)$$

The concavity is again given by finding its second derivatives:

$$\hat{y}_n'' = (2\hat{a}_2 x_n + \hat{a}_1)^2 e^{\hat{a}_2 x_n^2 + \hat{a}_1 x_n + \hat{a}_0} + 2\hat{a}_2 e^{\hat{a}_2 x_n^2 + \hat{a}_1 x_n + \hat{a}_0} \quad (3-11)$$

and substituting with  $x_r$  :

$$\hat{y}_n'' = 2\hat{a}_2 e^{\frac{\hat{a}_1^2}{4\hat{a}_2} - \frac{\hat{a}_1^2}{2\hat{a}_2} + \hat{a}_0} \quad (3-12)$$

Therefore the polarity of coefficient  $\hat{a}_2$  determines the concavity of the regression function. It follows that  $\hat{y}_n$  at  $x_r$  is at the maximum if  $\hat{a}_2 < 0$  and minimum if  $\hat{a}_2 > 0$ .

It can also be observed that type V exponential function and quadratic function has the same equation for the root and the same concavity condition.

### 3.3 Method Derivation

In the last section the general form of the type V exponential function is presented. In this section the procedure of estimating the phase positions will be described. This procedure will be named the Linear Exponential Regression Position Estimation Method(LERPPEM). As was done for the derivation of LQRPEM in Chapter 2, in the proposed estimation function  $\hat{x}_n$  and  $\hat{y}_n$  in (3-8) are replaced by  $\theta_e$  and  $L_{relative}(\theta_e)$ :

$$L_{relative}(\theta_e) = e^{a_2\theta_e^2 + a_1\theta_e^1 + a_0} \quad (3-13)$$

Therefore the relative inductance is modeled as having an exponential relationship with  $\theta_e$ . Fig. 3–1 below shows two type V exponential curves together with two periods of the inductance profile.

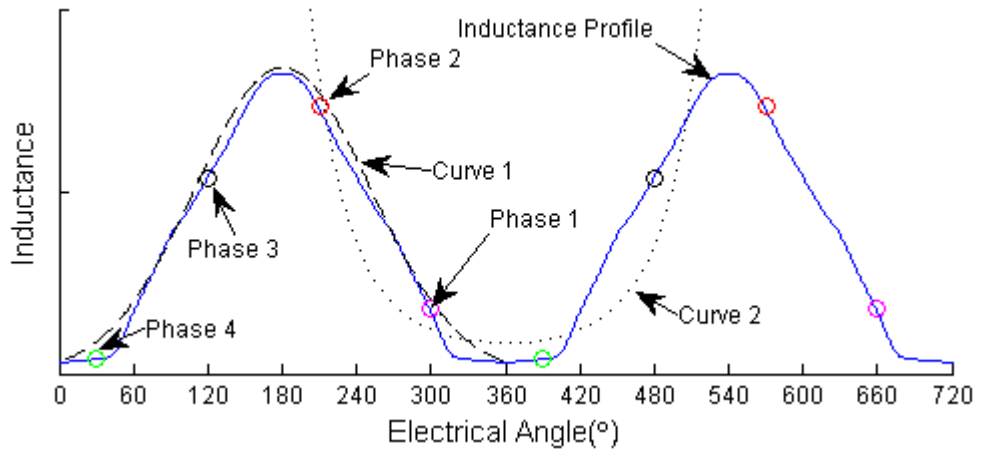


Fig. 3-1 Inductance of the phases repeated for 2 periods and superimposed with 2 Type V exponential functions

Curve 1 is a type V function that has a maximum vertex and curve 2 is another one with a minimum vertex. Unlike those of a polynomial function the two curves have very different shapes. Curve 1 is much more similar to the inductance profile whereas curve 2 looks like a parabola. For this reason it is therefore proposed that only curve 1 is used for the estimations. Later in the chapter examples will be given to illustrate this point.

The **D** matrix for solving for the coefficients are the same as in equation (2-19) of Chapter 2, restated here:

$$\mathbf{D} = \begin{bmatrix} 72900 & 270 & 1 \\ 32400 & 180 & 1 \\ 8100 & 90 & 1 \\ 0 & 0 & 1 \end{bmatrix} \quad (2-19)$$

But vector **y** is now:

$$\mathbf{y} = \begin{bmatrix} \ln(L_{relative\_1}) \\ \ln(L_{relative\_2}) \\ \ln(L_{relative\_3}) \\ \ln(L_{relative\_4}) \end{bmatrix} \quad (3-14)$$

Substituting  $\mathbf{D}$  and  $\mathbf{y}$  into the least squares solution equation (2-8), the coefficient vector  $\hat{\mathbf{z}}$  becomes:

$$\hat{\mathbf{z}} = \begin{bmatrix} 3.0864e-5 & -3.0864e-5 & -3.0864e-5 & 3.0864e-5 \\ -0.0050 & 0.0094 & 0.0072 & -0.0117 \\ 0.0500 & -0.1500 & 0.1500 & 0.9500 \end{bmatrix} \begin{bmatrix} \ln(L_{relative\_1}) \\ \ln(L_{relative\_2}) \\ \ln(L_{relative\_3}) \\ \ln(L_{relative\_4}) \end{bmatrix} \quad (3-15)$$

Similar to what was done with LQRPEM,  $\mathbf{y}$  has to be circular shifted to find the regression functions for all the angle combinations. The criteria to choose the correct function are also similar except that instead of using a regression function with the smallest *rms* residuals, the regression function with a maximum vertex as curve 1 in Fig. 3–1 is preferred as explained before. The procedure for finding the phase positions from the regression function is exactly the same as with LQRPEM. In the next section an example will be given to demonstrate the method.

### 3.4 An Example of LERPEM

In the last section the LERPEM is developed. This section will show an example of applying the method to estimate one arbitrary position. A motor as described by Table 2-1 is used. The angles chosen are  $36^\circ$ ,  $306^\circ$ ,  $216^\circ$ ,  $126^\circ$ , for Phase 1 through Phase 4, respectively. Through the same simulation steps as described in section 2.3, the corresponding currents are obtained as 1.1852A, 0.6461A, and 0.1396A, 0.1020A.

Following the procedure described in section 3.3, the four regression functions found are shown in Fig. 3–2.

Therefore the functions that can be used for position estimations are curve in Fig. 3–2b and Fig. 3–2c with their vertex positions between 90° and 180°. The estimated angles are then

$$\begin{bmatrix} \hat{\theta}_{1e} \\ \hat{\theta}_{2e} \\ \hat{\theta}_{3e} \\ \hat{\theta}_{4e} \end{bmatrix} = \begin{bmatrix} 34.94^\circ \\ 304.94^\circ \\ 214.94^\circ \\ 124.94^\circ \end{bmatrix} \quad (3-16)$$

For estimations using the curve in Fig. 3–2b, and

$$\begin{bmatrix} \hat{\theta}_{1e} \\ \hat{\theta}_{2e} \\ \hat{\theta}_{3e} \\ \hat{\theta}_{4e} \end{bmatrix} = \begin{bmatrix} 39.62^\circ \\ 309.62^\circ \\ 219.62^\circ \\ 129.62^\circ \end{bmatrix} \quad (3-17)$$

for estimations using the curve in Fig. 3–2c.

Comparing with the chosen phase angles, the curve of Fig. 3–2b gives more accurate estimations, which agrees with the hypothesis that the curve with a maximum vertex provides better results.

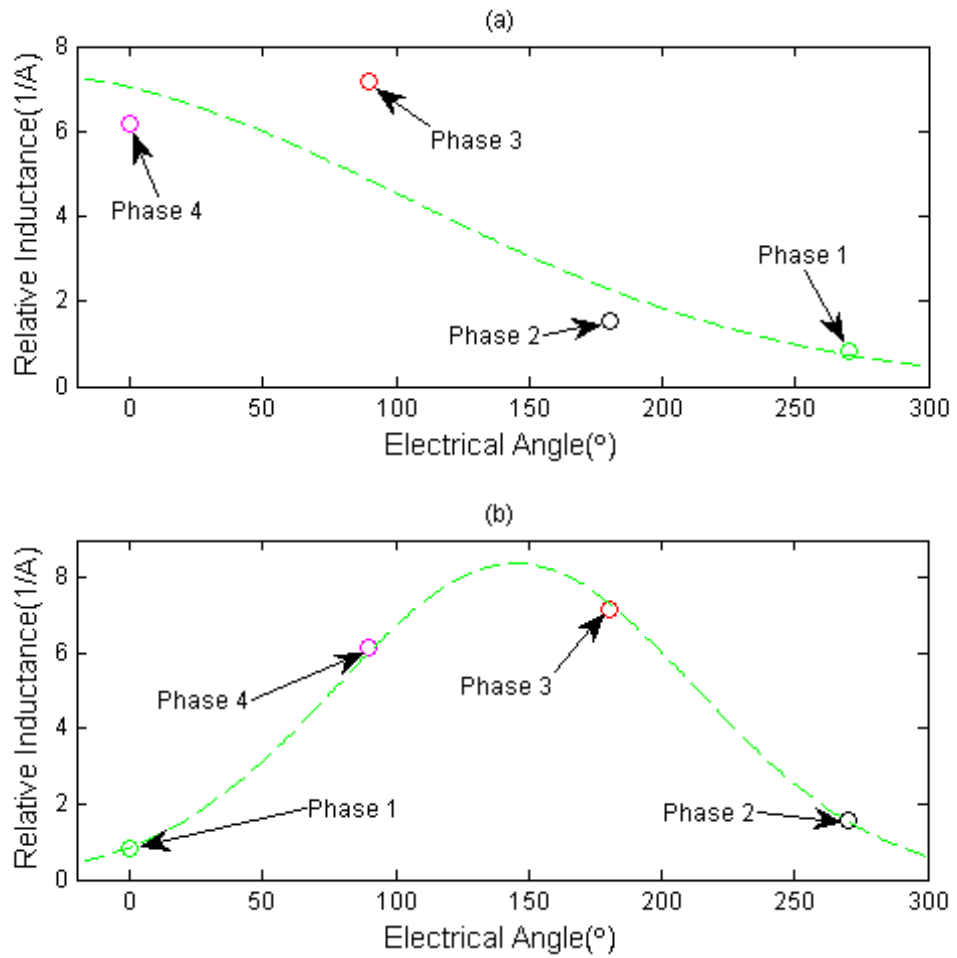
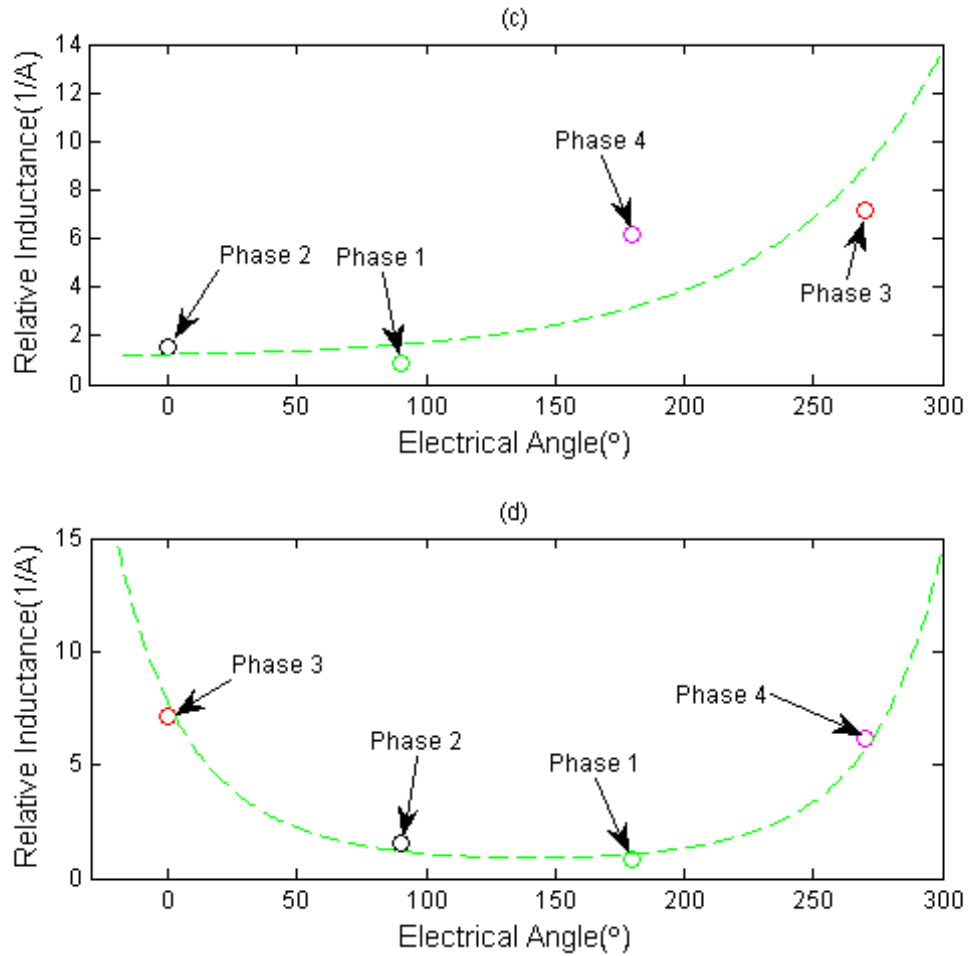


Fig. 3-2 Results from exponential regression.

a)Phase 1 assumed at 270°.  $\hat{a}_2=-0.000023$ ,  $\hat{a}_1=-0.002044$ ,  $\hat{a}_0=1.950714$ , *rms* residuals=2.581960°, maximum point at angle=-43.85°

b)Phase 2 assumed at 270°.  $\hat{a}_2=-0.000109$ ,  $\hat{a}_1=0.031540$ ,  $\hat{a}_0=-0.161798$ , *rms* residuals=0.229864°, maximum point at angle=145.06°



(Cont.)Fig. 3-2 Results from exponential regression.

c)Phase 3 assumed at 270°.  $\hat{a}_2=0.000023$ ,  $\hat{a}_1=0.001026$ ,  $\hat{a}_0=0.214877$ ,  $rms$  residuals=3.593118°, minimum point at angle=-22.00°

d)Phase 4 assumed at 270°.  $\hat{a}_2=0.000109$ ,  $\hat{a}_1=-0.030521$ ,  $\hat{a}_0=2.052427$ ,  $rms$  residuals=0.900348°, minimum point at angle=140.38°

### 3.5 Simulation Results

The same simulation as with LRPPEM is done with two motors as in Chapter 2, and the results are shown in Fig. 3-3 through Fig. 3-6:



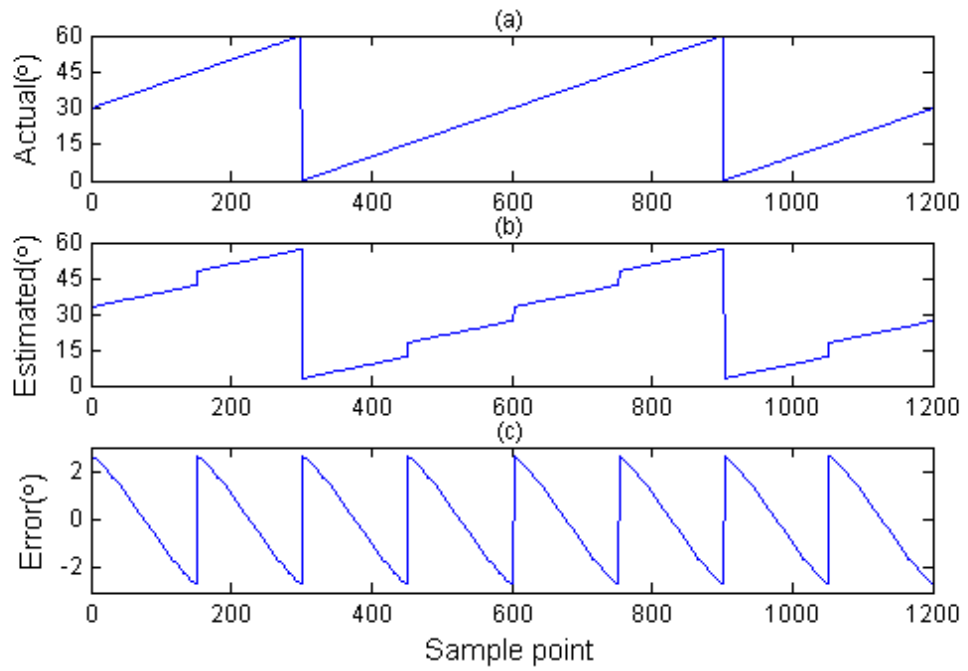


Fig. 3-3 Startup angle estimation simulation results of a 3kW four phase 8/6 switched reluctance motor using the curve with positive concavity. a) Actual angle. b) Estimated angle c) Error in estimation

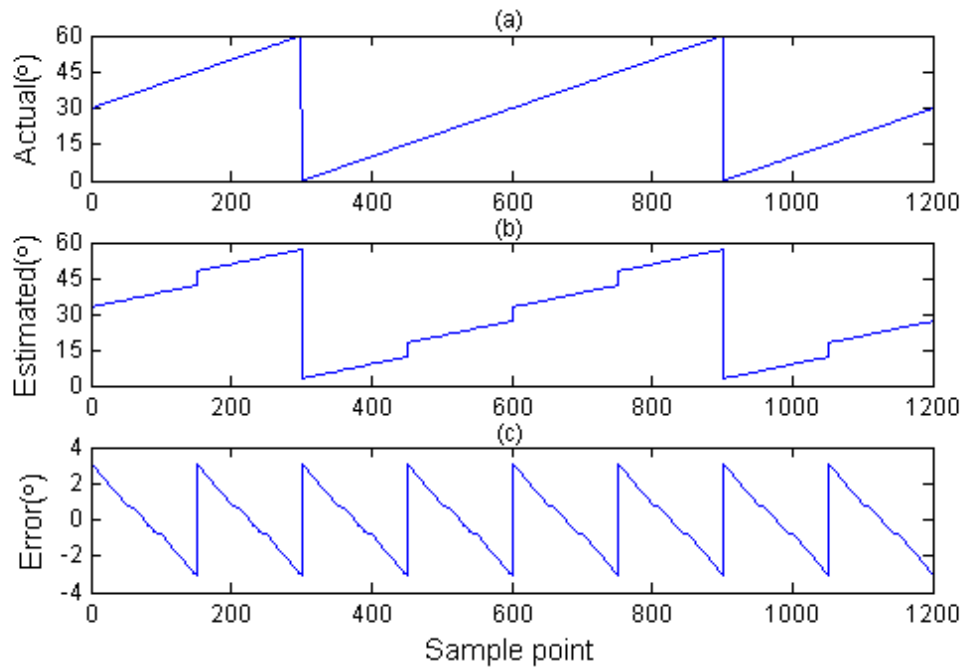


Fig. 3-4 Startup angle estimation simulation results of a 5kW four phase 8/6 switched reluctance motor using the curve with positive concavity. a) Actual angle. b) Estimated angle c) Error in estimations

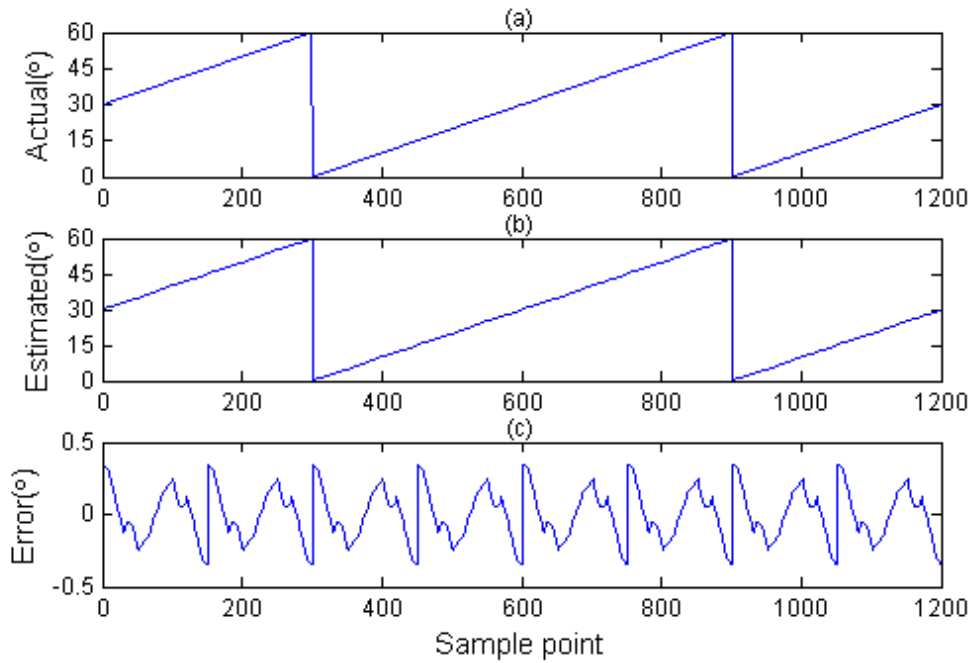


Fig. 3-5 Startup angle estimation simulation results of a 3kW four phase 8/6 switched reluctance motor using the preferred curve. a) Actual angle b) Estimated angle c) Error in estimation

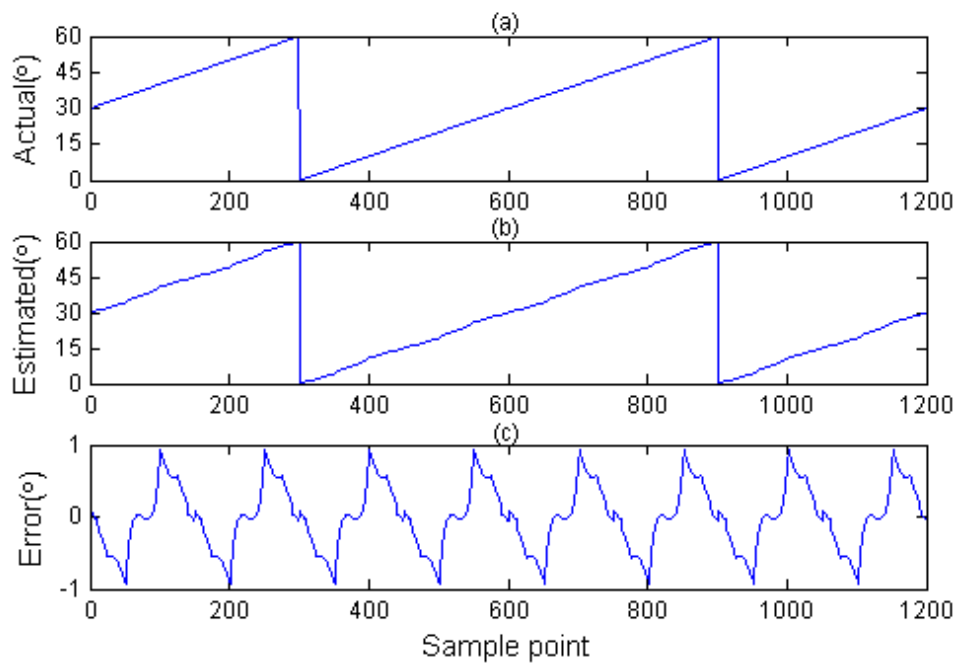


Fig. 3-6 Startup angle estimation simulation results of a 5kW four phase 8/6 switched reluctance motor using the preferred curve. a) Actual angle b) Estimated angle c) Error in estimations

Thus the simulation results further confirm that estimations done with the preferred regression function with a maximum vertex are more accurate. On the other hand the

results given by the function with a minimum vertex are similar to those given with a quadratic function, which is unsurprising due to the closeness in shape between the two curves.

To further compare the results, simulation is also performed using the inductance profile of phase 1 from the experimental 1.5kW motor. All other phases are assumed to have the same and symmetric inductance profile as phase 1. The results are shown in Fig. 3–7.

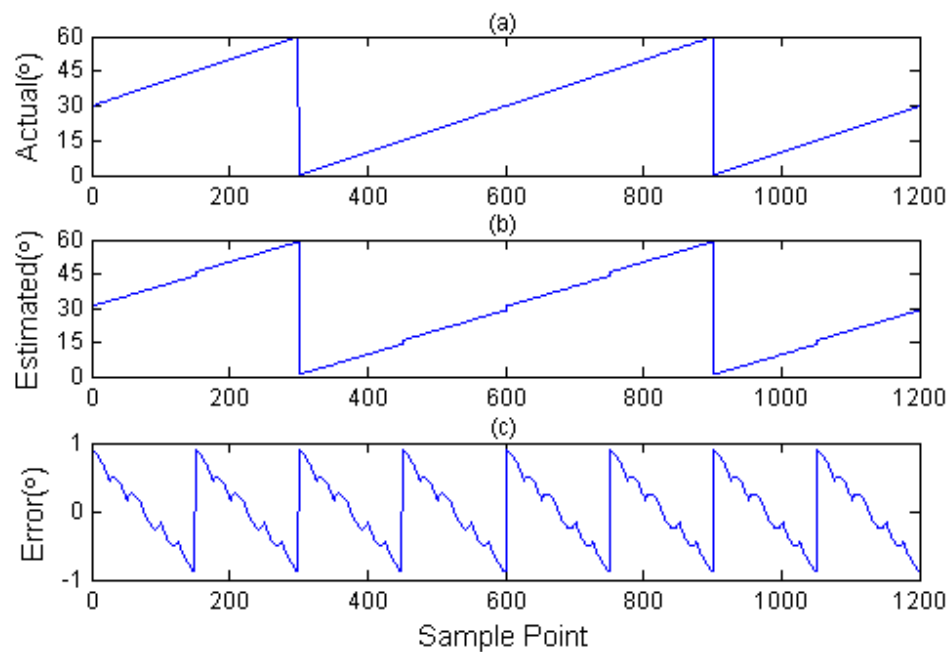


Fig. 3–7 Startup angle estimation simulation results of a 1.5kW four phase 8/6 switched reluctance motor using the preferred curve. a) Actual positions. b) Estimated positions c) Error in estimations.

It can be seen from the results that the estimation accuracies are not affected by the power ratings of the motors, as long as the phases are symmetric and balanced.

### 3.6 Experimental Results

Using the same data obtained with the experiment described in section 2.5, the developed LERPEM is used to estimate the phase positions with the preferred function. The final results are shown in Fig. 3–8.

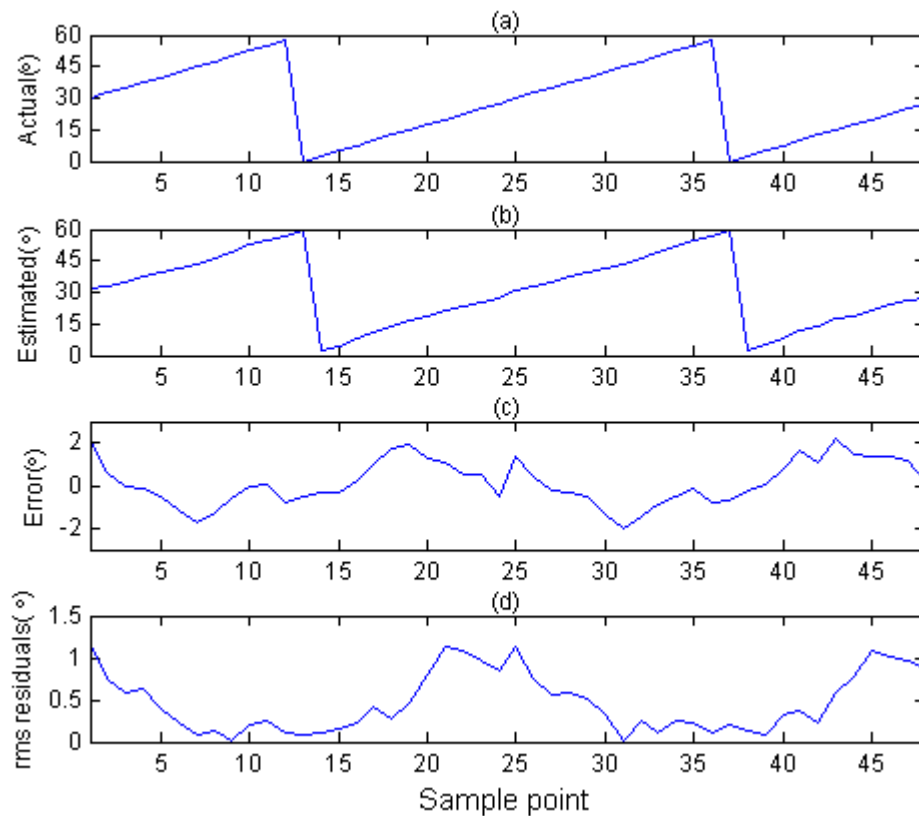


Fig. 3–8 Startup angle estimation experiment results of a 1.5kW four-phase 8/6 switched reluctance motor using LERPEM. a)Actual positions. b)Estimated positions c)Error in estimations d)rms residuals from the curve fit.

The positions estimated have a mean absolute error of  $0.88^\circ$  mechanical, and given the highly peculiar inductance profile of phase 2, the results therefore have shown that the LERPEM method can indeed provide very good estimates of the phase positions even without the assumption that all phases have the same inductance profile values.

### **3.7 Summary**

In this chapter LERPEM for sensorless starting of switched-reluctance motor is presented. A type V exponential function is used to model the inductance profile. This function is superior to the quadratic function of Chapter 2 that it resembles the inductance profile of an SRM more closely. The mean absolute error from the experiment is  $0.88^\circ$  mechanical. Compared with LQRPEM from Chapter 2 the LERPEM can provide more accurate estimates of the phase positions.

# **Chapter 4**

## **Position Estimation Using Co-sinusoidal function**

### **4.1 Introduction**

In Chapter 2 and Chapter 3 two different methods were developed to estimate the phase positions of a four-phase SRM through finding the vertex positions of the inductance modeling functions. Although they give accurate information for the positions, one drawback is that the correct angle order that fits the profile has to be found first and several calculations and comparisons have to be done before being able to make the final estimations. In this chapter we are going to investigate a new model where the trial and error process can be eliminated and thus providing a simpler algorithm for finding the phase positions.

### **4.2 Co-sinusoidal Regression Model**

#### **4.2.1 IEEE Standard 1057**

In this chapter a co-sinusoidal function for fitting the inductance profile will be investigated. The function analysis are based on content from The IEEE Standard

1057 which was originally developed by an IEEE committee to provide common terminology and test methods for describing the performance of waveform recorders[60, 61]. It was approved by the IEEE Standards Board on June 14, 1994 and revised in 2007. An important aspect of this standard is the use of sine wave signal and fitting algorithms to evaluate the performance of the recorders. Several algorithms for sine wave fitting based on the least square method were presented in [61] and the three parameter(known frequency) least squares fit to sine wave data using matrix operations will be adopted here in developing the regression model.

#### 4.2.2 Cosine Regression Function

A co-sinusoidal curve superimposed on two inductance periods is shown in Fig. 4–1.

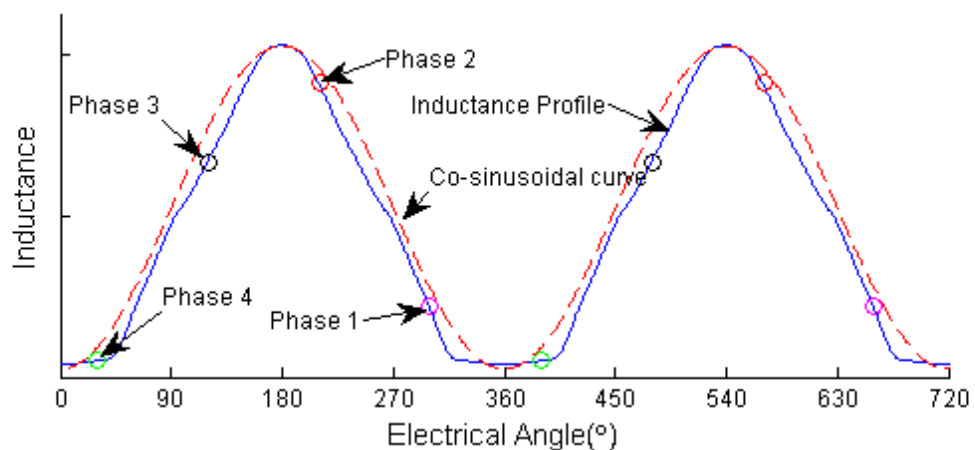


Fig. 4–1 Inductance of the phases repeated for 2 periods and superimposed with one co-sinusoidal function.

Unlike the quadratic and the exponential functions that each requires two curves of different concavities to model the inductance correctly, one co-sinusoidal function can model the inductance profile indefinitely. As can be observed in Fig. 4–1 the function can be considered as a 180° shifted cosine function with a DC offset. Therefore the modeling function to be used is defined as the following:

$$L_{relative\_n} = M \cos(\theta_{ne} + \phi) + C \quad (4-1)$$

where  $L_{relative\_n}$  represents the relative inductance of phase n,  $M$  the amplitude,  $\theta_{ne}$  the phase n's electrical position,  $\phi$  the phase shift, and  $C$  the offset. Like the quadratic or type V exponential function this function is not linear in parameter and therefore cannot be solved directly with linear least squares method. This problem is solved by transforming (4-1) into linear form using trigonometric identities:

$$L_{relative\_n} = A \cos(\theta_{ne}) + B \sin(\theta_{ne}) + C \quad (4-2)$$

where

$$M = \sqrt{A^2 + B^2} \quad (4-3)$$

$$\phi = \tan^{-1}\left(\frac{-B}{A}\right) \quad \text{for } A \geq 0 \quad (4-4)$$

$$\phi = \tan^{-1}\left(\frac{-B}{A}\right) + \pi \quad \text{for } A < 0 \quad (4-5)$$

The special condition for the inverse tangent is to ensure that  $\phi$  falls into the correct



quadrant.

### 4.2.3 Method Derivation

Now that the regression function is defined, its coefficients A, B and C can be found with the least squares method described in Chapter 2 and Chapter 3, with the following modifications to the regression matrix **D**:

$$\mathbf{D} = \begin{bmatrix} \cos(\theta_{1e}) & \sin(\theta_{1e}) & 1 \\ \cos(\theta_{2e}) & \sin(\theta_{2e}) & 1 \\ \cos(\theta_{3e}) & \sin(\theta_{3e}) & 1 \\ \cos(\theta_{4e}) & \sin(\theta_{4e}) & 1 \end{bmatrix} \quad (4-6)$$

The sample vector **y** remains the same as the relative inductance of the phases, as:

$$\mathbf{y} = \begin{bmatrix} L_{relative\_1} \\ L_{relative\_2} \\ L_{relative\_3} \\ L_{relative\_4} \end{bmatrix} \quad (4-7)$$

And the coefficient vector **z** as:

$$\mathbf{z} = \begin{bmatrix} A \\ B \\ C \end{bmatrix} \quad (4-8)$$

With the same angle assignments as before, the **D** matrix becomes:

$$\mathbf{D} = \begin{bmatrix} \cos(270) & \sin(270) & 1 \\ \cos(180) & \sin(180) & 1 \\ \cos(90) & \sin(90) & 1 \\ \cos(0) & \sin(0) & 1 \end{bmatrix} \quad (4-9)$$

which simplifies to:

$$\mathbf{D} = \begin{bmatrix} 0 & -1 & 1 \\ -1 & 0 & 1 \\ 0 & 1 & 1 \\ 1 & 0 & 1 \end{bmatrix} \quad (4-10)$$

Substituting this  $\mathbf{D}$  matrix and the  $\mathbf{y}$  vector into the least squares solution equation

(2-8), the solution coefficient vector  $\hat{\mathbf{z}}$  is obtained as:

$$\hat{\mathbf{z}} = \begin{bmatrix} 0 & -0.5 & 0 & 0.5 \\ -0.5 & 0 & 0.5 & 0 \\ 0.25 & 0.25 & 0.25 & 0.25 \end{bmatrix} \begin{bmatrix} L_{relative\_1} \\ L_{relative\_2} \\ L_{relative\_3} \\ L_{relative\_4} \end{bmatrix} \quad (4-11)$$

The  $\hat{\phantom{x}}$  superscript indicates a least squares solution quantity. The coefficients  $\hat{A}$ ,  $\hat{B}$ ,  $\hat{C}$  are thus found. Using these coefficients, the amplitude  $\hat{M}$ , phase shift  $\hat{\phi}$  and bias  $\hat{C}$  of the cosine expression (4-1) can be found using equations (4-3) through (4-5).

To determine the position of each phase it is only needed the value of the phase shift angle  $\hat{\phi}$ .  $\hat{M}$  and  $\hat{C}$  could give us an approximation of the aligned and unaligned inductances if the value of the volt-seconds applied is provided, but the accuracy is limited. The estimated electrical position is then simply:

$$\hat{\theta}_{ne} = \theta_{ne} - 180^\circ + \phi \quad (4-12)$$

If  $\hat{\theta}_{ne} < 0^\circ$  or  $> 360^\circ$ , it is needed to be wrapped around to fall between  $0^\circ$  and  $360^\circ$ .

The  $180^\circ$  degree adjustment in (4-12) is needed to transform the angles to the co-ordinate system of our inductance profile, which is a  $180^\circ$  shifted cosine curve. Other co-ordinate systems can easily be accommodated by proper shifting. The development of this method is completed and we will call it the Linear Sinusoidal Regression Position Estimation Method(LSRPEM).

### **4.3 Simulation Results**

The simulated results from applying LSRPEM to the same two motors as in Chapter 2 and Chapter 3 are shown below in Fig. 4–2 and Fig. 4–3.

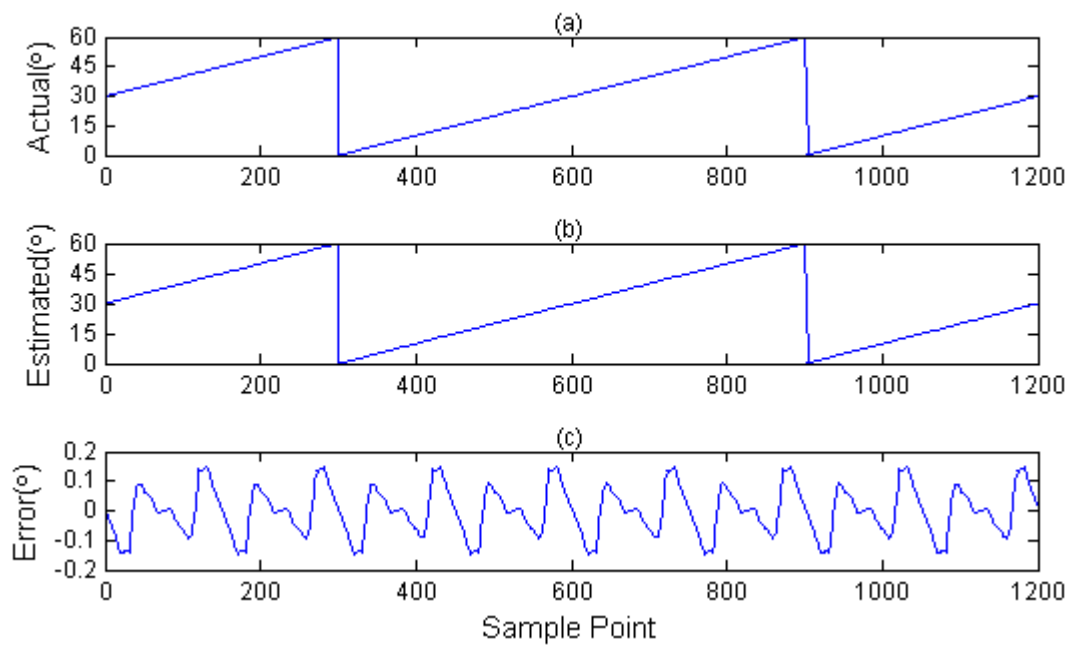


Fig. 4-2 Startup angle estimation simulation results using LSRPEM of a 3kW four-phase 8/6 switched reluctance motor. a) Actual angle. b) Estimated angle c) Error in estimation

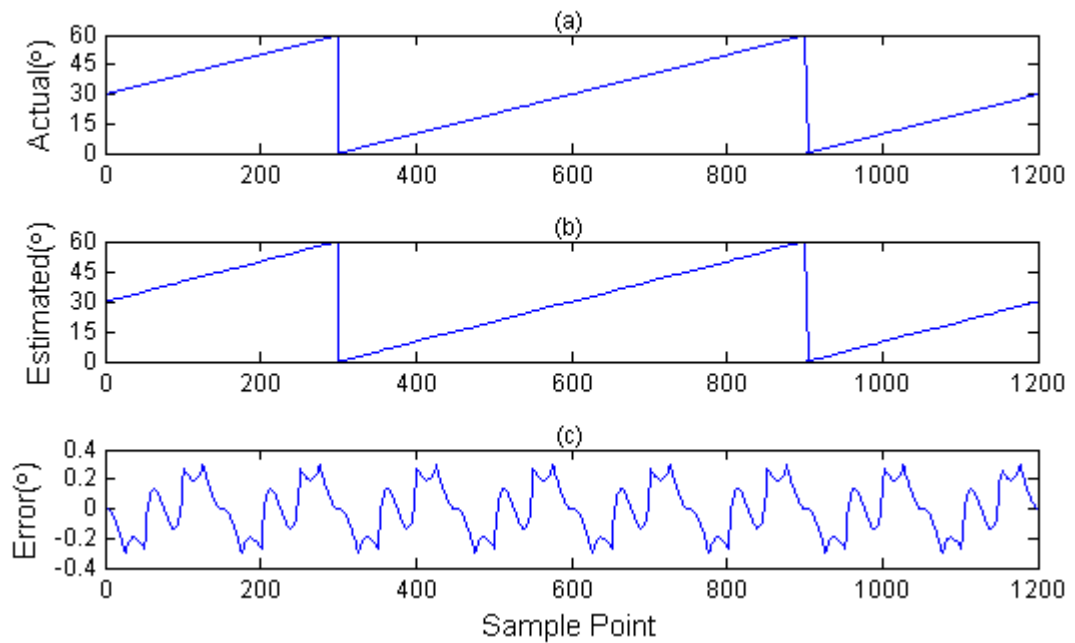


Fig. 4-3 Startup angle estimation simulation results using LSRPEM of a 5kW four-phase 8/6 switched reluctance motor. a) Actual angle. b) Estimated angle c) Error in estimation

By comparing the simulation results from Fig. 3–5 with those of Fig. 4–2, and Fig. 3–6 with those of Fig. 4–3, it can be seen that LSRPEM gives slightly better estimates than LERPEM with an ideal inductance profile which is symmetric about the aligned position and identical among phases.

#### **4.4 Experimental Results**

The LSRPEM is applied to the same experimental data as in Chapter 2 and Chapter 3. The results are shown in Fig. 4–4. The estimates have a mean absolute error of  $1.50^\circ$ , and a maximum error of  $4.16^\circ$ . The results show that in real situations LERPEM gives better estimates than LSRPEM.

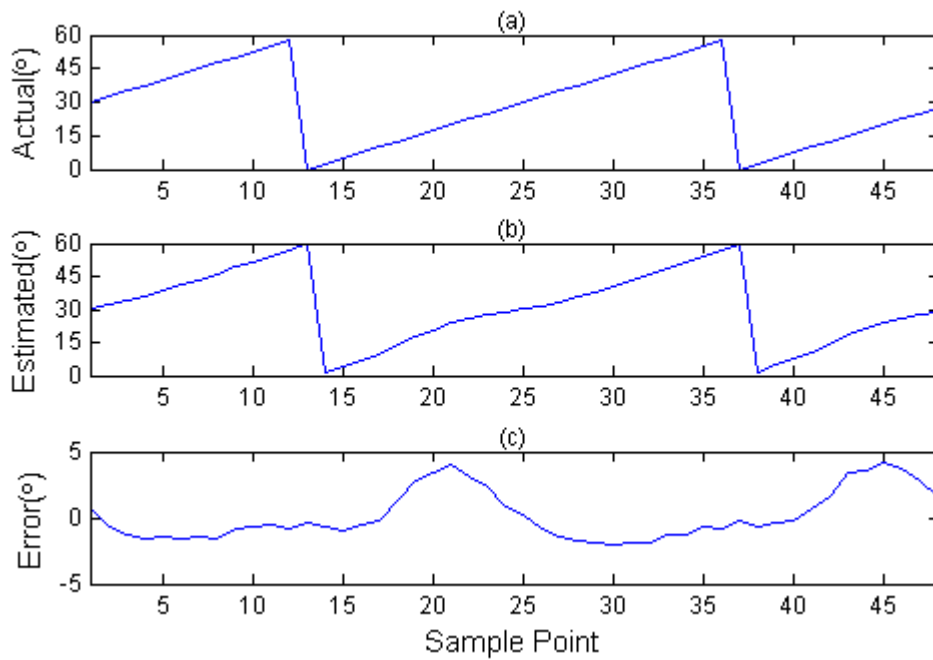


Fig. 4–4 Startup angle estimation experimental results using LSRPEM of a 1.5kW four-phase 8/6 switched reluctance motor. a) Actual angle b) Estimated angle c) Error in estimation

## 4.5 Models Comparison

In the last few chapters several models for sensorless rotor position estimation of switched reluctance motors are introduced. In this section their *rms* residuals resulting from the curve fit and the estimation accuracies will be shown and compared.

Fig. 4–5 and Fig. 4–6 show the estimation errors and the residuals from the different modeling methods, through simulation of the 3kW motor and the 5kW motor. It is noted that with the 3kW inductance profile, the sinusoidal method gives the most accurate results while the Type V method provides the smallest root mean square

residuals. The positions estimated by the Type V method are also quite accurate. The polynomial method performs worst in both quantities. With the 5kW profile, the sinusoidal method again gives the most accurate estimates, while Type V produces the smallest *rms* residuals. The polynomial method still performs the poorest. From the results of both profiles, it can be concluded that small residuals always leads to small errors, but large residuals do not necessarily produce the worst estimates.

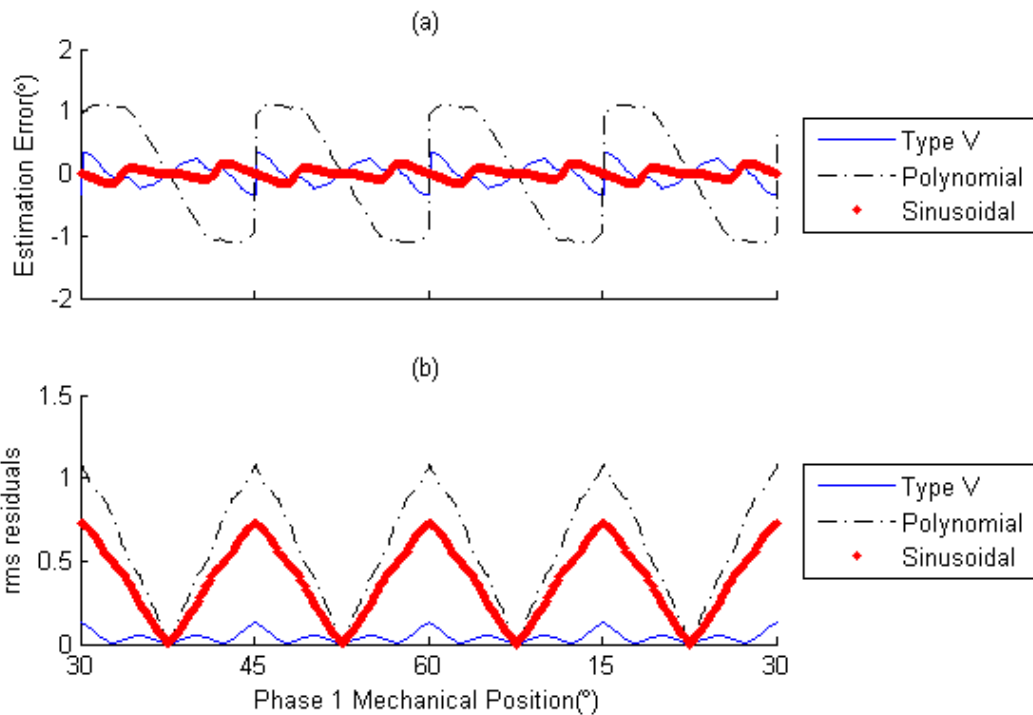


Fig. 4-5 Position estimation errors and *rms* residuals for the different methods using simulation result from the 3kW motor. a) Estimation Error. b) *rms* residuals

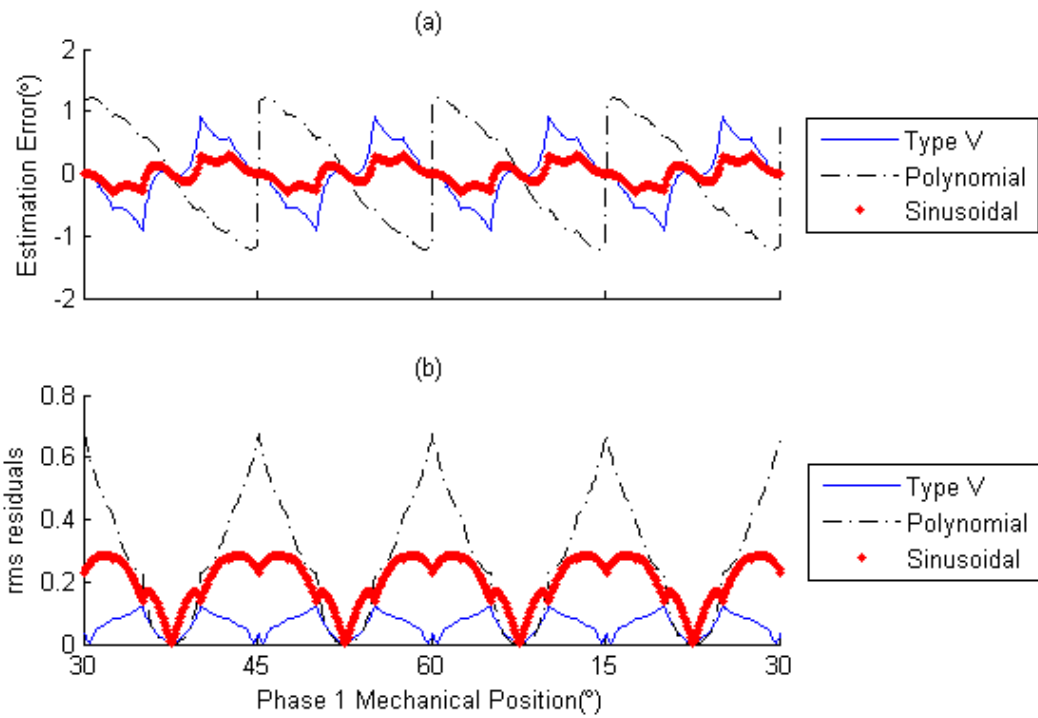


Fig. 4-6 Position estimation errors and *rms* residuals for the different methods using simulation result from the 5kW motor. a) Estimation Error. b) *rms* residuals

The results using data from the experimental 1.5kW motor are plotted in Fig. 4-7 below.



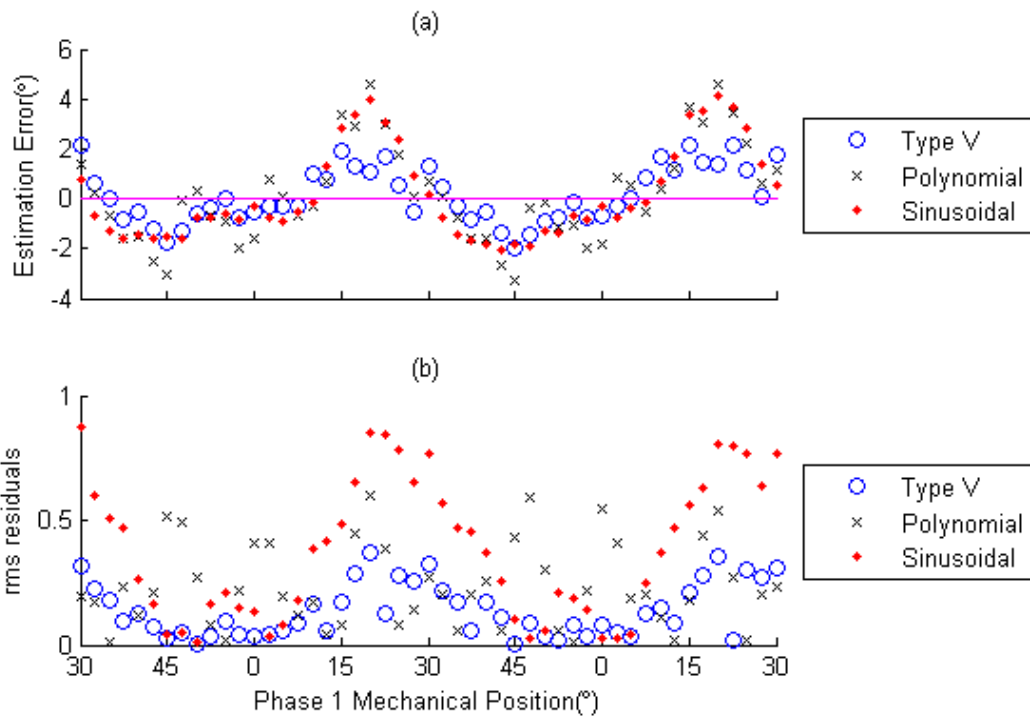


Fig. 4–7 Position estimation errors and *rms* residuals for the different methods using experimental result from the 1.5kW motor. a) Estimation Error. b) *rms* residuals

It can be noticed from Fig. 4–7 that the Type V method fares better under imperfect conditions. This is due to the fact that the Type V curve fits the motor’s inductance profile best, shown by the smaller residuals. It would then be more robust to inductance discrepancies because of the nature of least squares fitting. TABLE 4-1 summarizes the results. The calculation time is obtained by running the formulae programmed in C on a TI DSP F28335. All the calculations are done in fixed-point mathematics. It can be seen that the sinusoidal method is the fastest while Type V has the longest calculation time because of the logarithmic operations. With some more

modern processors with dedicated hardware for these operations, it is believed the clock cycles can be largely reduced.

TABLE 4-1  
COMPARISON OF THE DIFFERENT ESTIMATION METHODS

Category	Sinusoidal	Type V	Polynomial
3kW Avg. Absolute Estimation Error(°)	0.065	0.146	0.830
3kW Avg. Residuals(°)	0.382	0.042	0.578
5kW Avg. Absolute Estimation Error(°)	0.141	0.348	0.766
5kW Avg. Residuals(°)	0.206	0.062	0.289
Experiment Avg. Absolute Estimation Error(°)	1.50	0.88	1.56
Experiment Avg. Residuals(°)	0.383	0.138	0.237
Calculation Time(Clock Cycles)	216	3708	552

## 4.6 Summary

In this chapter the sinusoidal method called LSRPEM for position estimation at motor start-up is presented, and the results are compared with those obtained by the methods in Chapter 2 and Chapter 3. The accuracy of the estimations is similar to that of the LQRPEM and lower than LERPEM. Like those from the previous chapters, the merit in the new method lies in its purely mathematical approach and it has done away with the step of finding the right ordering of the phase positions needed in the previous two methods, facilitating a faster execution time.

## Chapter 5

# Position Estimation under Dynamic Conditions

### 5.1 Introduction

In the last three chapters, position estimation is based on static or free running conditions when there is no active phase and each can be applied with a probing voltage pulse train. In this chapter two dynamic position estimation methods will be introduced. With these two methods it is possible to control a running motor without position sensors.

Many methods on sensorless rotor position estimation under dynamic situations have been studied in the past. They can be crudely categorized into two groups, namely the energized phase methods and the un-energized phase methods. With the energized phase methods, the active phases are used for the estimation of positions. In [38] flux linkage method is used where the estimated flux of the active phase is compared with a reference value to commutate the phases. In [62] the change in current gradient is used to determine a commutation point close to the aligned position. In [63] the measured voltage and current are used to calculate the flux linkage, and through recursive least squares method the position is estimated from a lookup table. With the un-energized phase methods, inactive phases are used and in most cases probing

voltage pulses are applied to the motor phases and through the resultant phase currents, voltages or the derivatives of such, rotor position is estimated. In [64] a Fourier model of the inductance profile using the aligned and unaligned inductance is developed and inductance obtained using voltage injection method from an idle phase is used to look up the position from the model. Reference [65] describes a method that injects a voltage pulse to an idle phase to trigger a voltage resonance response. Through measuring this response the position is determined using a lookup table. In [66] voltage pulses are applied to an idle phase and the switching moment is determined by the measured current. Some methods combine both active and inactive phases, such as [67, 68].

The methods that will be introduced in this chapter use both the active and inactive phases to estimate the rotor position. Following the idea of the static methods introduced in the previous chapters, the methods to be developed do not require specific magnetic information of the motor to be known and only rely on the general properties of the phase inductance profile.

## **5.2 General Phase Inductance Profile property**

The general inductance against position plot for all phases superimposed is shown in

Fig. 5-1:

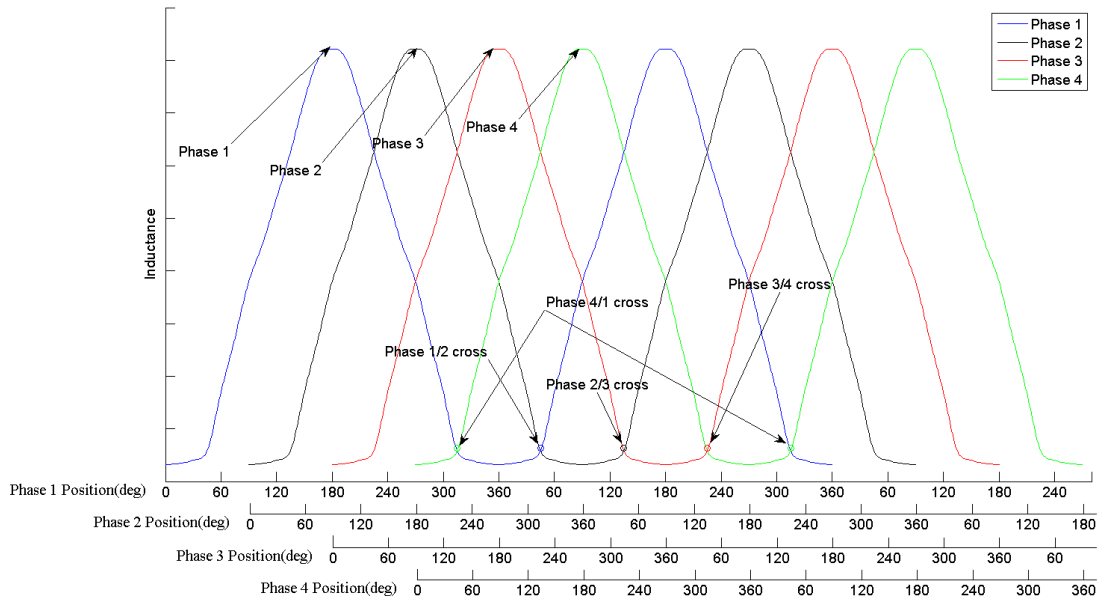


Fig. 5–1 General phase inductance profiles for all phases of an 8/6 SRM. Inductance profile crossing points for adjacent phases shown.

where the electrical positions for individual phases are shown on the x-axis. It can be noticed from the figure that the inductance profiles of two adjacent phases cross path at a particular point near the unaligned position, specifically at  $45^\circ$  for one and  $315^\circ$  for the other, on their own position axis. This event will be called “Adjacent Phase Inductance profiles crossing”, abbreviated as APC, for the rest of this work.  $APC_{n/m}$  will then stand for the APC of phase  $n$  and  $m$ , where phase  $n$  is at  $45^\circ$  and  $m$  at  $315^\circ$ . If the rotor is moving in the same direction, in one electrical cycle 4 APCs will occur. This special property will be used in the position estimation and phase switching schemes to be developed in this chapter for running a four-phase 8/6 SRM.

### 5.3 Using Kalman Filter For SRM Control

Chapter 1 gave an introduction of the Kalman filter. There are numerous literatures describing the use of Kalman filters in motor control to estimate the speed, position, and torque [35, 37, 69-79]. In [73] the extended Kalman filter was used to estimate the speed and rotor flux of an induction motor, and the estimates were then utilized for vector control. In [76] an alternate approach was taken where the states estimated were the speed and the stator flux, and they were used in direct torque control of the induction motor. The authors of [80] used an unscented Kalman filter to better estimate the true mean and covariance of a nonlinear permanent magnet synchronous motor model. The use of Kalman filters in the control of switched reluctance motors was also described in [29, 81]. In [29] models of different complexities were presented and compared. In [81] the extended Kalman filter was applied to find the speed, position and current of the motor. With all these methods, the magnetic characteristics of the motor must be known such that a process model can be built.

Given the multitude of studies on motor control utilizing the Kalman filter, it is still not commonly seen in practice. One contributing factor is the need of a large amount of machine data to build up the model, which is sometimes impossible or difficult to obtain in a manufacturing environment. Calculation complexity also prohibits its use

in low end microcontrollers. Rapid advances in DSP technologies have now made it possible to include the filter in the control software, but the complexity of the motor model is still needed to be reduced such that the amount of data required is more practical for real life applications.

The same issues also plague the use of the filter in the control of switched reluctance motors, because a large amount of machine details are required. The nonlinearity nature of the motor model due to magnetic saturation further aggravates the problems, making it necessary to provide to the model the inductance/flux linkage at different position and current combinations, and the necessity to use the extended Kalman filter or other nonlinear variations of the filter for estimating the system states.

On the other hand, Kalman filters have been successfully and widely used in navigation, ever since their first well known application in the Apollo 11 spacecraft. Many modern navigation systems also utilize the filter as a core component in the control. Inspecting the models that the filter used in these applications reveals the reason: the models are relatively simple and do not require large amount of information on the controlled target. The dynamic equations governing the models mostly involve simple kinematic equations of acceleration, velocity and position. These information, or states of the process, can be obtained easily from sensors. This is in contrast with the common models used in switched reluctance motors that have

states that can only be obtained indirectly through some prior knowledge of the motors, and only through the usage of nonlinear methods. This chapter will describe a method that utilizes the discrete Kalman filter using simple dynamic state equations, and the estimated states are used directly in controlling the motor.

## 5.4 The State Space model

### 5.4.1 Conventional State Space model

In [29] the system states for a four-phase switched reluctance motor is formulated as follow:

$$x = \begin{bmatrix} I_1 \\ I_2 \\ I_3 \\ I_4 \\ \omega \\ \theta \\ T_{Load} \end{bmatrix} \quad (5-1)$$

where  $I_n$  stands for current of phase n. Similar to the state vector of (5-1), in common practice for sensorless control using the filter the state vector comprises speed, position, current and load torque. The position is determined by the inductance at a certain current level and speed is not directly measured but only as a function of output torque and load torque. Including the output torque in the state equations is



very complex since it is necessary to know the change in co-energy with respect to position at every angle and current. System states are mingled with each other with some states dependent on the others through linear and non-linear relationships. Applying the model requires in-depth knowledge of the motor and also large amount of data memory in the control systems. The nonlinear dynamic relationships also prohibit the use of linear Kalman filter and therefore stability and optimality are not guaranteed. In this study these problems are resolved by modification of the general model such that it only involves linear kinematic relationships. Measurements are also made available for all states to enhance the predictions from the filter.

#### 5.4.2 Proposed State Space model

The proposed discrete state space model for the SRM in the form of (1-4) is as follow:

$$\begin{bmatrix} s \\ \dot{s} \end{bmatrix}_{k+1} = \begin{bmatrix} 1 & T \\ 0 & 1 \end{bmatrix} \begin{bmatrix} s \\ \dot{s} \end{bmatrix}_k + w_k \quad (5-2)$$

where  $s$  represents the position and  $T$  the sampling period. The state vector

$$\mathbf{x} = \begin{bmatrix} s \\ \dot{s} \end{bmatrix} \quad (5-3)$$

consists only of position and speed. The usual states of current and torque are omitted to avoid having to know the precise model of the motor. There is no input vector  $\mathbf{u}$  in this model and  $\mathbf{w}_k$  is the zero mean process noise vector where the effects of torque

and load are modeled as part of the speed process noise. This assumption is valid as long as the speed can reach a steady state in a reasonable time. The measurements of the states to be used for the filter will be made available with the special switching techniques shown in the next section.

## **5.5 Position Estimation Procedure and Phase Switching**

### **Strategy**

The proposed method comprises two switching schemes, one for low speed control and the other for high speed. Under the low speed switching scheme, which will hereafter be referred to as Type I switching mode, the general characteristics of the inductance profile is utilized for phase switching. In the high speed scheme, which will be called the Type II switching mode, the Kalman filter is used. Type I switching is also needed to prime the Kalman filter for Type II switching, which will be shown later. The flux linkage relationship, described by (2-14), is again used for comparing the magnitudes of the phase inductance.

#### **5.5.1 Type I Switching Mode**

The first switching mode has dual functionality: first it starts up the motor and keeps it running, second it prepares the Kalman filter for Type II switching by providing

position and speed measurements. This is accomplished by utilizing the APC event of the SRM inductance profile described in section 5.2. The simulated current waveform under Type I switching mode for the first 0.08s after the motor starts is shown below in Fig. 5–2.

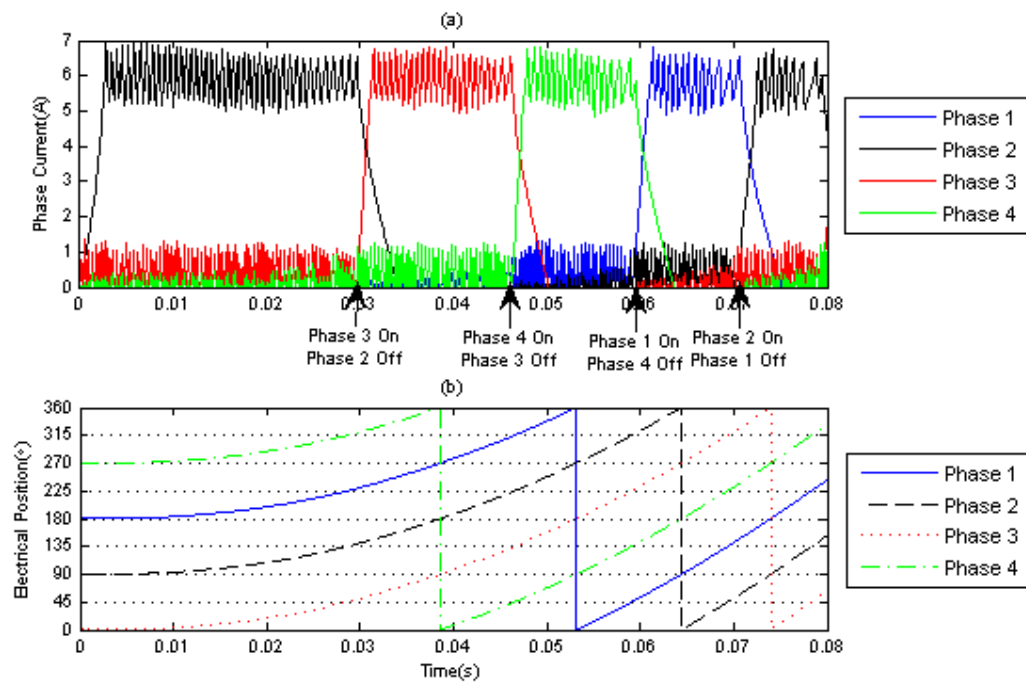


Fig. 5–2 Current switching waveforms for all phases of an 8/6 SRM under Type I Switching Mode.

a)Current waveforms. b) Actual Electrical Positions

Under this mode, each phase is turned on between  $45^\circ$  and  $135^\circ$ , meaning also only one phase will be on at any time. To start the motor, static methods developed from the previous chapters are used to determine the starting phase, which lies between  $45^\circ$  and  $135^\circ$ . When the motor starts running probing voltage pulses are applied to the two phases which will have the next APC. This is illustrated In Fig. 5–2. For this

simulation the motor starts with Phase 1 aligned. Therefore Phase 2 is the first active phase and Phase 3 and 4 are the next APC phases. Probing pulses with the same amount of volt-seconds are applied to these two phases and their current measured. When the difference in current values between the two probing phases changes sign, it is an indication that APC3/4 has occurred. This happens at around 0.03s in the figure. It is known from section 5.2 and also can be seen in the figure that, at this time Phase 2 reaches  $135^\circ$ , phase 3 is at  $45^\circ$  and phase 4 at  $315^\circ$ . Phase 2 will then be turned off and Phase 3 turned on. The new probe phases become Phase 4 and Phase 1, since their APC will happen next.

To keep the motor running this switching and probing sequence continues, such that at each APC the APC phase which is at  $45^\circ$  is turned on and the current active phase turned off. Fig. 5–2 shows the switching sequence. Under this switching sequence the motor will keep running, and each phase will turn on at an angle of  $45^\circ$  and turn off at  $135^\circ$ . This gives a dwell angle of  $90^\circ$  electrical for each active phase which for an 8/6 SRM is equivalent to  $15^\circ$  mechanical. The drawbacks of this switching scheme are

- 1) Compared with a theoretical maximum dwell span of  $180^\circ$  this imposes a limitation on the maximum speed and torque of the motor.
- 2) Only one phase is active at a time.

These limitations could be removed once the controller goes into Type II switching

mode, to be described in the forthcoming subsection. Nevertheless, under this switching scheme the motor is able to run normally.

As a consequence of the above switching process, the position and speed information required by the Kalman filter can also be obtained, since at each profile crossing the position of the rotor is known, and four such crossings occur and thus four positions can be detected in one electrical cycle with an 8/6 SRM. For instance when phase 1 is active, phase 2 and 3 will be probing. When APC2/3 happens, phase 2 will be at  $45^\circ$ , which also corresponds to phase 1's position of  $135^\circ$ . When phase 2 is active, phase 3 and 4 are the probing phases. APC3/4 will occur at phase 3's position of  $45^\circ$ , which also is phase 1's position of  $225^\circ$ . And by the same token at APC4/1, phase 1 will be at  $315^\circ$  when phase 4 reaches its turn on angle, again at  $45^\circ$ . Therefore 4 distinct positions can be identified at each APC within one electrical cycle. Now that these positions are available, the speed of rotation can also be found. Since each phase is turned on at the same position in every cycle, the time between same-phase APCs are equal to the time needed to travel one electrical cycle. With the very accurate timer in the DSP, this time can be measured precisely. Thus using this information the speed of the rotor can be determined. By dividing  $360^\circ$  by this time, the speed in electrical degrees per second can be found. Although theoretically it is also known that the distance between sequential APCs is  $90^\circ$ (since there are four crossings in one cycle),

it is usually not a good idea to use the time between sequential phase crossings for speed calculation since inductance among phases varies and it cannot be guaranteed that sequential APCs are  $90^\circ$  apart. Two APCs of the same phase-pair are much more reliable for determining the angular distance travelled.

The speed for the first electrical cycle after starting cannot be determined, because as explained above it is calculated by the time between two same-phase APCs. But after the first cycle speed information is available every  $90^\circ$ , i.e. once at every APC. After feeding these speed and position measurements to the filter, the estimated states of speed and position can then be obtained.

### **5.5.2 Type II Switching Mode**

Under Type II switching mode, with the position information available from the filter, the turn-on and turn-off angles can be chosen freely. The simulation result illustrating the scheme is shown below in Fig. 5-3.

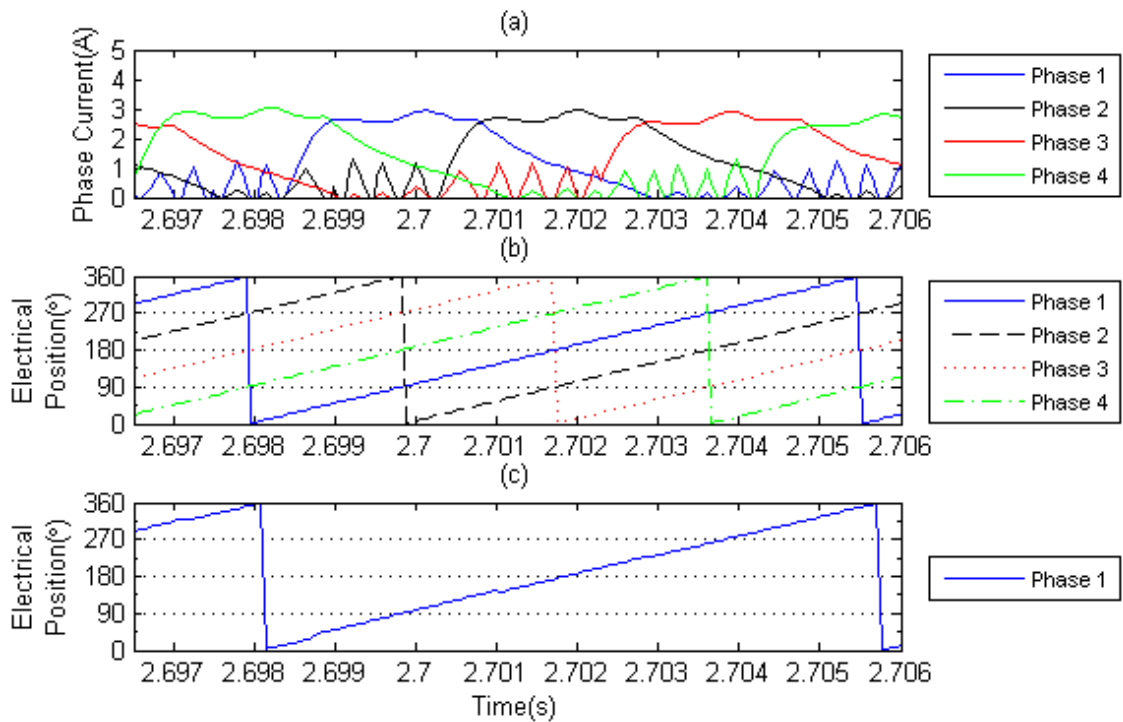


Fig. 5-3 Current switching waveforms for all phases of an 8/6 SRM under Type II Switching Mode.

a)Current waveforms. b)Actual Electrical Positions c) Estimated Phase 1 Electrical Position from filter

The turn on angle is chosen to be  $15^\circ$  and the turn off angle  $126^\circ$ . The position information is provided by the Kalman filter, shown in plot c). It is shown in the figure that the phases are commutated correctly. The choice of the probe phases are still the two phases to have the next APC but the probing process is different to Type I since it might not be possible to apply probing pulses of equal volt-seconds to the two phases when one of them become active before their APC, as in the current case with the turn-on angle at  $15^\circ$ . This is shown in the expanded current waveforms in Fig. 5-4. As can be seen phase 1 becomes active before APC<sub>1/2</sub>, so now only to phase 2 the probing pulses can be applied and phase 1 has to be switched according to the set

reference current. Therefore the APC1/2 event cannot be detected by just comparing the probe phase current magnitudes as in Type I mode but their relative inductances have to be found first by dividing the difference between on-time and off-time of the probe phases by the measured current value. Some errors might be introduced by the various voltage drops and mutual inductive couplings that lead to volt-seconds difference. In the experiment section their effects will be shown.

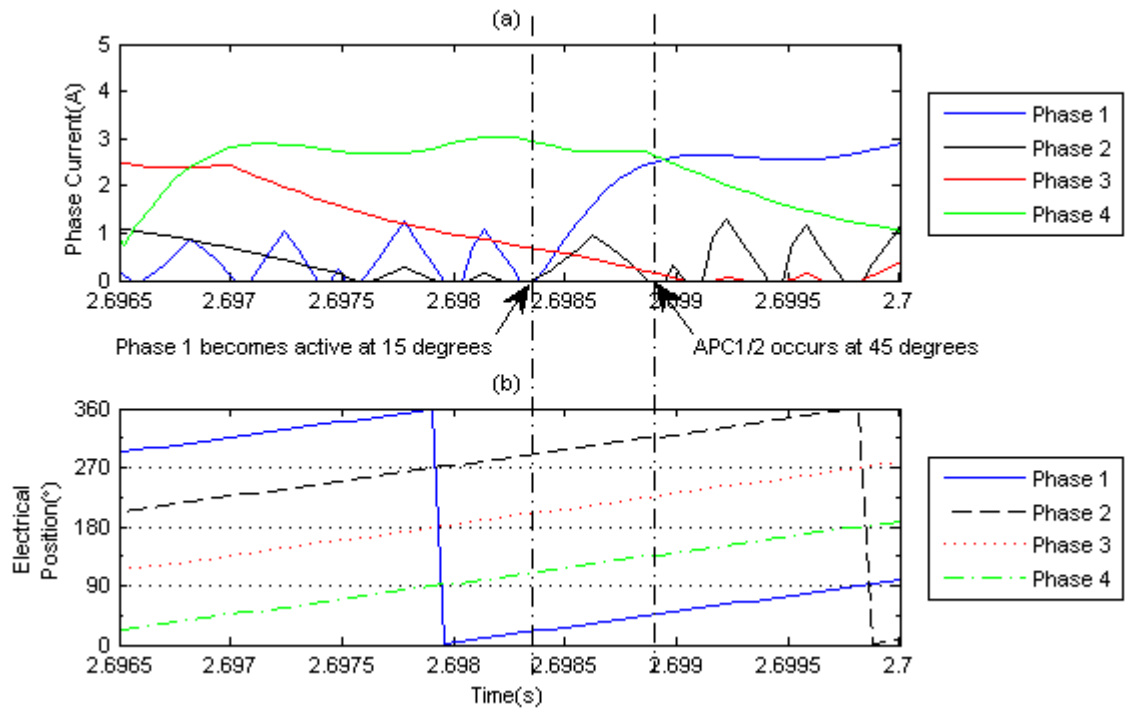


Fig. 5-4 Expanded current switching waveforms for all phases of an 8/6 SRM under Type II Switching Mode. a)Current waveforms. b)Actual Electrical Positions



## **5.6 Some Implementation Issues**

In the last section the methods for sensorless control of SRM utilizing the Kalman filter was described. In this section some practical aspects affecting the physical implementation will be discussed.

### **5.6.1 Update frequency of the Kalman filter**

The measurable states in the system model are the position and velocity, and they are used in the Kalman filter equations. Two issues must be resolved before the filter can be applied using these states, which is the availability of the measurements and the time between measurements, discussed below.

#### **a) Availability Of Measurements**

In a general implementation, for every iteration of the Kalman-filtering equation (1-10) there is a measurement update, meaning the filter expects to have the state measurements available to correct the estimations. It is not possible in the present case since position and speed info only arrives every 90 electrical degrees, and to use the filter as a position estimator for commutation it must be run more frequently.

#### **b) Asynchronous Measurements**

Since the measurements come at instants of phase crossings, the time intervals between measurements are not deterministic and dependent on speed. This again will affect the time between measurement updates when using the filter. This particular form known as multi-rate system is investigated in previous research works[82-86]. But if the filter is run in multi-rate the process noise covariance  $\mathbf{Q}_k$  and the state transition matrix  $\mathbf{A}_k$  are different at each filter execution. This is because  $\mathbf{A}_k$  contains the value of the execution period, which is now variable, and  $\mathbf{Q}_k$  will propagate through time, therefore the time between filter executions will affect its value. This can be shown by inspecting equation (1-11) for the calculation of the state estimation covariance, repeated here:

$$\mathbf{P}_k^- = \mathbf{A}_{k-1} \mathbf{P}_{k-1}^+ \mathbf{A}_{k-1}^T + \mathbf{Q}_{k-1} \quad (1-11)$$

where  $\mathbf{A}_{k-1} = \mathbf{A}_k = \begin{bmatrix} 1 & T \\ 0 & 1 \end{bmatrix}$

Letting  $k = k + 1$  to simplify the expression, and assuming there is no measurement update, at  $n$  sampling periods after the instant  $k$  the state estimation covariance becomes:

$$\begin{aligned} P_{k+n} = & \mathbf{A}_k^n P_k \mathbf{A}_k^{T^n} + \mathbf{A}_k^{n-1} \mathbf{Q}_k \mathbf{A}_k^{T^{n-1}} + \mathbf{A}_k^{n-2} \mathbf{Q}_{k+1} \mathbf{A}_k^{T^{n-2}} \\ & + \mathbf{A}_k^{n-3} \mathbf{Q}_{k+2} \mathbf{A}_k^{T^{n-3}} + \dots + \mathbf{A}_k^0 \mathbf{Q}_{k+n-1} \mathbf{A}_k^{T^0} \end{aligned} \quad (5-4)$$

Expanding  $\mathbf{A}_k$  in the first term we get

$$\begin{aligned}
P_{k+n} &= \begin{bmatrix} 1 & T \\ 0 & 1 \end{bmatrix}^n P_k \begin{bmatrix} 1 & 0 \\ T & 1 \end{bmatrix} + A_k^{n-1} Q_k A_k^{T^{n-1}} + A_k^{n-2} Q_{k+1} A_k^{T^{n-2}} \\
&+ A_k^{n-3} Q_{k+2} A_k^{T^{n-3}} + \dots + A_k^0 Q_{k+n-1} A_k^{T^0}
\end{aligned} \tag{5-5}$$

=>

$$\begin{aligned}
P_{k+n} &= \begin{bmatrix} 1 & nT \\ 0 & 1 \end{bmatrix} P_k \begin{bmatrix} 1 & 0 \\ nT & 1 \end{bmatrix} + A_k^{n-1} Q_k A_k^{T^{n-1}} + A_k^{n-2} Q_{k+1} A_k^{T^{n-2}} \\
&+ A_k^{n-3} Q_{k+2} A_k^{T^{n-3}} + \dots + A_k^0 Q_{k+n-1} A_k^{T^0}
\end{aligned} \tag{5-6}$$

Comparing this to the state estimation covariance if the filter is run with a period of  $nT$ :

$$P_{k+1} = \begin{bmatrix} 1 & nT \\ 0 & 1 \end{bmatrix} P_k \begin{bmatrix} 1 & 0 \\ nT & 1 \end{bmatrix} + Q_k \tag{5-7}$$

Therefore for filters with different execution periods, at the same time instant if the state estimation covariance  $\mathbf{P}_k$  is to agree, their process noise covariance  $\mathbf{Q}_k$  must be different. After every iteration of the filter the past process noise covariance propagates. It is therefore important to realize that, even though the Kalman filter can be run with any desired frequency, the choice of the discrete process noise covariance has to be prudent such that its propagation downstream is considered. If the sampling periods are varying, then  $\mathbf{Q}_k$  has to be recalculated for each iteration of the filter.

For the reasons above the filter in the present application will run with a fixed sampling period  $T$  much smaller than the measurement period, and with an empirical

choice of the process noise covariance  $\mathbf{Q}_k$ . This will guarantee a frequent position and speed output from the filter, a constant state transition matrix and process noise covariance vector for ease of implementation, and a state estimation covariance which can be calculated offline if desired. To take care of the missing data between measurements, the Riccati equation is modified such that the measurement update step is skipped when measurements are not available. This can be accomplished by setting the Kalman gain to zero in (1-10). The point to pay attention to is therefore the choice of  $\mathbf{Q}_k$  and to make sure measurement updates are frequent enough such that the state estimation follows the actual states closely. This can assure the convergence of the filter.

## **5.7 Simulation Results**

Simulations are done with several scenarios to show the system behavior of the two control methods. Type I switching is always used to start the motor and prime the Kalman filter. Hysteresis current control and hard chopping is used for the simulations.

### 5.7.1 Type I only switching with applied load

The settings used for this simulation are shown in TABLE 5-1 and results shown in Fig.

5–5. The plots begin after the motor has reached a steady state no-load speed.

TABLE 5-1  
SIMULATION SETTINGS FOR TYPE I SWITCHING

Time(s)	Control Type	Set Current(A)	Load(Nm)	On Angle(°)	Off Angle(°)
$t < 3.6$	I	6	0	45	135
$3.6 \leq t < 9$	I	6	2.3	45	135
$9 \leq t < 12$	I	6	0	45	135

The speed estimates from the filter have a mean error of 0.762rpm with motor unloaded and 0.987rpm loaded. The position estimates have a mean mechanical error of  $-1.465^\circ$  unloaded and  $-0.450^\circ$  loaded. The simulation step time is set at 60 microseconds in order to match the real time execution cycle time of the dSPACE hardware in the experiment section. If this step time is reduced the errors are also smaller. Speed estimations have a larger error at load change but in general the filter performance is satisfactory. Position estimates lag the actual ones at no load with higher speed because the larger execution step size of the Kalman filter and some control logic lead to delayed position information. Therefore as expected position errors reduce under load when the speed is lower.

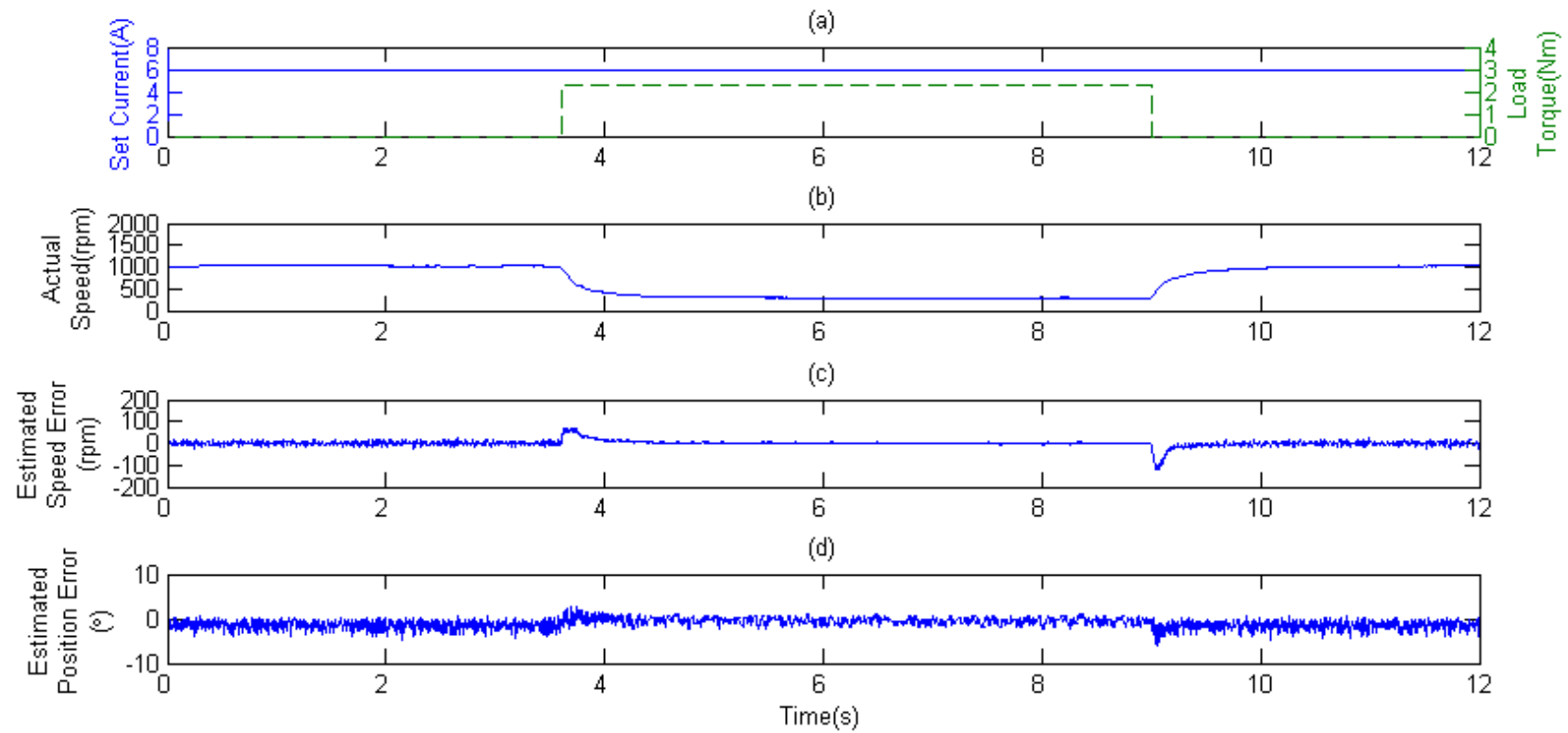


Fig. 5-5 Simulation results using Type I switching method with and without load a)Set Current and Load. b)Actual Speed c)Estimated Speed Error d)Estimated Position Error

### 5.7.2 Type II switching

The settings used for the simulation are shown in TABLE 5-2 and results shown in Fig. 5-6. The recording starts after the motor has reached a steady state no-load speed.

TABLE 5-2  
SIMULATION SETTINGS FOR TYPE II SWITCHING

Time(s)	Control Type	Set Current(A)	Load(Nm)	On Angle(°)	Off Angle(°)
$t < 2.9$	II	6	0	15	126
$2.9 \leq t < 7.9$	II	6	2.3	15	126
$7.9 \leq t < 12$	II	6	0	15	126

For the time range shown, the speed estimates from the filter have a mean error of 1.014rpm with motor unloaded and 0.450rpm loaded. The position estimates have a mean mechanical error of  $-0.884^\circ$  unloaded and  $-0.640^\circ$  loaded. Notice that under Type II switching without considering the resistive voltage drop, the active phase which carries a larger current will have a larger apparent relative inductance(because volt-seconds is larger than actual), causing an earlier than actual detection of phase inductance crossing. This could reduce the effect of the longer simulation step time, leading to a smaller position lag. But in general due to the almost perfect conditions both Type I and Type II switching produce good results. It could also be seen that since it is now possible to turn on the winding earlier, the torque is increased and thus a higher speed is reached using Type II switching.

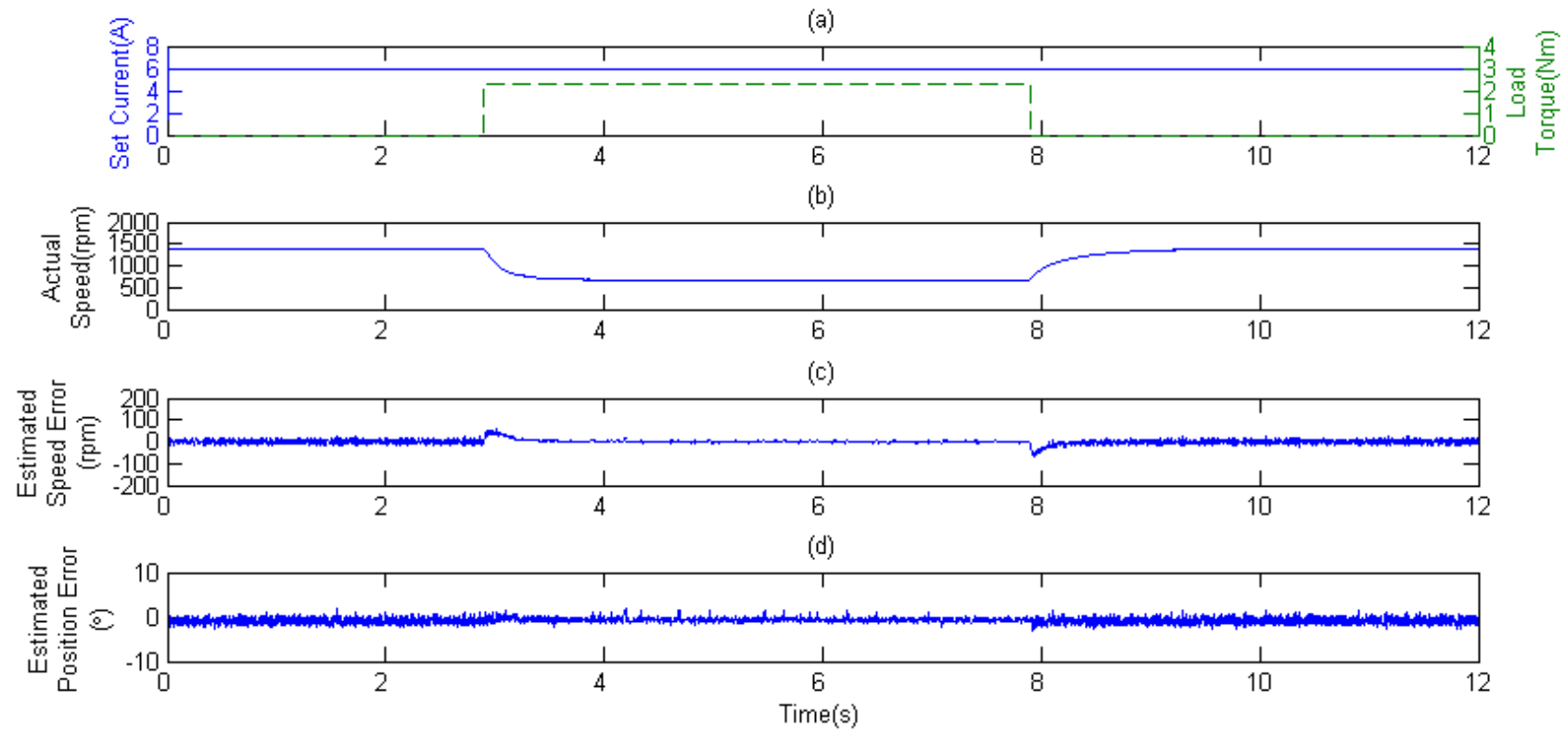


Fig. 5-6 Simulation results using Type II switching method with and without load a)Set Current and Load. b)Actual Speed c)Estimated Speed Error d)Estimated Position Error



### 5.7.3 Type I to Type II transition

The settings used for the simulation are shown in TABLE 5-3 and results shown in Fig. 5-7. It shows the system behavior when switching scheme changes from Type I to Type II. The recording starts from motor idle state.

TABLE 5-3  
SIMULATION SETTINGS FOR TYPE I TO II TRANSITION

Time(s)	Control Type	Set Current(A)	Load(Nm)	On Angle(°)	Off Angle(°)
$t < 2$	I	6	0	45	135
$2 \leq t < 4$	II	6	0	15	126

It is observed that the filter takes some times from the idle state to produce the correct position and speed detection, as expected. But this will not affect the startup performance of the motor since Type I switching does not use the Kalman filter's outputs. The speed change from Type I to Type II is gentle enough that the Kalman filter's output does not show a big error during the mode transition.

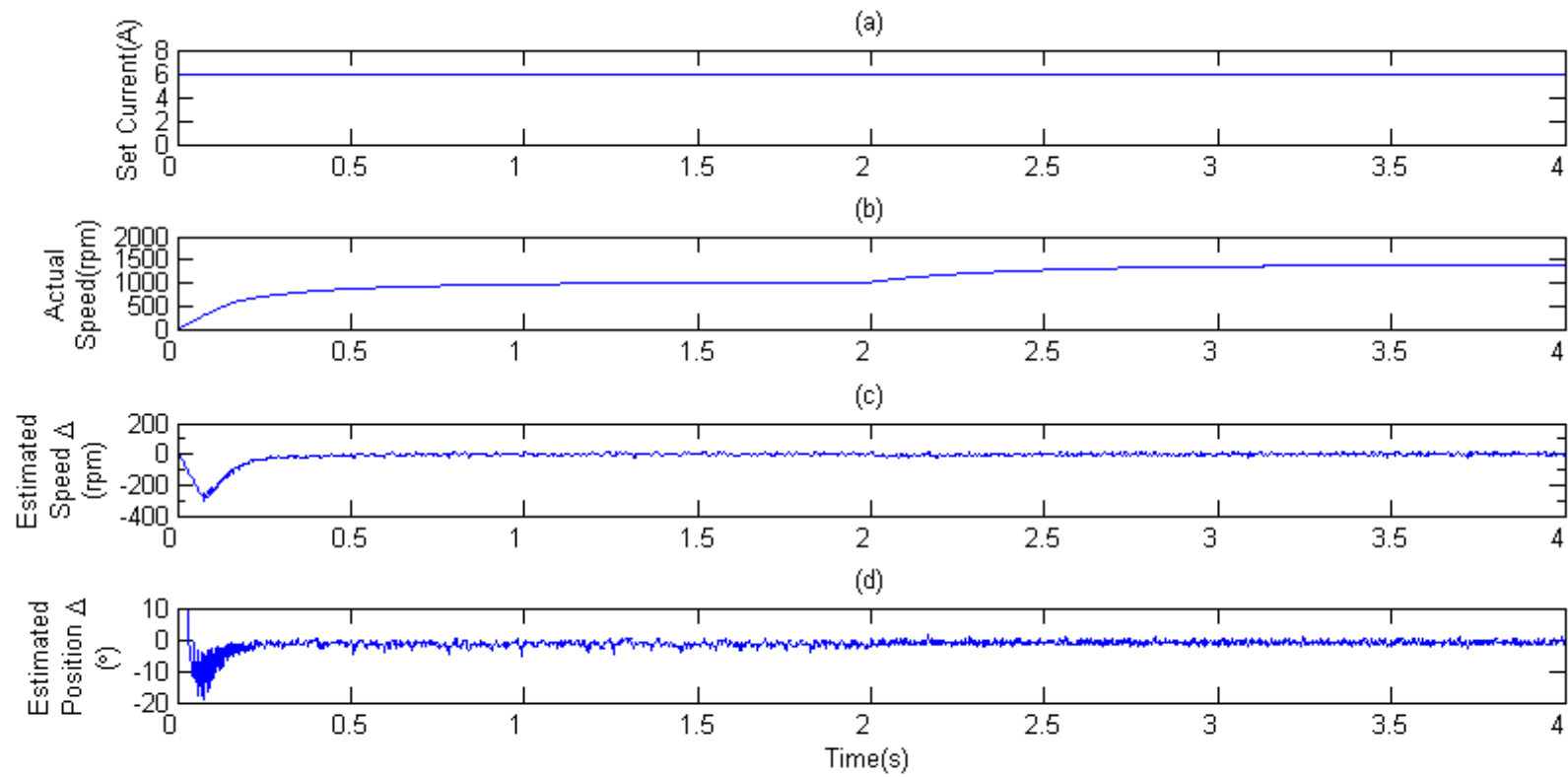


Fig. 5-7 Simulation results using Type I and Type II switching methods with load a)Set Current. b)Actual speed c)Speed Estimation delta d)Position Estimation delta.

## 5.8 Experimental Results

The experimental setup was described in section 2.5. The motor is the same one used for the static methods but the applied voltage is now changed to 65V. The results are shown below.

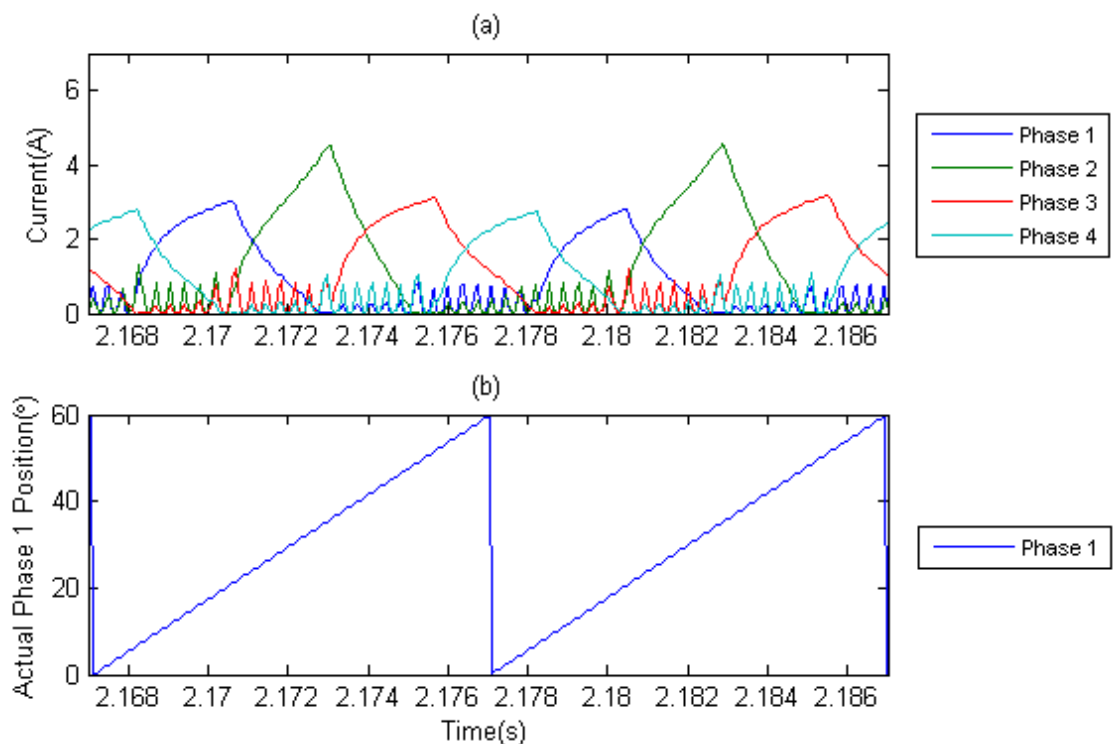


Fig. 5-8 Current waveforms under Type I switching without load a)Phase Currents. b)Phase 1 Mechanical Position

Fig. 5-8 shows the phase current waveforms and the corresponding phase 1 position of the motor at no load for Type I switching scheme. It can be seen that phase 2 has a higher maximum current than the other. This is due to its lower inductance as shown in Fig. 2-11. Although the set reference current is 6A actual phase currents cannot

reach this value due to the speed of the motor leading to short turn on time. The triangular shaped current pulses are the probing currents. Fig. 5–9 shows the same waveforms with the motor under a 2.3Nm load. It can be seen that now all phases can reach a current of 6A due to the lower speed of the motor. The figure is expanded into Fig. 5–10 for a better view of the waveforms. Fig. 5–11 illustrates the Kalman filter performance under Type I switching. The speed estimates from the filter have a mean error of 0.50rpm with motor unloaded and 1.03rpm loaded. The position estimates have a mean mechanical error of 1.05° unloaded and 2.64° loaded. The mean speed error is slightly higher when the motor is loaded due to the higher current that leads to higher torque ripples, but the effect is small. Differing to the simulation results, the position estimates has a positive delta. This is probably contributed by the effect of the mutual inductance which was not considered in the simulations. But the overall results agree.

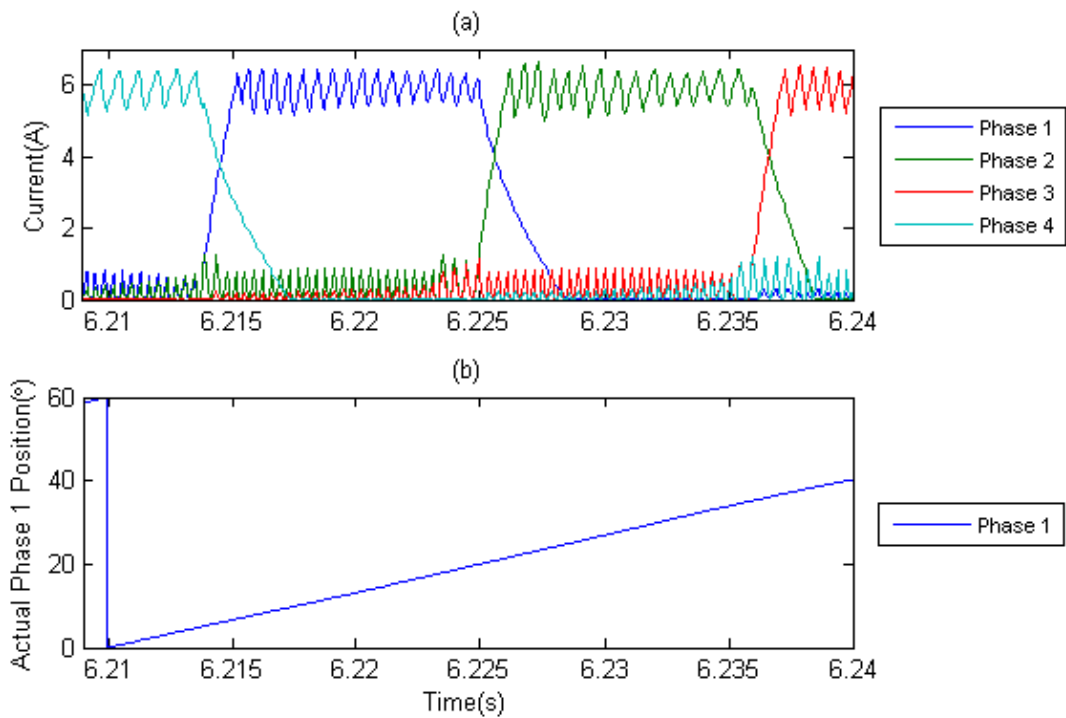


Fig. 5-9 Current waveforms under Type I switching with load a)Phase currents. b)Phase 1 Mechanical Position

Fig. 5-12 shows the current waveforms and the corresponding phase 1 position under Type II switching scheme. In general the current waveforms are not so consistent among phases due to the error in the position estimates used for phase switching. The different inductance profile of phase 2 also contributes to its higher current amplitude.

Fig. 5-13 shows the same quantities with the motor under a 2.3Nm load. Here the phase current waveforms are more consistent since it is now possible to reach the full reference current of 6A. Fig. 5-14 illustrates the Kalman filter performance under Type II switching. The speed estimates from the filter have a mean error of 2.69rpm with motor unloaded and 0.53rpm loaded. The position estimates have a mean

mechanical error of  $3.49^\circ$  unloaded and  $4.39^\circ$  loaded. As expected, due to volt-seconds errors, the position estimates have larger errors than Type I. The speed estimates are still quite good since using APCs from the same phase-pairs eliminate these volt-seconds errors.

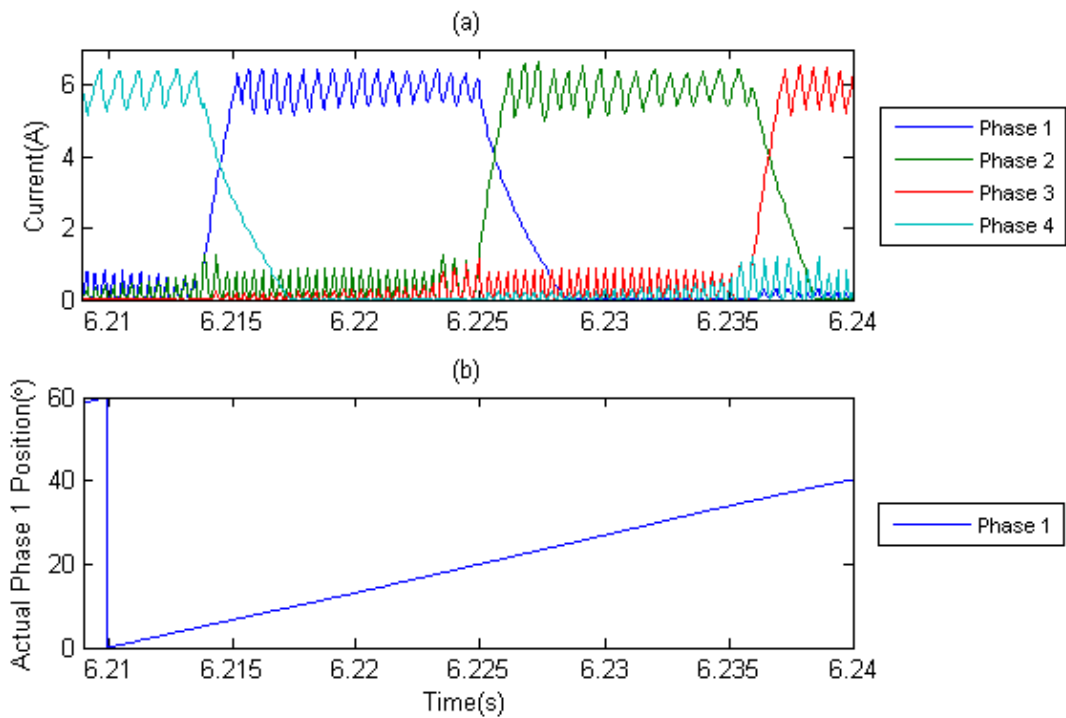


Fig. 5-10 Current waveforms under Type I switching mode with load in expanded view. a)Phase currents. b)Phase 1 Mechanical Position

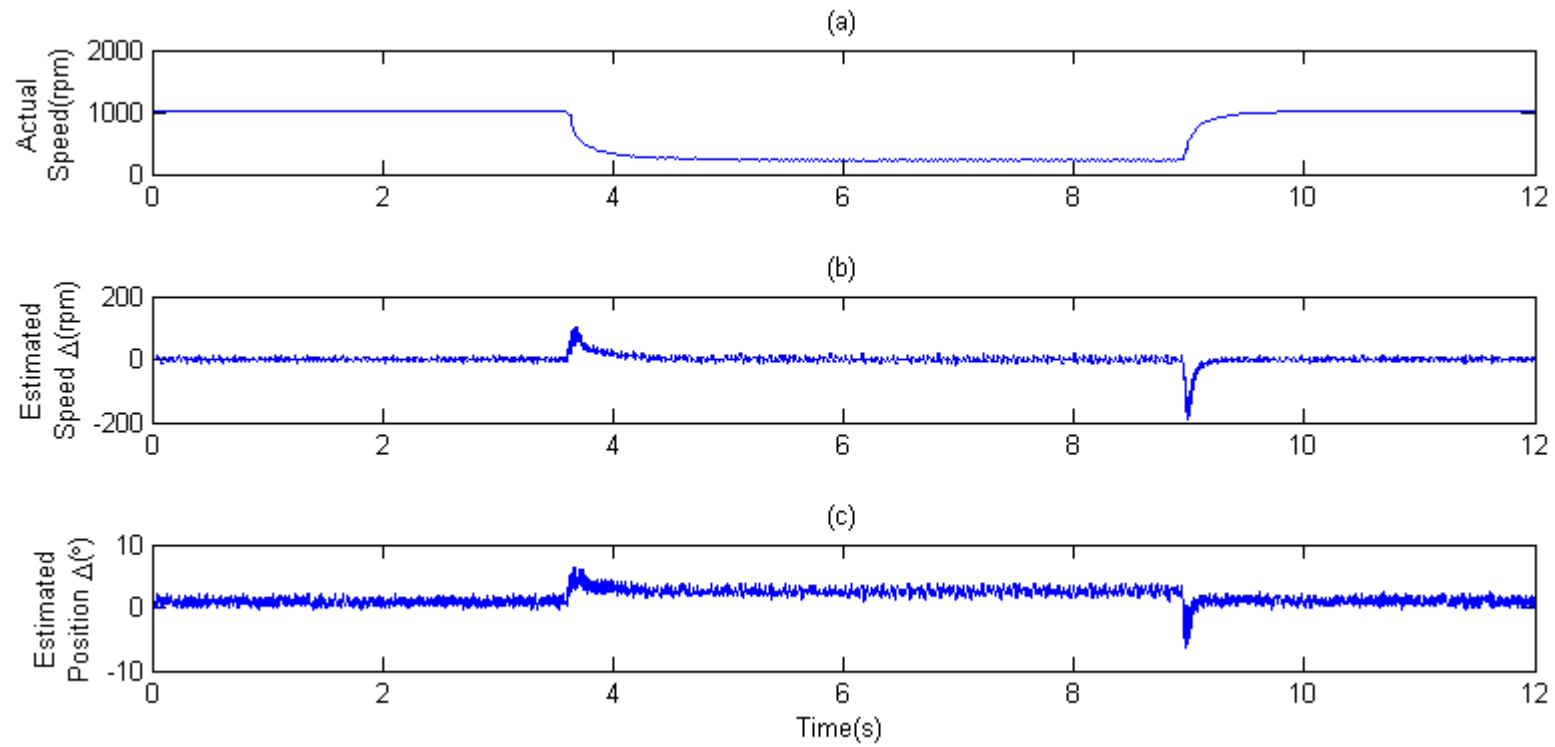


Fig. 5-11 Kalman Filter performance under Type I switching. a)Actual Speed b)Filter Speed Estimation error c)Filter Position Estimation Error

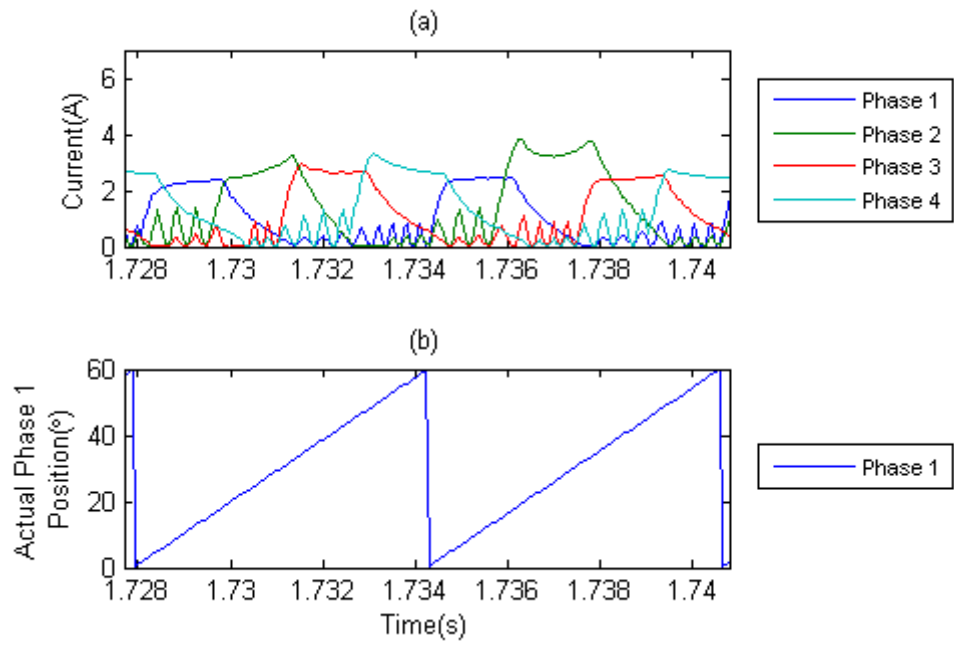


Fig. 5-12 Current waveforms under Type II switching without load a)Phase currents. b)Phase 1 Mechanical Position

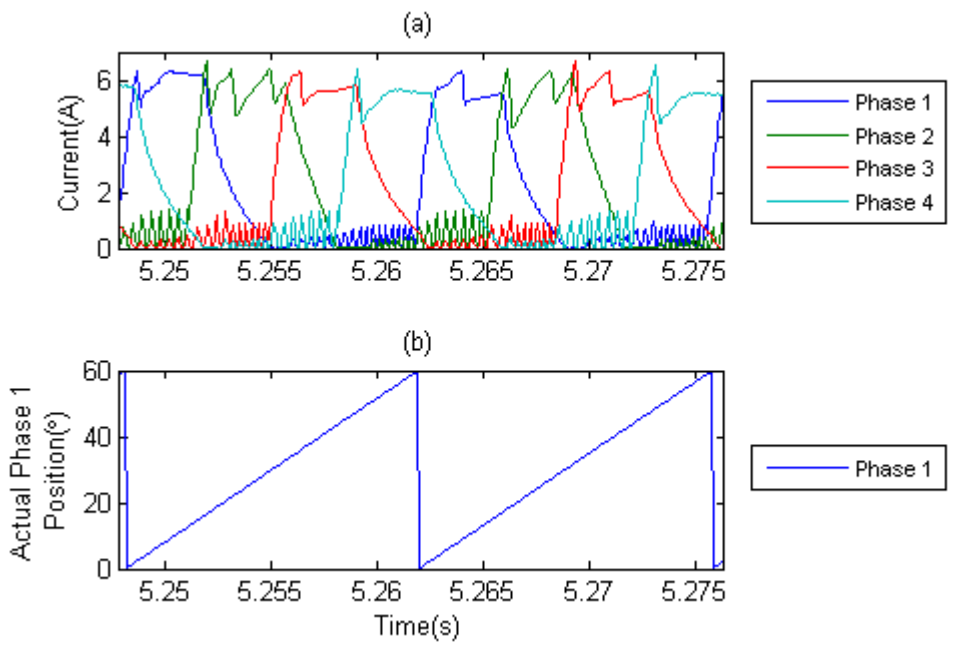


Fig. 5-13 Current waveforms under Type II switching with load a)Phase currents. b)Phase 1 Mechanical Position



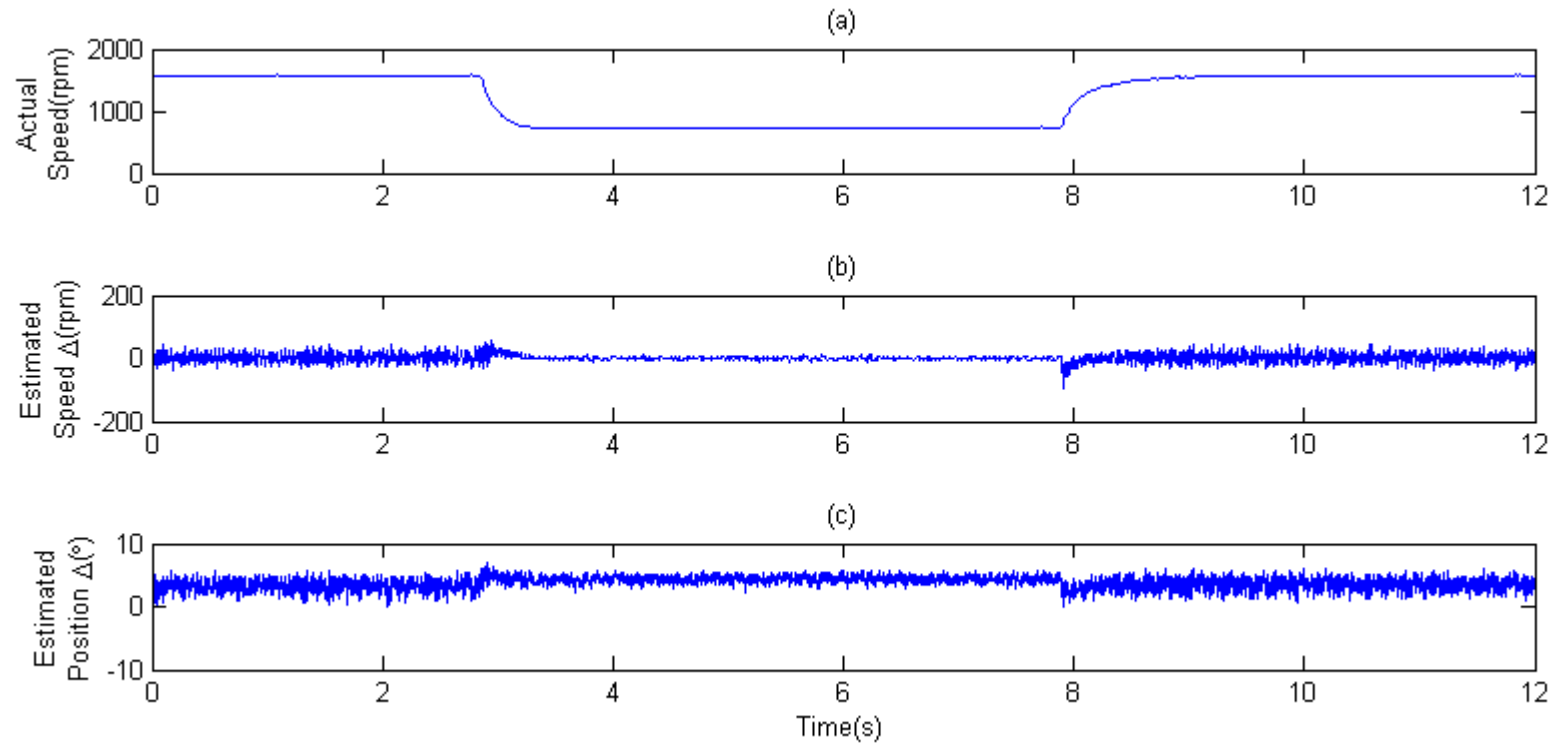


Fig. 5-14 Kalman Filter performance under Type II switching. a)Actual Speed b)Filter Speed Estimation error c)Filter Position Estimation error

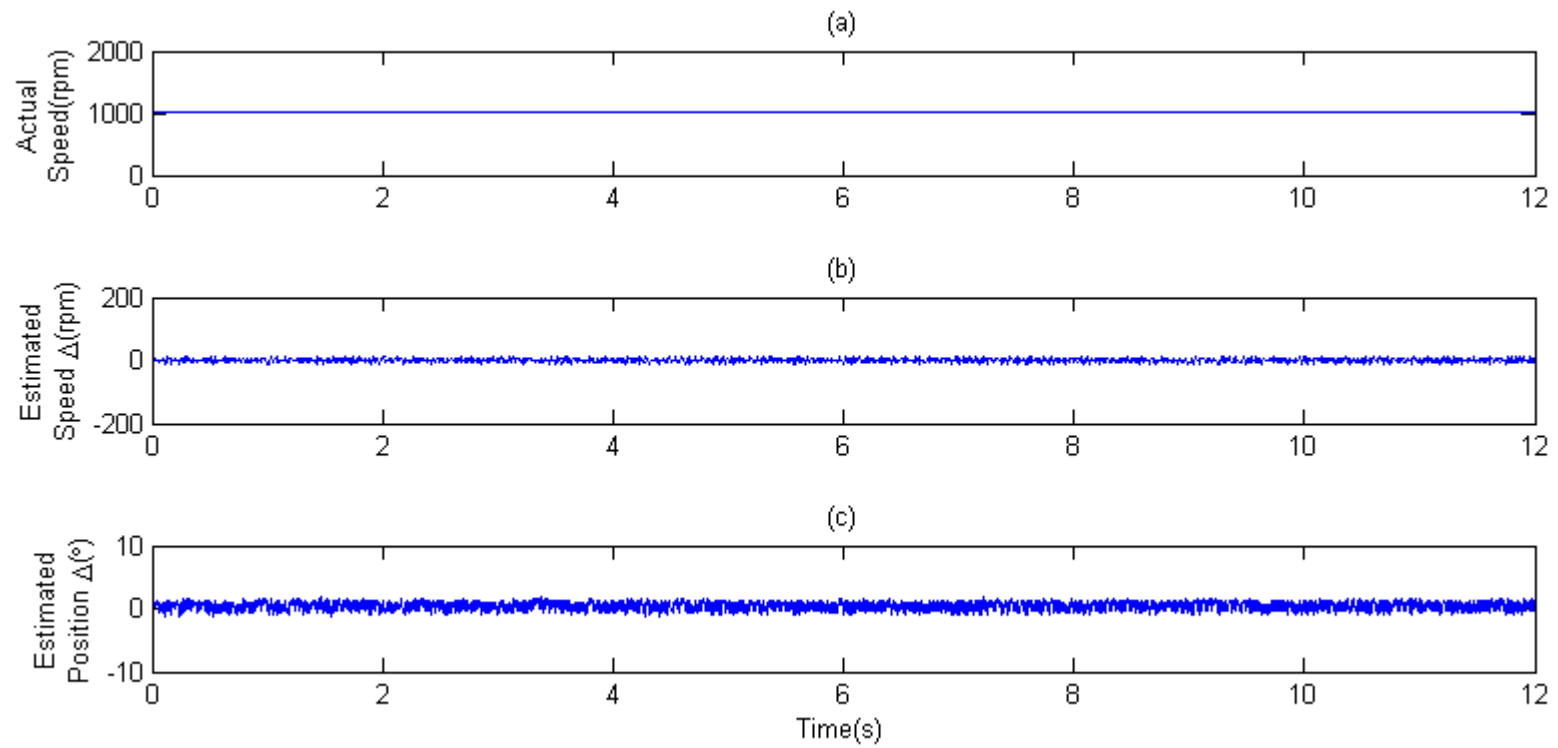


Fig. 5–15 Kalman Filter performance with no switching. a)Actual Speed b)Filter Speed Estimation error c)Filter Position Estimation error

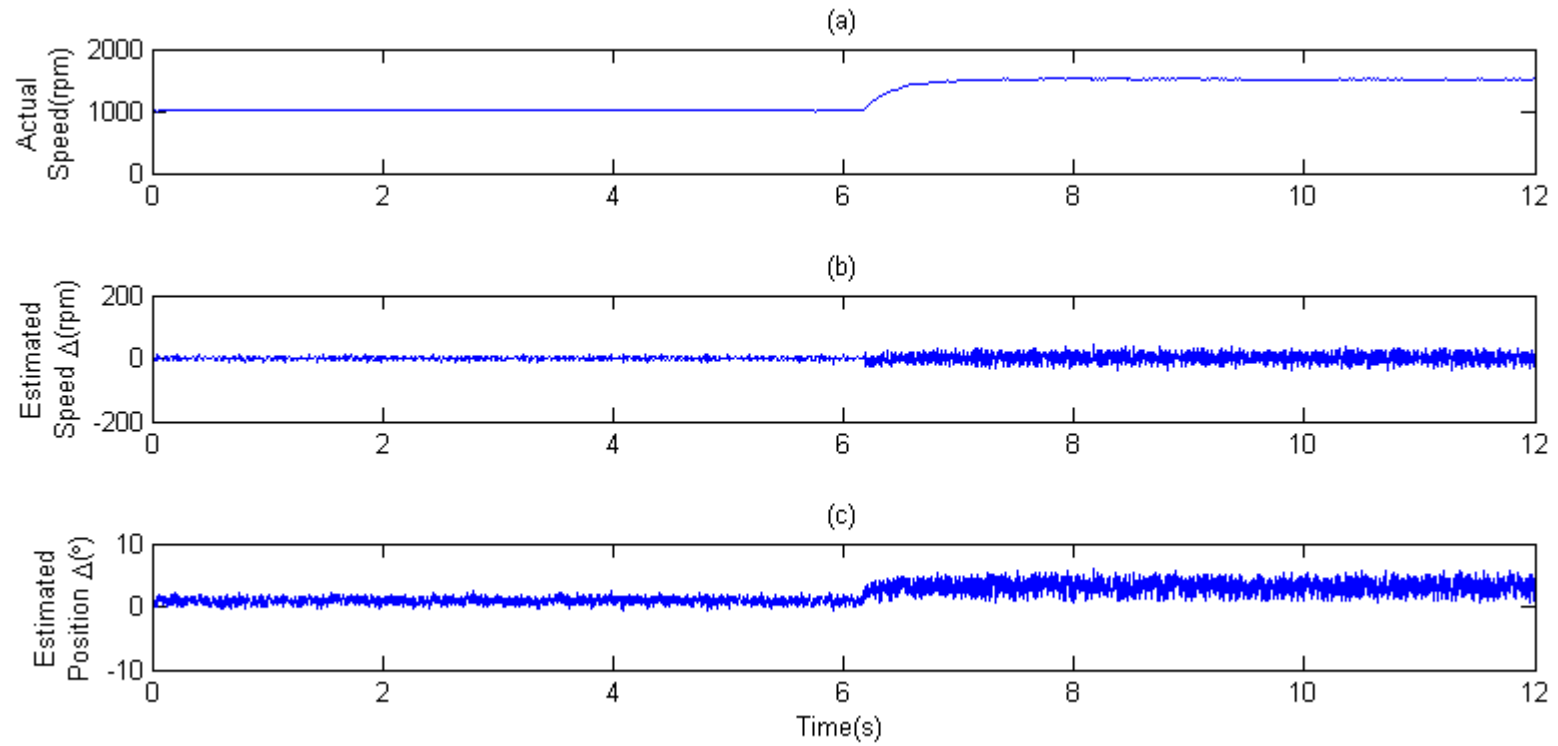


Fig. 5–16 Kalman Filter performance when switching goes from Type I to Type II. a)Actual Speed b)Filter Speed Estimation error c)Filter Position Estimation error

Fig. 5–15 shows a special case where there is no active phase and the SRM is driven by an external servo motor at 1000rpm. This is to test the filter performance with minimal mutual inductive influence. The mean speed estimation error is found to be 0.74rpm and the mean position estimation error is  $0.51^\circ$ . It thus shows that without the influence of mutual inductance the position estimation accuracy improves.

In order to have a clearer picture of the positions where APCs occur, the identified APCs for each phase pair in all electrical cycles within the experiment time range are isolated and shown in Fig. 5–17 through Fig. 5–24. Each figure shows the difference between the actual detected and expected APC positions for each type of switching schemes and for the condition with no active phase. Fig. 5–17 through Fig. 5–20 shows the difference at no load and Fig. 5–21 through Fig. 5–24 shows the difference when the motor is loaded at 2.3Nm. The difference between the actual detected APC position and the expected APC position will be denoted by  $\Delta P_{APC}$

Fig. 5–17 shows the difference between actual and expected positions when APC4/1 happens. The expected phase 1 position should be 52.5 mechanical. It can be seen that when there is no active phase the expected and actual positions have  $0^\circ$  mean difference. With Type I switching the difference is  $-1^\circ$  and with Type II the difference is  $-4^\circ$ . Under loaded conditions, shown in Fig. 5–21, with Type I switching the

difference is  $-2.1^\circ$  and with Type II the difference is  $-5.4^\circ$ . Loaded condition with no active phase is not tested.

Fig. 5–18 shows the difference between actual and expected positions when APC1/2 occurs. The expected phase 1 position should be  $7.5^\circ$  mechanical. When there is no active phase the expected and actual positions have  $-0.9^\circ$  mean difference. With Type I switching the mean difference is  $-1.5^\circ$  and with Type II the mean difference is  $-3.9^\circ$ . Under loaded conditions, shown in Fig. 5–22, with Type I switching the difference is  $-2.7^\circ$  and with Type II the difference is  $-4.4^\circ$ . Again loaded condition with no active phase is not tested.

Fig. 5–19 shows the difference between actual and expected positions when APC2/3 happens. This expected phase 1 position should be  $22.5^\circ$  mechanical. When there is no active phase the expected and actual positions have  $-1.2^\circ$  mean difference. At no load, with Type I switching the mean difference is  $-1.8^\circ$  and with Type II the mean difference is  $-4.8^\circ$ . Under loaded conditions, shown in Fig. 5–23, with Type I switching the difference is  $-2.6^\circ$  and with Type II the difference is  $-4.5^\circ$ .

Fig. 5–20 shows the difference between actual and expected position when APC3/4 takes place. This expected phase 1 position should be  $37.5^\circ$  mechanical. When there is no active phase the expected and actual positions have a mean difference of  $-1^\circ$ .

With Type I switching the mean difference is  $-1.2^\circ$  and with Type II the mean difference is  $-2.9^\circ$ . Under loaded conditions, shown in Fig. 5–24, with Type I switching the difference is  $-3.05^\circ$  and with Type II the difference is  $-4.03^\circ$ .

With these results, some observations can be made. Since the detection method is the same for the case with Type I switching mode and with no active phase mode, the difference in the detected position can only be contributed by the effect from mutual inductance. It seems that the mutual inductance will cause premature detections of the APCs. With Type II switching, the detected APC positions are even smaller than those of Type I, which is believed to be contributed by the errors when calculating the total volt-seconds when the various voltage drops are not considered. Under loaded conditions, the effect of mutual inductance is even more pronounced, which can be seen by the more negative  $\Delta P_{APCs}$ . However, the lower motor speed under loaded condition also can contribute to a smaller position lag caused by the execution time of the program. It is interesting to see that although phase 2 has a very different aligned inductance, this has very little effect on its detected APC positions. It is believed to have to do with its similar unaligned inductance to the other phases. With this characteristic inductance profile among phases are similar near the unaligned position where the APCs are detected.

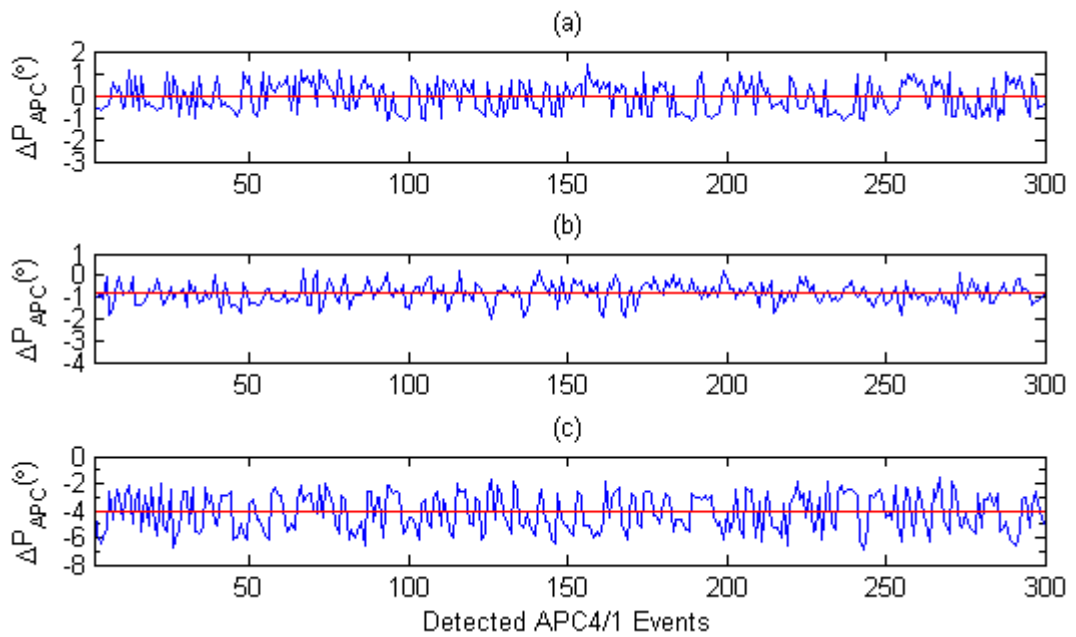


Fig. 5-17 Position variations from expected at APC4/1 under different switching conditions with no load. Red lines indicate mean values. a)No switching. b)Type I switching c)Type II switching

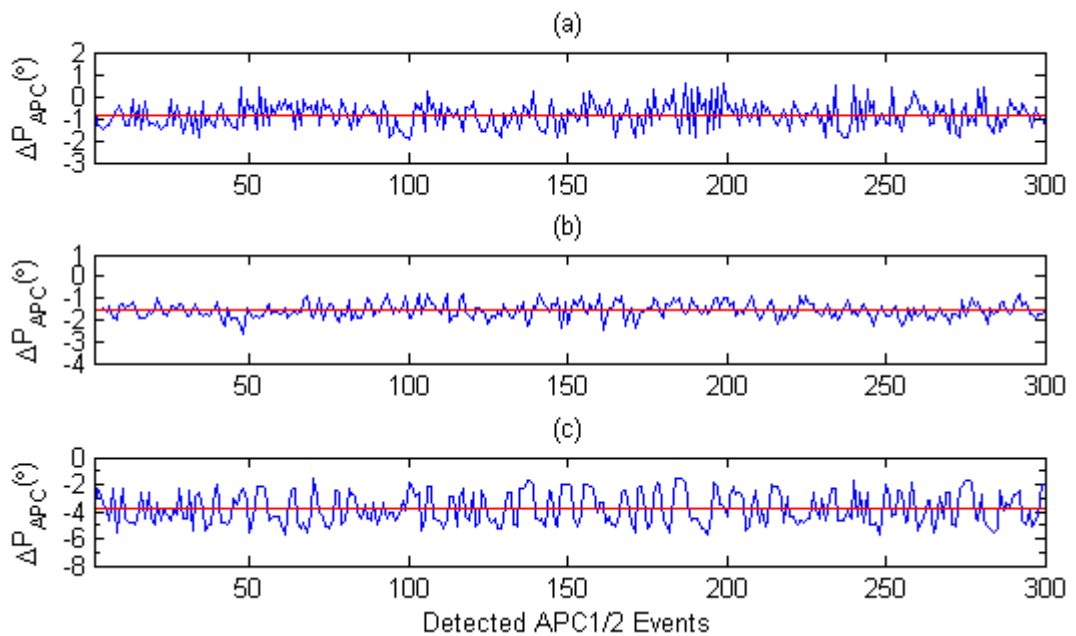


Fig. 5-18 Position variations from expected at APC1/2 under different switching conditions with no load. Red lines indicate mean values. a)No switching. b)Type I switching c)Type II switching

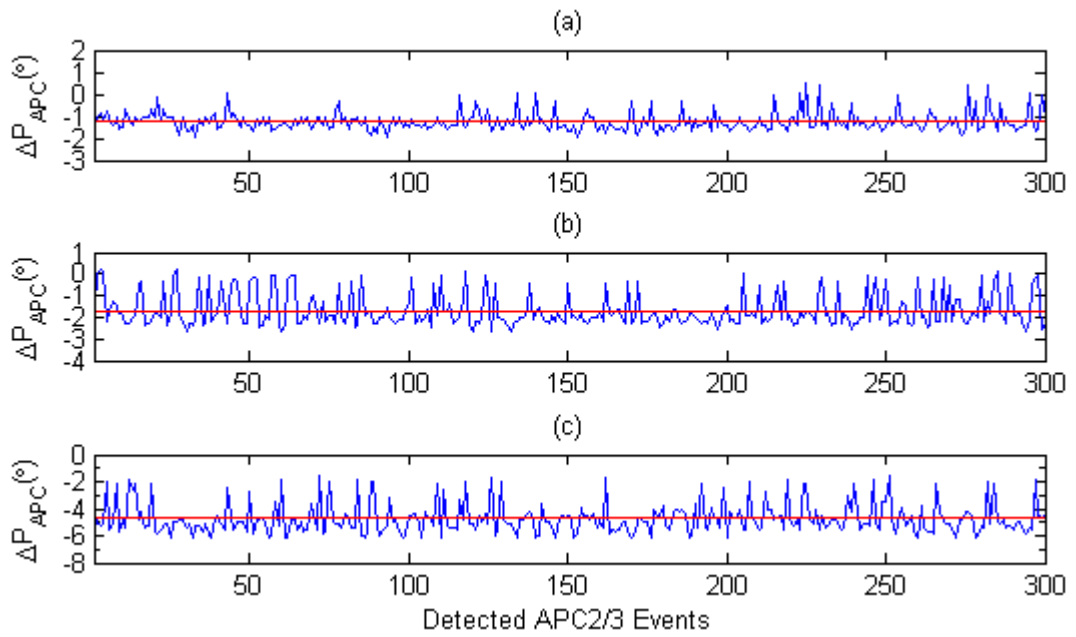


Fig. 5–19 Position variations from expected at APC2/3 under different switching conditions with no load. Red lines indicate mean values. a)No switching. b)Type I switching c)Type II switching

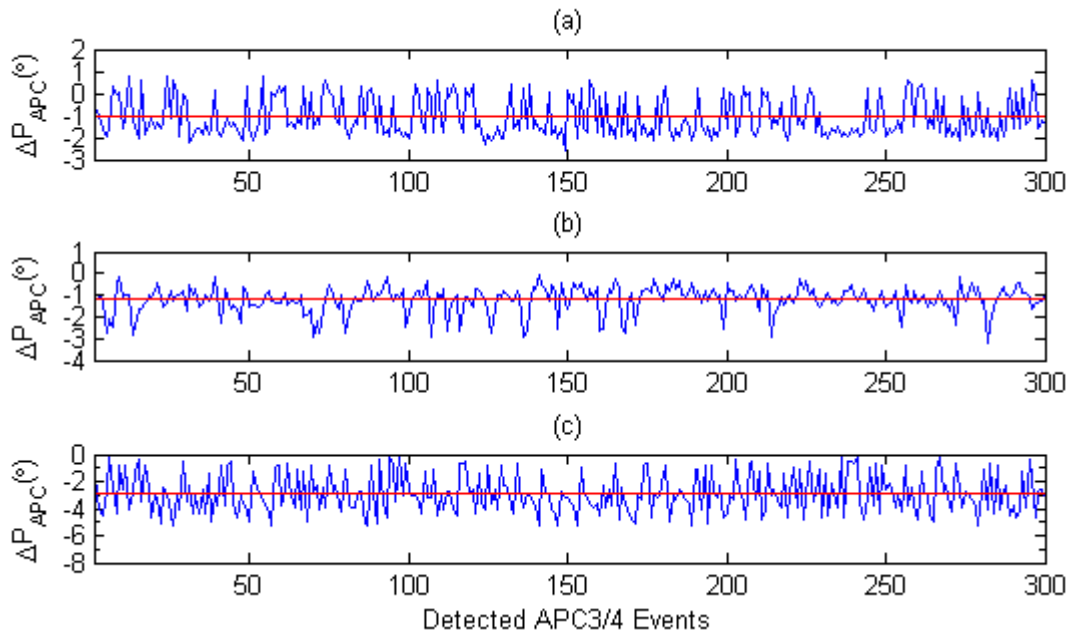


Fig. 5–20 Position variations from expected at APC3/4 under different switching conditions with no load. Red lines indicate mean values. a)No switching. b)Type I switching c)Type II switching



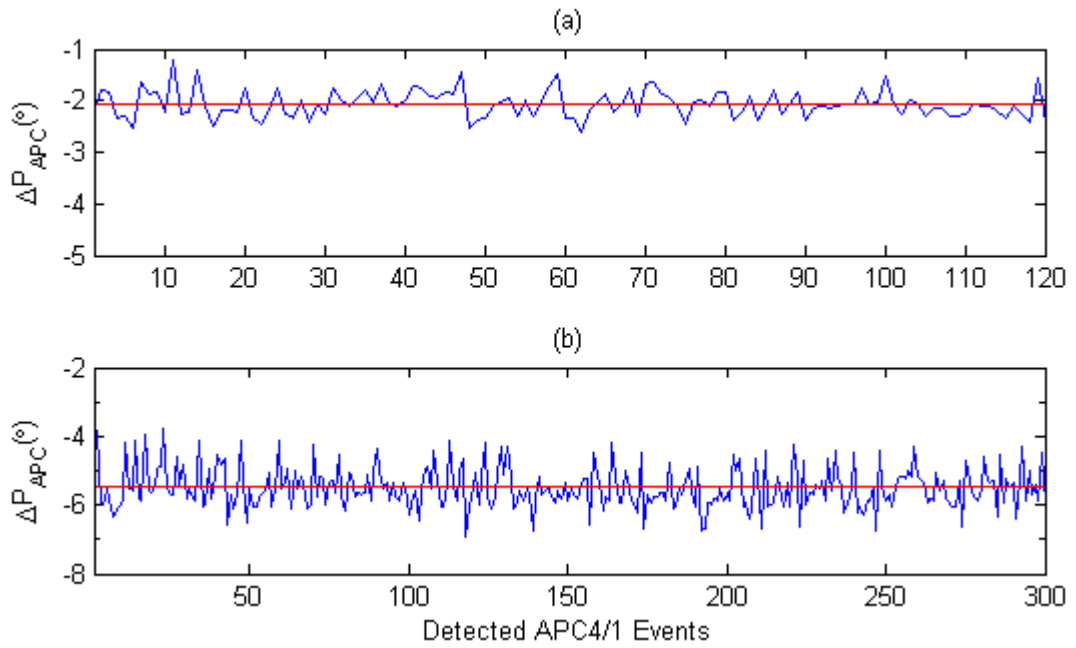


Fig. 5-21 Position variations from expected at APC4/1 under different switching conditions under load. Red lines indicate mean values. a)Type I switching b)Type II switching

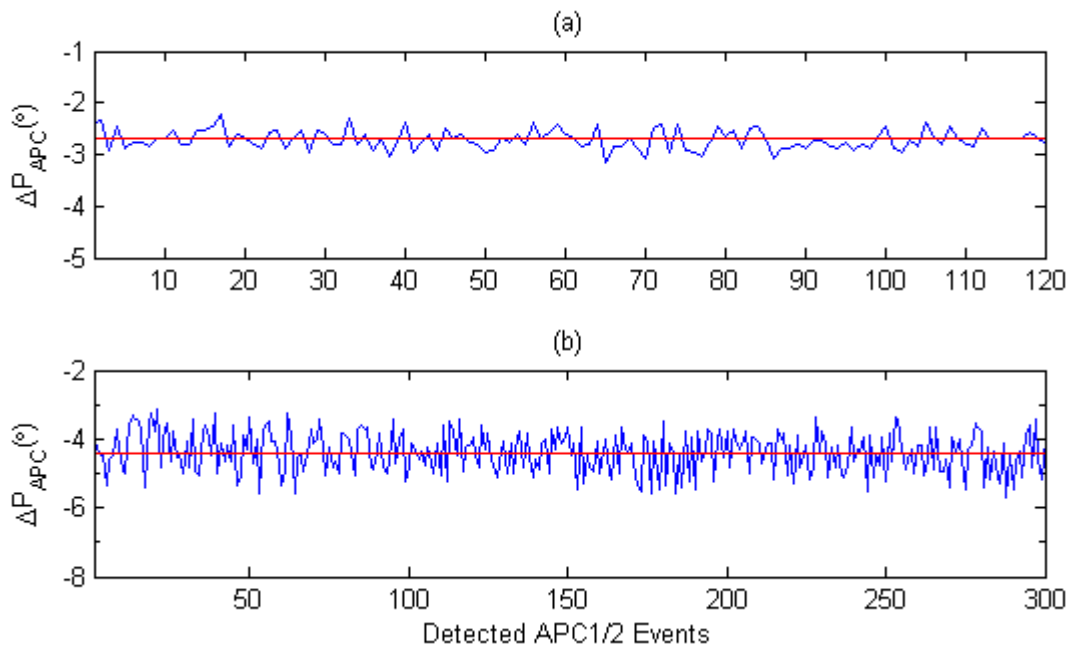


Fig. 5-22 Position variations from expected at APC1/2 under different switching conditions under load. Red lines indicate mean values. a)Type I switching b)Type II switching

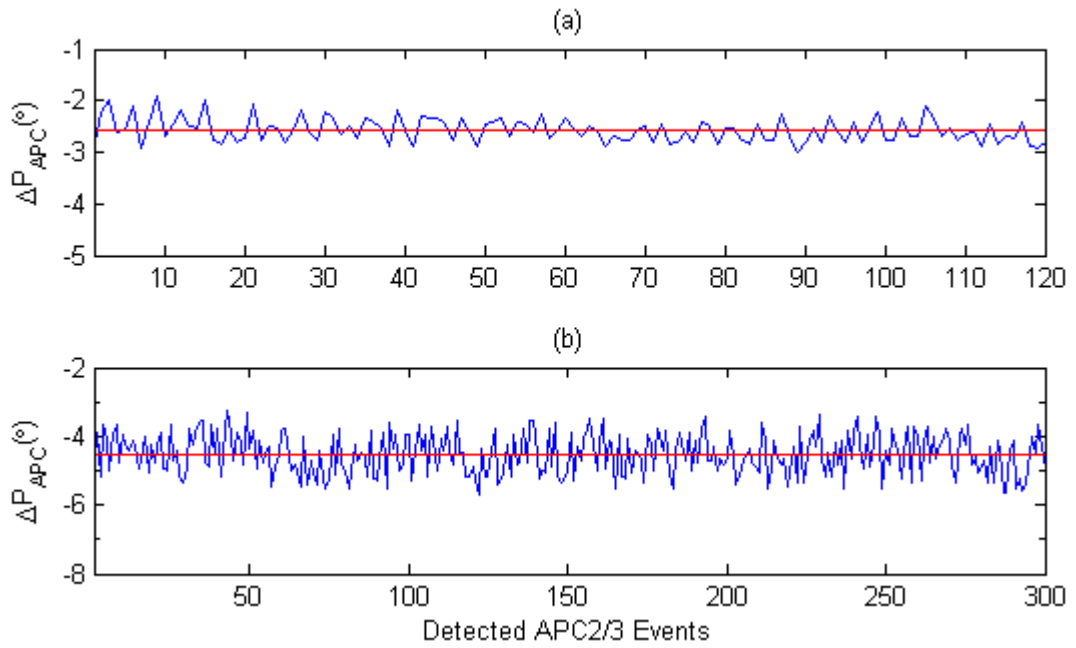


Fig. 5–23 Position variations from expected at APC2/3 under different switching conditions under load. Red lines indicate mean values. a)Type I switching b)Type II switching

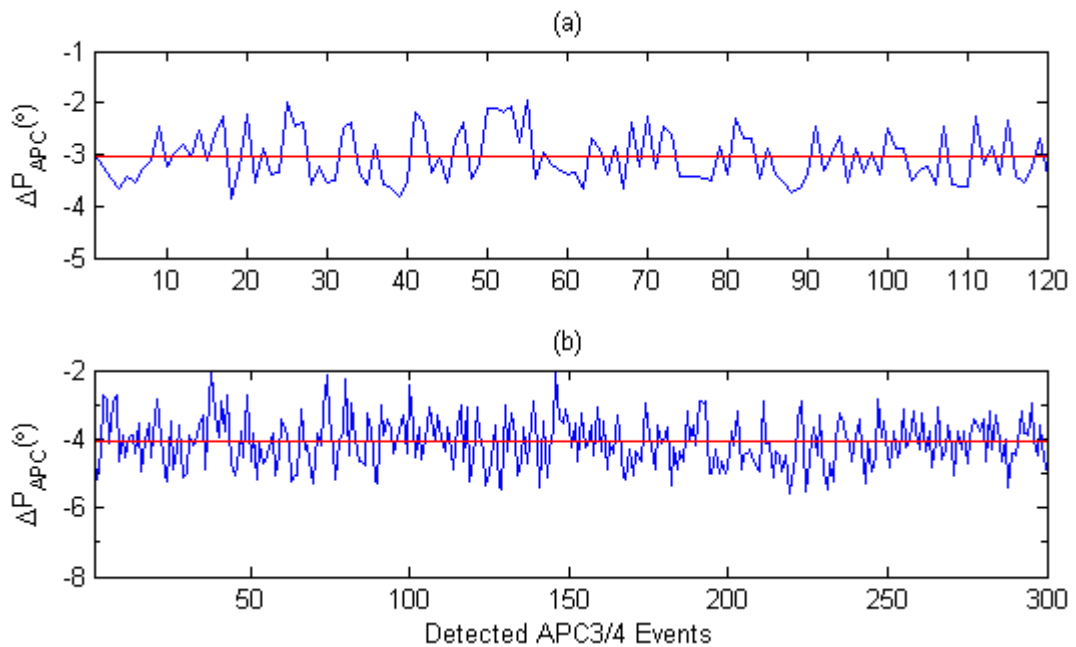


Fig. 5–24 Position variations from expected at APC3/4 under different switching conditions under load. Red lines indicate mean values. a)Type I switching b)Type II switching

## 5.9 Comparison to other methods

TABLE 5-4 compares the two dynamic methods against three other methods described in the literature.

TABLE 5-4  
COMPARISON OF DIFFERENT DYNAMIC METHODS

	Type I	Type II	Ref 30	Ref 63	Ref 68
Lookup Tables Needed	No	No	Yes	Yes	Yes
Position Estimated	Yes	Yes	Yes	Yes	Yes
Average Position Error( $^{\circ}$ )	$\sim 3$	$\sim 5$	$\sim 3$	$\sim 2$	$\sim 0.9$
Speed Estimated	Yes	Yes	Yes	Yes	No
Average Speed Error(%)	$\sim 0.5$	$\sim 0.16$	$\sim 0.1$	$\sim 0.5$	N/A

Comparing to other methods, it can be seen that the type I and II switching methodologies can provide reasonable estimations of position and speed without lookup tables created using specific magnetic information on the motors used

## 5.10 Summary

In this chapter two sensorless methods using the general inductance characteristic of four-phase 8/6 SRM are presented. The first method, Type I switching mode uses the intersection of the inductance profiles of two adjacent phases for commutation, and at the same time provides measurements to the Kalman filter. The second method Type

II switching mode then uses the output from the Kalman filter to remove the switching constraints imposed by the first method to raise the motor output torque and speed capability. The speed and filter performance from the two switching schemes are shown and the effects of mutual inductance are investigated. Simulation and experimental results have shown the validity of the methods. It is shown that both switching schemes provide reasonably accurate commutation while Type I provides slightly accurate results under loaded condition. Mutual inductance is shown to have a lead effect on the crossing point detection which cause earlier than expected commutation. This is acceptable since an earlier turn on position actually has a beneficial effect to the average torque and an earlier turn off position does not affect the torque by much.

## Chapter 6

### Conclusion

In this thesis different methods to estimate rotor position of a four-phase SRM have been developed and tested. The static methods, which estimate positions with no active phases, are all based on linear regression analysis, using different functions to connect the different phase inductances together. Through these connections the model parameters are found and then used to estimate the rotor positions. Different model functions have different accuracies and complexities and the choice should be based on available system resources. Type V exponential regression function provides the best position estimates and the co-sinusoidal function consumes the least resources. Two methods were developed to detect rotor position while the motor is running. The first method is based on the general characteristic of the inductance profile of a four-phase SRM, and phase commutations are done at fixed rotor positions. The second method utilizes the Kalman filter to estimate rotor position and based on this information carry out the commutations of the phases. All the techniques developed in this thesis have the unique advantage that no specific magnetic information is required to be known or stored, while providing specific rotor position information. This chapter summarizes the methods developed and the contributions made.

## 6.1 Developed Techniques for Position Estimations

Chapter 2 modeled the inductance relation among phases using a quadratic regression function. By using linear regression technique the parameters of the fitting functions for different positions were found. The vertices of the functions were then used to find the rotor positions. The developed technique was referred to as the Linear Quadratic Regression Position Estimation Method(LQRPEM).

Chapter 3 used a type V exponential function to model the inductance relationship among phases. A special form of least squares technique is used to find the parameters of the fitting functions. The vertex positions were again used to estimate the positions of the rotor. Compare with the LQRPEM this new method has improved accuracies for the estimates, even with the non-ideal phase 2 inductance profile. The developed technique was referred to as the Linear Exponential Regression Position Estimation Method(LERPEM).

Chapter 4 used a cosine function as the model function to link the different phase inductances together, and the phase positions are estimated by finding the phase shift of the model functions. The method was referred to as the Linear Sinusoidal Regression Position Estimation Method(LSRPEM). LSRPEM is more straightforward and numerically efficient compared with the LQRPEM and LERPEM, where it is needed to find the correct orderings of the phases on the inductance profile. A co-sinusoidal function can link the inductances from different phases across cycles and therefore can eliminate the comparison steps required by both LQRPEM and LERPEM. Simulation results have shown that out of the three methods, theoretically LSRPEM can provide the best estimates. However, using data from experiments,

LERPEM gives the best results, indicating that it is more robust and useful in practical situations where phases have different inductance profile values.

All the developed static techniques are collectively called the Linear Regression Position Estimation Methods(LRPEM).

Chapter 5 introduced two techniques for rotor position detection and phase commutation. In the first technique, called the Type I switching mode, current pulses were applied to the inactive phases to identify APC events. These events were then used to commutate the phases and at the same time, unique rotor position and speed information were extracted. By using a Kalman filter, the position information was interpolated to provide fine rotor positions. Under Type II switching mode the positions are then used for phase commutations. While Type I switching imposes some speed and torque limitations, Type II switching can utilize the full speed and torque capability of the motor. Experimental results have shown that both switching schemes can successfully control the motor in both unloaded and loaded situations.

## **6.2 Main Contributions**

There are several significant contributions from this research:

### **1) Fastest static algorithms**

The series of static algorithms developed are the fastest methods available to estimate rotor positions for a four-phase 8/6 SRM. The approach is mathematical, there is no need to compare and sort the magnitudes of the measured currents which are unreliable. No lookup table is required and only a

few lines of codes are enough to implement the methods. The estimated positions also have adequate accuracies.

## **2) Fine Position estimations without magnetic characteristic information**

In comparison with conventional sensorless methods, including those for permanent magnet and induction motors[69-80], no specific magnetic characteristics of the SRM are required to estimate fine rotor positions. This is advantageous for their practical applications.

## **3) Robust using information from four phases.**

With the static techniques all four phases are utilized to estimate the positions with a regression function. With the dynamic techniques, the Kalman filter combines information from all four phases. Detrimental effects from sampling errors and unbalanced, imperfect inductance profiles are thus minimized. This advantage is demonstrated through the experimental motor with a peculiar phase 2 inductance.

## **4) Applicable to all SRM with three phases or more**

The presented methods are not restrictive. All the methods can be used to estimate positions for SRM with at least three phases. Calculation overhead is minimal with increasing number of phases. For the static techniques each additional phase induces only two extra multiply-and-add operations. For the dynamic techniques there is almost no extra overhead.



### **6.3 Future Research**

For the developed static techniques, it is discovered that different model functions will give different accuracies under unbalanced phase inductance situations. It is hoped some other modeling functions can be found that can provide better robustness of the estimating scheme.

The static methods can also be further extended to the application on running motors, where the effects of various voltage drops, mutual couplings and inductance saturation will have a larger impact on the estimation quality. Measures should be taken so that these effects could be minimized and better methods to estimate volt-seconds should be found.

In the current research for the dynamic methods, no considerations were given to the effects of voltage drops, mutual couplings or inductance saturation. This leads to larger deviations of the estimated positions from the actual ones, especially when under Type II switching mode. Future effort will be to concentrate on how to mitigate the various effects in order to achieve better estimation results.

## References

- [1] D. S. Reay, T. C. Green, and B. W. Williams, "Minimisation of torque ripple in a switched reluctance motor using a neural network," presented at The Third International Conference on Artificial Neural Networks, 1993.
- [2] Z. Lin, D. S. Reay, and B. W. Williams, "Torque ripple reduction in switched reluctance motor drives using B-spline neural networks," Conference Record of the Fourtieth IAS Annual Meeting, 2005.
- [3] H. M. Cheshmehbeigi, S. Yari, and E. Afjei, "Design and analysis of low torque ripple switched reluctance motor using 3-dimensional finite element method," presented at European Conference on Circuit Theory and Design, 2009.
- [4] N. Inanc, A. Derdiyok, and V. Ozbulur, "Torque ripple minimization of a switched reluctance motor including mutual inductances via sliding mode control technique," presented at Proceedings of the IEEE International Symposium on Industrial Electronics, 1997.
- [5] F. Sahin, H. B. Ertan, and K. Leblebicioglu, "Optimum geometry for torque ripple minimization of switched reluctance motors," *IEEE Transactions on Energy Conversion*, vol. 15, issue 1, pp. 30-39, 2000.
- [6] X. Changliang, J. Fuchen, X. Mei, and F. Hongwei, "Commutation signal identification for switched reluctance motors based on fuzzy neural networks," presented at IEEE International Conference on Automation and Logistics, 2008.
- [7] N. K. Sheth and K. R. Rajagopal, "Optimum pole arcs for a switched reluctance motor for higher torque with reduced ripple," *IEEE Transactions on Magnetics*, vol. 39, issue 5, pp. 3214-3216, 2003.
- [8] S. Changjing, D. Reay, and B. Williams, "Adapting CMAC neural networks with constrained LMS algorithm for efficient torque ripple reduction in switched reluctance motors," *IEEE Transactions on Control Systems Technology*, vol. 7, issue 4, pp. 401-413, 1999.
- [9] Z. Jingjun, Z. Haijun, G. Ruizhen, and W. Lili, "Fuzzy compensation control for minimum torque ripple of switched reluctance motor system based on finite element model," presented at The 3rd IEEE Conference on Industrial Electronics and Applications, 2008.
- [10] J. O. Fiedler and R. W. De Doncker, "Extended analytic approach to acoustic noise in switched reluctance drives," presented at The 33rd IEEE Annual Power Electronics Specialists Conference, 2002.
- [11] J. O. Fiedler, K. A. Kasper, F. Chaparro, and R. W. De Doncker, "Effectiveness of Noise Reducing Measures in Switched Reluctance Drives," presented at The 41st IAS Annual Meeting, 2006.

- [12] J. O. Fiedler, K. A. Kasper, and R. W. De Doncker, "Acoustic noise in switched reluctance drives: an aerodynamic problem?," presented at The IEEE International Conference on Electric Machines and Drives, 2005.
- [13] K. A. Kasper, M. Bosing, R. W. De Doncker, S. Fingerhuth, and M. Vorlander, "Noise Radiation of Switched Reluctance Drives," presented at The 7th International Conference on Power Electronics and Drive Systems, 2007.
- [14] K. A. Kasper, J. O. Fiedler, D. Schmitz, and R. W. De Doncker, "Noise Reduction Control Strategies for Switched Reluctance Drives," presented at IEEE Vehicle Power and Propulsion Conference, 2006.
- [15] X. Ojeda, M. Gabsi, M. Lecrivain, and X. Mininger, "Noise Reduction Using Piezoelectric Active Control on High Speeds Switched Reluctance Drives," presented at The 42nd IAS Annual Meeting, 2007.
- [16] D. W. J. Pulle, J. C. S. Lai, J. F. Milthorpe, and N. Huynh, "Quantification and analysis of acoustic noise in switched reluctance drives," presented at The Fifth European Conference on Power Electronics and Applications, 1993.,
- [17] A. A. Goldenberg, I. Laniado, P. Kuzan, and C. Zhou, "Control of switched reluctance motor torque for force control applications," *IEEE Transactions on Industrial Electronics*, vol. 41, issue 4, pp. 461-466, 1994.
- [18] R. B. Inderka and R. W. A. A. De Doncker, "High-dynamic direct average torque control for switched reluctance drives," *IEEE Transactions on Industry Applications*, vol. 39, issue 4, pp. 1040-1045, 2003.
- [19] B. H. Jeong, K. Y. Lee, J. D. Na, G. B. Cho, and H. L. Baek, "Direct torque control for the 4-phase switched reluctance motor drives," presented at Eighth International Conference on Electrical Machines and Systems, 2005.
- [20] Z. Lin, D. Reay, B. Williams, and X. He, "High-performance current control for switched reluctance motors based on on-line estimated parameters," *IET Electric Power Applications*, vol. 4, issue 1, pp. 67-74.
- [21] M. Miller, "Dynamic torque control for switched reluctances drives based on a new online machine model," presented at European Conference on Power Electronics and Applications, 2005.
- [22] C. R. Neuhaus, N. H. Fuengwarodsakul, and R. W. De Doncker, "Predictive PWM-based Direct Instantaneous Torque Control of Switched Reluctance Drives," presented at The 37th IEEE Power Electronics Specialists Conference, 2006.
- [23] K. Tungpimolrut, R. Pupadubsin, N. Chayopitak, S. Kachapornkul, P. Jitkreeyarn, and P. Somsiri, "Torque compensation for switched reluctance drives," presented at International Conference on Electrical Machines and Systems, 2008.
- [24] Z. Zhu, N. C. Cheung, K. W. E. Cheng, X. Xiangdang, and L. Jiongang, "Direct Instantaneous Force Control With Improved Efficiency for Four-Quadrant Operation of Linear Switched Reluctance Actuator in Active Suspension System," *IEEE Transactions on Vehicular Technology*, vol. 61, issue 4, pp. 1567-1576.

- [25] O. Ahmed, K. Ohyama, Y. Narumoto, H. Fujii, and H. Uehara, "Sensorless operation of SRM drives from starting to steady state," presented at IEEE International Symposium on Industrial Electronics, 2009.
- [26] T. Bamba, A. Komatsuzaki, and I. Miki, "Estimation of Rotor Position for Switched Reluctance Motor at Standstill," presented at Power Conversion Conference - Nagoya, 2007.
- [27] J. Bekiesch, G. Schroder, K. Tae-Hyoung, and A. Jin-Woo, "A simple excitation position detection method for sensorless SRM drive," presented at European Conference on Power Electronics and Applications, 2007.
- [28] A. Bellini, F. Filippetti, G. Franceschini, C. Tassoni, and P. Vas, "Position sensorless control of a SRM drive using ANN-techniques," presented at The Thirty-Third IAS Annual Meeting, 1998.
- [29] A. Brosse, G. Henneberger, M. Schniedermeier, R. D. Lorenz, and N. Nagel, "Sensorless control of a SRM at low speeds and standstill based on signal power evaluation" presented at 24th Annual Conference of the IEEE Industrial Electronics Society(IECON), 1998.
- [30] M. Divandari, A. Koochaki, M. Jazaeri, and H. Rastegar, "A Novel Sensorless SRM Drive via Hybrid Observer of Current Sliding Mode and Flux linkage," presented at IEEE International Electric Machines & Drives Conference, 2007.
- [31] B. Fahimi, A. Emadi, and R. B. Sepe, Jr., "Four-quadrant position sensorless control in SRM drives over the entire speed range," *IEEE Transactions on Power Electronics*, vol. 20, issue 1, pp. 154-163, 2005.
- [32] H. Gao, F. R. Salmasi, and M. Ehsani, "Sensorless control of SRM at standstill," presented at The Sixteenth Annual IEEE Applied Power Electronics Conference and Exposition, 2001.
- [33] T. Guojun, M. Zhenglan, K. Songyan, and Z. Xulong, "Four-quadrant position sensorless control in Switched Reluctance Motor drives based on Sliding Mode Observer," presented at International Conference on Electrical Machines and Systems, 2009.
- [34] C. Hai-Jin, S. Long-Xing, Z. Rui, and J. Wei-Ping, "A robust non-reversing starting scheme for sensorless switched reluctance motors," presented at International Conference on Mechatronics and Automation, 2009.
- [35] Y. lee-Woo, K. Young-Seok, and L. Yong-Geun, "The rotor speed and position sensorless control of SRM using the binary observer," presented at The Thirty-Fourth IAS Annual Meeting, 1999.
- [36] B. Jianrong and X. Longya, "Eliminating starting hesitation for reliable sensorless control of switched reluctance motors," *IEEE Transactions on Industry Applications*, vol. 37, issue 1, pp. 59-66, 2001.
- [37] C. Jun and D. Zhiquan, "Sensorless Control of Switched Reluctance Motor Based on Phase Inductance Vectors," *IEEE Transactions on Power Electronics*, vol. 27, issue 7, pp. 3410-3423.

- [38] T. Koblara, C. Sorandaru, S. Musuroi, and M. Svoboda, "A low voltage sensorless Switched Reluctance Motor drive using flux linkage method," presented at The 12th International Conference on Optimization of Electrical and Electronic Equipment (OPTIM), 2010.
- [39] H. Lin, S. Hexu, G. Jie, and B. Jie, "A new method to detect the initial position for sensorless SRM," presented at International Conference on Electronics, Communications and Control (ICECC), 2011.
- [40] L. Ming-Tsan and L. Tian-Hua, "Sensorless synchronous reluctance drive with standstill starting," *IEEE Transactions on Aerospace and Electronic Systems*, vol. 36, issue 4, pp. 1232-1241, 2000.
- [41] K. Min-Huei, B. Won-Sik, K. Dong-Hee, K. Nam-Hun, and C. Kyeong-Ho, "A position sensorless control system of SRM over wide speed range," presented at The 7th International Conference on Power Electronics, 2007.
- [42] K. Trakrancharoungsook and S. Kittiratsatcha, "Position Estimation Technique of a Switched Reluctance Motor at Standstill," presented at Power Conversion Conference - Nagoya, 2007.
- [43] D. van Treek, P. Matuschek, H. J. Brauer, T. Schoenen, and R. W. De Doncker, "An automatic identification of phase inductance for operation of switched reluctance machines without position sensor," presented at IEEE International Electric Machines and Drives Conference, 2009.
- [44] K. F. Wong, K. W. E. Cheng, and S. L. Ho, "On-line instantaneous torque control of a switched reluctance motor based on co-energy control," *IET Electric Power Applications*, vol. 3, issue 4, pp. 257-264, 2009.
- [45] B. Won-Sik, K. Min-Huei, K. Nam-Hun, and K. Dong-Hee, "Position sensorless control system of SRM using neural network," presented at The 35th IEEE Annual Power Electronics Specialists Conference, 2004.
- [46] L. Zhenguo, H. Baoying, L. Caihong, L. Dong-Hee, and A. Jin-Woo, "SRM sensorless speed control based on the improved simplified flux method," presented at International Conference on Electrical Machines and Systems (ICEMS), 2011.
- [47] M. Krishnamurthy, C. S. Edrington, and B. Fahimi, "Prediction of rotor position at standstill and rotating shaft conditions in switched reluctance machines," *IEEE Transactions on Power Electronics*, vol. 21, issue 1, pp. 225-233, 2006.
- [48] B. Deng, T. Tian, and J. Pan, "DSP based sensorless control for induction motor using extended Kalman filter," presented at The 7th IEEE International Conference on Electronics, Circuits and Systems, 2000.
- [49] K. Fuat, G. Hiroki, G. Hai-Jiao, and I. Osamu, "Artificial neural networks and inductance vector based sensorless torque estimation in switched reluctance motor drive," presented at the International Conference on Electrical Machines and Systems(ICEMS), 2007.
- [50] M. M. Beno, L. Rajaji, V. M. Varatharaju, and A. N. Santos, "Rotor position estimation of 6/4 Switched Reluctance Motor using a novel neural network algorithm," presented at IEEE GCC Conference and Exhibition (GCC), 2011.

- [51] C. A. Hudson, N. S. Lobo, and R. Krishnan, "Sensorless Control of Single Switch-Based Switched Reluctance Motor Drive Using Neural Network," *IEEE Transactions on Industrial Electronics*, vol. 55, issue 1, pp. 321-329, 2008.
- [52] J. A. Makwana, P. Agarwal, and S. P. Srivastava, "ANN based sensorless rotor position estimation for the Switched Reluctance Motor," presented at Nirma University International Conference on Engineering (NUICONE), 2011.
- [53] S. Paramasivam, R. Arumugan, B. Umamaheswari, S. Vijayan, S. Balamurugan, and G. Venkatesan, "Accurate rotor position estimation for switched reluctance motor using ANFIS," presented at Conference on Convergent Technologies for Asia-Pacific Region(TENCON), 2003.
- [54] D. S. Reay, Y. Dessouky, and B. W. Williams, "The use of neural networks to enhance sensorless position detection in switched reluctance motors," presented at IEEE International Conference on Systems, Man, and Cybernetics, 1998.
- [55] [http://en.wikipedia.org/wiki/Regression\\_analysis](http://en.wikipedia.org/wiki/Regression_analysis), "Regression Analysis."
- [56] R. E. Kalman, "A new approach to linear filtering and prediction problems," *Journal of basic Engineering*, vol. 82, pp. 35-45, 1960.
- [57] [http://en.wikipedia.org/wiki/Polynomial\\_regression](http://en.wikipedia.org/wiki/Polynomial_regression), "Polynomial Regression."
- [58] [http://en.wikipedia.org/wiki/Vandermonde\\_matrix](http://en.wikipedia.org/wiki/Vandermonde_matrix), "Vandermonde Matrix."
- [59] V. S. a. M. Poulin-Costello, *Catalog of Curves for Curve Fitting*: Forest Science Research Branch, Ministry of Forests, 1994.
- [60] "IEEE Standard for Digitizing Waveform Recorders - Redline," *IEEE Std 1057-2007(Revision of IEEE Std 1057-1994) - Redline*, pp. 1-210, 2008.
- [61] "IEEE Standard for Digitizing Waveform Recorders," *IEEE Std 1057-1994*, pp. 0\_1, 1994.
- [62] X. Kai, Z. Qionghua, M. Zhiyuan, W. Shuanghong, and S. Jianbo, "Sensorless Position Estimation of Switched Reluctance Motors Based on Gradient of Phase Current," presented at IEEE International Conference on Industrial Technology, 2006.
- [63] K. R. Thompson, P. P. Acarnley, and C. French, "Rotor position estimation in a switched reluctance drive using recursive least squares," *IEEE Transactions on Industrial Electronics*, vol. 47, issue 2, pp. 368-379, 2000.
- [64] A. Khalil and I. Husain, "Four Quadrant Sensorless Operation of a Switched Reluctance Machine Using Fourier Model," presented at The 37th IEEE Power Electronics Specialists Conference, 2006.
- [65] K. R. Geldhof, A. P. M. Van den Bossche, and J. A. Melkebeek, "Rotor-Position Estimation of Switched Reluctance Motors Based on Damped Voltage Resonance," *IEEE Transactions on Industrial Electronics*, vol. 57, issue 9, pp. 2954-2960.
- [66] H. J. Guo, M. Takahashi, T. Watanabe, and O. Ichinokura, "A new sensorless drive method of Switched Reluctance Motors based on motor's magnetic characteristics," *IEEE Transactions on Magnetics*, vol. 37, issue 4, pp. 2831-2833, 2001.

- [67] S. A. Hossain, I. Husain, H. Klode, B. Lequesne, A. M. Omekanda, and S. Gopalakrishnan, "Four-quadrant and zero-speed sensorless control of a switched reluctance motor," *IEEE Transactions on Industry Applications*, vol. 39, issue 5, pp. 1343-1349, 2003.
- [68] I. H. Al-Bahadly, "Examination of a Sensorless Rotor-Position-Measurement Method for Switched Reluctance Drive," *IEEE Transactions on Industrial Electronics*, vol. 55, issue 1, pp. 288-295, 2008.
- [69] A. Dell'Aquila, F. Cupertino, L. Salvatore, and S. Stasi, "Kalman filter estimators applied to robust control of induction motor drives," presented at The 24th Annual Conference of the IEEE Industrial Electronics Society, 1998.
- [70] M. Farasat, E. Karaman, A. M. Trzynadlowski, and M. S. Fadali, "Hybrid field orientation and direct torque control for electric vehicle motor drive with an extended Kalman filter," presented at IEEE Energytech, 2012.
- [71] D. Janiszewski, "Sensorless control of Permanent Magnet Synchronous Motor based on Unscented Kalman Filter," presented at International Conference on Power Engineering, Energy and Electrical Drives (POWERENG), 2011.
- [72] M. Jannati and E. Fallah, "A new method for speed sensorless vector control of single-phase induction motor using Extended Kalman Filter," presented at The 19th Iranian Conference on Electrical Engineering (ICEE), 2011.
- [73] Y. R. Kim, S. Seung-Ki, and M. H. Park, "Speed sensorless vector control of induction motor using extended Kalman filter," *IEEE Transactions on Industry Applications*, vol. 30, issue 5, pp. 1225-1233, 1994.
- [74] M. S. Merzoug, H. Benalla, and H. Naceri, "Speed Estimation Using Extended Filter Kalman for the Direct Torque Controlled Permanent Magnet Synchronous Motor (PMSM)," presented at The Second International Conference on Computer and Electrical Engineering, 2009.
- [75] K. H. Ng, C. F. Yeong, E. L. M. Su, and A. R. Husain, "Current sensorless control of a PMDC motor using Kalman filter and cascaded PID controller," presented at The 4th International Conference on Intelligent and Advanced Systems (ICIAS), 2012.
- [76] D. Pai A, L. Umanand, and N. J. Rao, "Direct torque control of induction motor with extended Kalman filter," presented at The Third International, Power Electronics and Motion Control Conference, 2000.
- [77] S. Praesomboon, S. Athaphaisal, S. Yimman, R. Boontawan, and K. Dejhan, "Sensorless speed control of DC servo motor using Kalman filter," presented at The 7th International Conference on Information, Communications and Signal Processing, 2009.
- [78] G. Terorde, K. Hameyer, and R. Belmans, "Sensorless control of a permanent magnet synchronous motor for PV-powered water pump systems using the extended Kalman filter," presented at The Ninth International Conference on Electrical Machines and Drives, 1999.
- [79] P. Zhongbo, H. XueFeng, and D. Zixue, "Direct Torque Control for Electric Vehicle Driver Motor Based on Extended Kalman Filter," presented at The 72nd IEEE Vehicular Technology Conference Fall (VTC 2010-Fall), 2010.

- [80] M. Cheol, N. Kee Hyun, J. Mun Kyu, C. Chang Ho, and K. Young Ahn, "Sensorless speed control of permanent magnet synchronous motor using Unscented Kalman Filter," presented at SICE Annual Conference (SICE), 2012.
- [81] Y.-z. Li and K.-g. Zhao, "Sensorless speed control of the switched reluctance motor using extended Kalman filter," presented at The 2nd International Conference on Information Science and Engineering (ICISE), 2010.
- [82] L. P. Yan, D. H. Zhou, M. Y. Fu, and Y. Q. Xia, "State estimation for asynchronous multirate multisensor dynamic systems with missing measurements," *IET Signal Processing*, vol. 4, issue 6, pp. 728-739.
- [83] S. Roshany-Yamchi, M. Cychowski, R. R. Negenborn, B. De Schutter, K. Delaney, and J. Connell, "Kalman Filter-Based Distributed Predictive Control of Large-Scale Multi-Rate Systems: Application to Power Networks," *IEEE Transactions on Control Systems Technology*, vol. 21, issue 1, pp. 27-39.
- [84] B. Sridhar, P. Smith, R. E. Suorsa, and B. Hussien, "Multirate and event-driven Kalman filters for helicopter flight," *IEEE Control Systems*, vol. 13, issue 4, pp. 26-33, 1993.
- [85] L. Weihua and S. Shah, "Data-driven Kalman filters for non-uniformly sampled multirate systems with application to fault diagnosis," presented at the American Control Conference, 2005.
- [86] L. Young Ok, L. Seung-Hi, S. Youngseop, and C. Chung Choo, "Robust multirate state estimator for autonomous vehicles with uncertain vision processing period," presented at The 11th International Conference on Control, Automation and Systems (ICCAS), 2011.